CONTROL OF A VSC-HVDC SYSTEM WITH LARGE WIND POWER INTEGRATION FOR POWER SYSTEM TRANSIENT STABILITY IMPROVEMENT

JAMES KINYUA MURIUKI

DOCTOR OF PHILOSOPHY IN

(Electrical Engineering)

JOMO KENYATTA UNIVERSITY OF

AGRICULTURE AND TECHNOLOGY.

2018

Control of a VSC-HVDC system with large wind power Integration for power system transient stability Improvement

James Kinyua Muriuki

A thesis submitted in partial fulfillment for the Degree of Doctor of Philosophy in Electrical Engineering in the Jomo Kenyatta University of Agriculture and Technology.

2018

DECLARATION

This thesis is my original work and has not been presented for a degree in any other university.

Signature: ..... Date: .....

Eng. James Kinyua Muriuki

This thesis has been submitted for examination with our approval as University Supervisors.

Signature: ..... Date: .....

Prof. Christopher Maina Muriithi

Muranga University of Technology (MUT)

Signature: ..... Date: .....

Prof. Dr-Eng. Livingstone M. Ngoo

Multi Media University

Signature: ..... Date: .....

Prof. George Nyakoe

JKUAT, Kenya

DEDICATION

I dedicate this thesis to my lovely wife Sophie, son Dylan and daughters Maryann and Nyakio. Surely, as the saying goes, two are better than one because when one is down the other can help lift one up. My family accorded me great support during my research; it has not been easy but you stood with me at all times. You gave me the best of what any person would expect from his loved ones and may the Lord Almighty, the Creator of things including all animals and birds that crawl, walk, swim, fly, hop, slither and navigate bless you in abundance.

ACKNOWLEDGEMENT

The completion of this work could not have been possible without the involvement of many individuals who contributed in one way or the other even without knowing that their inputs were valuable. The PhD flight has been long and demanding both mentally and physically, I thank you all. Though I may not enumerate all your names in this work, your contributions are sincerely appreciated and gratefully acknowledged. However, I would particularly wish to express my deep appreciation to the following great Kenyans and financial institutions:

Professor Muriithi you were readily available when called upon to give directions. You guided me from the research initiation to its successful completion. Thank you for your endless support, constant and insightful feedback on my PhD work. Your prompt interventions to my many queries and understanding during the research were tremendous. Professor Ngoo you were at all times available and encouraged me to pursue my research even when I felt low; you ignited and lifted my spirits during the many visits in your office and at times in your house to discuss the research progress. Your responses to my many queries whenever I got stuck were timely and helpful. You are such a team player and I salute you. Professor Nyakoe I cannot lay it on with a trowel the assistance and contributions I got from you. Whenever I put a request for a meeting to discuss about the research progress, you were readily available and if committed, you always made arrangements for a meeting at the next available opportunity and for that I remain indebted.

The financial support I received from higher education loans board (HELB) is highly appreciated. Further, the research grant from national research fund (NRF) enabled me to carry out the research effectively and disseminated the results of my findings at various conferences and published widely in both local and international journals. Consequently, I remain grateful and i will utilize the knowledge gained to make the world a better habitation for humanity.

TABLE OF CONTENTS

LIST OF TABLES

LIST OF FIGURES

LIST OF APPENDICES

LIST OF ABBREVIATIONS

AC:	Alternating current
AVR:	Automatic voltage regulator
ABB:	Asea brown boveri
CB:	Circuit breaker
CSC-HVDC:	Current source converter-high voltage direct current
DC:	Direct current
dq:	Direct quadrature rotating frame
EWEA:	European wind energy association
FACTS:	Flexible alternating current transmission system
GTO:	Gate turn off thyristor
HVDC:	High voltage direct current
HVAC:	High voltage alternating current
IEEE:	Institute of Electrical and Electronic Engineers
IPFC:	Interline power flow controller

IGBT:	Insulated gate bipolar transistor
LCC:	Line commutated converters
LCC-HVDC:	Line commutated converters-high voltage direct current
MOC:	Modulus optimum criterion
NFDCB:	Novel fast direct current breaker
PI:	Proportional and Integral controller
PSS:	Power system stabilizer
PLL:	Phase-locked loop
PWM:	Pulse width modulation
RoW:	Right of way
STATCOM:	Static synchronous compensator
SOC:	Symmetrical optimum criterion
SSSC:	Static synchronous series compensator
SVC:	Static VAr compensator
TCSC:	Thyristor controlled series compensator
TCPS:	Thyristor controlled phase shifter
WPP:	Wind power plant

WTG: Wind turbine generator

VSC-HVDC: Voltage source converter- high voltage direct current

UFD: Ultra-fast disconnector

UPFC: Unified power flow controller

LCS: Load commutator switch

LIST OF SYMBOLS

a	Symmetrical distance
A_r	Swept area of the turbine rotor blades in (m^2)
C_{dc}	DC capacitance.
ρ	Density of air in (Kg/m^3)
C_p	Power coefficient of the wind turbine
i_{abc}	AC current through the reactor in abc reference frame
L_f	Phase reactor inductance
λ	Tip speed ratio between the turbine blade tip speed
θ	Blade pitch angle in [degrees]
T_{eq}	First order time constant of the inner current control loop,
x_d	*d*-axis reactance (p.u.)

x'_d d axis transient reactance (p.u.)

x_q q-axis reactance (p.u.)

x'_q q-axis transient reactance (p.u.)

T_a Average time delay of the converter (s)

T'_{do} d-axis time constant (s)

T'_{qo} q-axis time constant (s)

T''_{do} d-axis sub-transient open-circuit

T''_{qo} q-axis sub-transient open-circuit

x''_d d-axis sub-transient reactance

x''_q q-axis sub-transient reactance

H Inertia constant (p.u.)

i_{dc} Converter output DC current

i_L DC current through DC inductor link

U_{dc} Steady-state DC voltage

W_R Total energy absorbed by the surge arrestors and suppressed at the time of fault clearance

L_{dc} System inductance.

I^2_o Short-circuit current.

L Reactor inductance

R Reactor resistance.

u_{abc} Converter AC side output voltage in abc reference frame

V Wind speed upstream the rotor in (m/s)

v_{abc} Grid AC voltage in abc reference frame

V_{dc} Direct voltage controller

V_g Rated voltage at transformers converter side

V_c Rated voltage at transformers AC grid side

P	Active power (Kw)
P_g	Active power at transformer's converter side
Q	Reactive power (Kvar)
Q_g	Reactive power at transformer's converter side
R_f	Phase reactor resistance
s_g	Complex power
i_f^d	Direct current reference
i_f^q	Quadrature current reference
X_o	Zero-sequence reactance

ABSTRACT

Majority of wind farms are located far away from the load centers thus requiring long distance transmission of electrical power. One of the traditional methods of power transmission is based on alternating current (AC) and is not suitable for bulk power transmission over long distances. In addition, AC systems do not have full controllability of the active and reactive power compared to direct current (DC) systems. Besides, transient faults may cause high transient currents that can damage the power systems equipment. This necessitated the development of DC transmission based on line commutated converter-high voltage direct current (LCC-HVDC) and voltage source converter-high voltage direct current (VSC-HVDC) power transmission systems. Although, LCC-HVDC provides improved power controllability compared to AC systems, VSC-HVDC system is the most efficient and reliable for bulk and long distance transmission of electrical power. It also has the ability to operate in all the four converter quadrants allowing independent control of active and reactive power.

Although VSC-HVDC systems are better than any other available transmission systems, they have challenges under short-circuit faults. The high current generated can cause the rated voltage across the diode to be exceeded thereby damaging the converter valves. In addition, the currently developed and commercialized DC breakers for protection of the VSC-HVDC system have a fault clearing time of 5ms. This is a major deterrent towards providing excellent protection for converters and the transmission network.

This research provides solutions to converters and the transmission systems that often fail under the influence of short-circuit faults. Further, three scenarios were analyzed; conventional generation with and without wind power and that with wind power integrated through a VSC-HVDC system. In each of the three scenarios, a three-phase short-circuit fault was created on the transmission line and the critical clearing time was used to assess the performance of the proposed scheme. A novel fast DC breaker was developed in this work which has double protection against high voltage spikes provided by inclusion of the freewheeling diodes and high pass filters that divert the high frequency harmonics to the ground consequently protecting the converters and the AC network.

Simulation results were done and from which a novel fast DC breaker developed in this research has a fault clearing time of 1ms. This is a great milestone in the development of a fast switching device. The findings of this research are major contributions towards the improvement of the power system transient stability of a VSC-HVDC system with large wind power integration.

CHAPTER ONE

INTRODUCTION

1.1 Background

Globally, the depletion and increase in fossil fuel prices, climate change, environmental pollution, high cost of power, unprecedented growth in energy insecurity, etc., have all contributed to the interest in renewable energy sources. Furthermore, the long term cost of non-renewable generation are projected to increase in subsequent years due to fast economic growth in the emerging nations, increasing electricity demand, depletion of the stocked non-renewable energy resources etc. as a result, it is anticipated that in the next 20 years, a high portion of world electricity generation would come from renewable energy. Renewable energy sources such as solar, wind, geothermal energy have enormous potential in contributing to the world's electricity portfolio and security, as well as mitigating the increasing emissions of greenhouse gases. However, the integration of renewable energy sources such as wind power and solar power into the power grid will bring new operational and technical challenges. For instance, in the case of wind generator, it will be important to know what would be acceptable level of penetration of wind power generation without compromising the power system stability. It is therefore prudent to carryout investigation of the current power system and finds out if wind energy can be used to support the grid and at the same time achieve safe and reliable operation without compromising system stability.

Many incentives have been put in place to attract investors interested in setting up wind power plants (WPPs). However, the intermittent behavior of wind power causes voltage variations that may result to system instability. In addition, WPPs are located far from the load centers thus necessitating reliable and efficient mode of power transmission. Though with these disadvantages, wind power still remains the most competitive source of renewable energy and precautions for WPPs have been put in place to prevent system collapse under short-circuit faults as provided in the grid code (National Grid Electricity Transmission plc [NGET], 2013). As a requirement for connecting wind turbines to the grid, the voltage should reduce to zero for a period of 150ms before disconnection from the grid to allow the system to recover the lost generation from wind power and replace

with the available energy reserves thus preventing the power system from voltage collapse.

One of the earliest and dominant approaches to electrical power transmission is based on alternating current (AC) systems. The reason for its dominance is because most of the heavy power consuming devices were designed for AC power support. Nevertheless, over the years, high voltage alternating current (HVAC) has been challenged. The most common issues is reactive power management that necessitate the use of large power compensation devices like capacitor banks and automatic voltage regulators at the generating stations, along the power transmission lines and at the load points to boost and regulate the voltage. HVAC systems have higher power losses and cannot transmit bulk power efficiently over long distances. Furthermore, HVAC systems lack the capability for full controllability of the active and reactive power and require large space to construct the three-phase power line and the primary substations. These challenges have made High Voltage Direct Current (HVDC) favourable for long distance power transmission (Ackermann, 2005) HVDC system is classified into two technologies based on Line Commutated Converter-High Voltage Direct Current (LCC-HVDC) and Voltage Source Converter-High Voltage Direct Current (VSC-HVDC) (Shewarega & Erlich, 2014).. LCC-HVDC is applied in high power transmission and has low conversion power losses because they utilize thyristors for switching purposes. However, lack of full controllability for active and reactive power and the need for large reactive power compensation devices has made it less attractive (Shewarega & Erlich, 2014). VSC-HVDC system is a relatively innovative system for large power transmission and has gained global interest from researchers and power transmission utilities. It has the ability to independently control active and reactive power, capability for power reversal by simply changing the direction of current flow and can be connected to weak networks. The outputs of VSC-HVDC systems are determined exclusively by rating of the equipment, efficiency of the system and its control system. This gives total flexibility regarding the location of the converters in the AC system since Short-Circuit Ratio (SCR) is no longer a limiting factor (Cole & Belmans, 2011). However, VSC-HVDC systems are not available for high voltage applications and have higher conversion power losses compared to LCC-HVDC system.

DC breakers are the most reliable and efficient for fault discrimination and isolation on the DC network however, the existing DC breakers have a fault clearing time ranging from 5-100ms (Hausler, 1999) which is considered not very effective to protect the modern equipment. This delay damages the VSC-HVDC valves and transmission system under short-circuit faults. It is therefore important to develop DC breakers that have fast fault clearing time and superior fault discriminative features. The increasing interest in energy mix predominantly wind power demands the development of VSC-HVDC power systems with fast HVDC breakers that can withstand challenges emanating from short-circuit faults and other disturbances affecting the power system stability and security.

1.2 Problem statement

The integration of large amount of wind power to a conventional grid has been a challenge predominantly due to the short-circuit faults, failure to adequately invest in the state of art forecasting equipment, weakness of the transmission technology and the unstable power system. Also, the choice of the wind turbine technology contributes largely on the amount of wind power that can be integrated to a grid. The situation is made worse by the erratic wind characteristic that often causes voltage variations and can negatively affect the power system stability. Majority of the wind farms are located far away from the load centers thus necessitating efficient and reliable technology for electrical power transmission. VSC-HVDC systems employing pulse width modulation (PWM) and insulated gate bipolar transistors (IGBT) for fast switching operation are used for long distance transmission of electrical power and several commercial projects are in operation (Railing, et al., 2004). VSC-HVDC power systems have challenges under short-circuits faults. The smaller resistance in DC system causes large current magnitudes during short-circuits faults that damage the converter valves and the power transmission network. Further, the recently available DC breakers for protection of the VSC-HVDC power systems have a fault clearing time of 5ms (Negari, 2015) which are considered long to adequately protect the power system. Also, the incorrect selection of the controller's parameters can lead to poor performance of the power system and affect the system stability.

1.3 Justification

VSC-HVDC system is preferred to LCC-HVDC for long distance bulk power transmission. Most of the VSC valves uses IGBT for fast DC switching operation and continues to attract a lot of interest from researchers (Gomis-Bellmunt, Liang, Ekanayake, King & Jenkins, 2011). VSC-HVDC power transmission system enhances large integration of wind power because it has the ability to independently control active and reactive power, a characteristic deficient in LCC-HVDC power transmission system. It can also easily reverse the direction of power flow whenever required, it requires smaller spacing for the substations and the way leaves trace for the power line is relatively smaller compared to any other mode of power transmission thus making VSC-HVDC the most preferred mode of power transmission over long distances (Gomis-Bellmunt, et. al, 2011).

Short-circuit faults are the common type of faults in power systems and damages the VSC-HVDC converter valves and the transmission network because the available DC breakers have long fault clearing time. The wind turbines are supposed to meet the current grid codes that stipulate fault ride through (FRT) capability of wind power plants down to zero voltage for fault durations up to 150ms (Adapa, 2012) subsequently improving the grid stability. Therefore, despite the challenges facing VSC-HVDC power transmission systems connected with wind power, they still have better controllability of DC voltage, frequency, active and reactive power than LCC-HVDC system or any other transmission system available. A DC breaker with fast response time will provide the much needed intervention against short-circuit faults in VSC-HVDC and transmission systems. The tuning of the VSC controllers are based on the principle adopted for the basic electrical derives that require appropriate controllers tuning for enhanced stability and fast system response time (Liserre , 2001). However, achieving these two conditions is not an easy task and requires a good compromise between the two parameters.

1.4 Objectives

1.4.1 Main objective

The main objective of this thesis was to investigate the best control strategy among the existing ones for a VSC-HVDC power transmission system with high wind power penetrations and develop a novel DC breaker for transient stability improvement.

1.4.2 Specific objectives

1 To model a wind farm and VSC-HVDC power system with a vector current control.

2 To test the performance of the developed model of a VSC-HVDC system with vector current control and carry out time domain simulations with and without wind farm and with VSC-HVDC transmission scheme.

3. To design and analyze a novel model of DC breaker for VSC-HVDC power system transient stability improvement.

1.5 Contributions of the Thesis

From the theoretical analysis and simulation results, the following are the summarized main contributions of this thesis:

a) Previous researchers such as (Machaba, 2008; Preitl & Precup, 1999) concluded that based on SOC, the system is only stable when the symmetrical distance is between $a = 2 \; and \; 4 \; respectively$. However, in this thesis, it has been shown in figure A.1 of the appendix, that wider tuning of the DC voltage controller based on SOC provided a stable system with good response time at symmetrical distance of a=8. Further, wider tuning of the inner current controller by modulus optimum criterion (MOC) delivered an optimal system response and stability at a=8. Though the overshoot for various values of symmetrical distance is almost the same, the time at which it occurred for a=8 is optimal. The result further indicates fast rise and settling time and the system is the most stable compared to other values of symmetrical distances.

The novel fast DC breaker model developed in this research has a fault clearing time of 1ms. The amount of energy absorbed and dissipated under fault affects the time the fault will be cleared in the system. In this research, two topologies of solid state DC breaker are discussed; these are solid state DC breaker with CB paralleling a surge arrestor and a solid state DC breaker with a freewheeling diode (Eriksson, Backman & Halen, 2014),. Based on equations (2.6) and (2.7), it is shown that under the influence of fault in the

system, the energy absorbed by the surge arrestor for equation (2.6) is larger than that for equation (2.7). Therefore, based on this reasoning and the need to develop a fast DC breaker, the topology with DC circuit breaker and freewheeling diode was modeled and included in the VSC-HVDC system in figure 3.16. The DC breaker was inserted between the freewheeling diodes and the RC circuit to bypass any reverse voltage impulse thus ensuring protection of the DC breaker from fault emanating from the rectifier side and the inverter side. A company like asea brown boveri (ABB) has developed fast DC breakers that can overcome the power loss by use of a mechanical breaker with a solid-state valve ((Steurer, Frohlich, Holaus, Kaltenegger, 2003; Holaus, Frohlich, 2002; Schroder, Meyer, De Doncker, 2002; Decesaro & Porter, 2009)

b) The developed novel fast DC circuit breaker in this research has a fault clearing time of 1ms which is faster than the currently available DC breakers response time of 5ms (Negari, 2015; Eriksson, Backman & Halen, 2014),.
c) This thesis established that wind power integration to a conventional power system can be more than 20% as long as the power system is stable and the designed controllers meet certain high performance specifications based on the application desired. Three scenarios were investigated to find out how much wind power can be integrated without affecting the grid stability. The configuration without wind power attained a critical clearing time of 0.123 s while the system with wind power at 22% and 34% had a critical clearing time of 0.129 s and 0.127 s respectively. The configuration with 22% wind power integration had its synchronous generator (G3) removed and replaced with a wind farm model of equivalent rating while the configuration with 34% wind power integration had its synchronous generator (G2) removed and replaced with an equivalent wind farm model. This indicates that power system with wind power integration have improved transient stability compared to system without wind power. Even though the critical clearing time reduced from 0.129 s at 22% wind power penetration to 0.127 s at 34% wind power penetration, the system was stable hence, in this research wind power penetration level of 34% was achieved. In addition, three scenarios were investigated and compared to find the best configurations for large wind power integration. Based on the three configurations, the one with wind power and developed VSC-HVDC system

attained power transient stability at 2.45 s while the other two configurations were unstable at the same time. This shows that wind power and the VSC-HVDC system improves transient system stability. The finding in this research is important particularly at the moment when the global attention and interests are focused towards renewable energy sources that have unique and dynamic characteristics.

1.6 Author's Publications

This thesis is based on the research contained in the following publications:

Journals published:

1. J. Muriuki, C. Muriithi, L. Ngoo and G. Nyakoe, ''Wider range of tuning the proposed VSC-HVDC system for improved controller performance''. **International Journal of Electrical Engineering & Technology (IJEET)** Volume 6, Issue 9, Nov-Dec, 2015, pp.01-06, Article ID: IJEET_06_09_001 available online at http://www.iaeme.com/IJEET/issues.asp JType=IJEET& VType=6&IType=9 ISSN Print: 0976-6545 and ISSN Online: 0976-6553 © IAEME Publication
2. J. Muriuki, C. Muriithi, L. Ngoo and G. Nyakoe, ''Assessment of VSC-HVDC System for Transient Stability Improvement of a Power system with Large Wind Power Injection''***, IOSR Journal of Electrical and Electronics Engineering (IOSR-JEEE) e-ISSN: 2278-1676,p-ISSN: 2320-3331, Volume 11, Issue 6 Ver. III (Nov. – Dec. 2016), PP 63-75 www.iosrjournals.org***
3. J. Muriuki, C. M. Muriithi, L. Ngoo, G. Nyakoe. ''Review of HVDC Circuit Breakers Topologies''. IOSR Journal of Electrical and Electronics Engineering (IOSR-JEEE) e-ISSN: 2278-1676, p-ISSN: 2320-3331, Volume 12, Issue 3 Ver. II (May – June 2017), PP 109-117 www.iosrjournals.org.
4. J. Muriuki, G. Nyakoe, C. Muriithi, L. Ngoo. (2017), "Novel Modeling of a Fast DC Breaker for a VSC-HVDC Transmission System Protection". J Electr Electron Syst 6: 241. Doi: 10.4172/2332-0796.1000241. November 2017. Volume 6, Issue 3.

Conference proceedings:

1 J. Muriuki, C. Muriithi, L. Ngoo and G. Nyakoe, ‘‘Performance Review of the VSC-HVDC Based Controllers’’, ***Proceedings of the 2016 Annual Conference on Sustainable Research and Innovation, 4-6 May 2016.*** **p. 104-113, may 2016. ISSN 2079-6226. Available at:** ***http://sri.jkuat.ac.ke/ojs/index.php/proceedings/article/view/406***

2 J. Muriuki, C. Muriithi, and L. Ngoo, ‘‘Analysis of Wind Power Integration for Power System Transient Stability’’, **Proceedings of the *Sustainable Research and Innovation (SRI)***.Conference 6-8May, 2015. ISSN: 2079-6226.

sri.jkuat.ac.ke/ojs/index.php/proceedings/article/view/313/23

1.7 Thesis layout

This thesis is structured into five chapters. In chapter one, an introduction of the VSC-HVDC system with its various controllers is discussed. An overview of the present global status of renewable energy is highlighted. Also, comparison is made between the DC transmission systems, namely; LCC-HVDC and the VSC-HVDC, and why the latter is the most preferred mode for long distance transmission of electrical power. In addition, this chapter includes the objectives, problem statement and justification that necessitated the carrying out of this thesis. It also contains the thesis main contributions and publications based on the thesis findings and review. In chapter two, a layout of the VSC-HVDC system with its various components is presented. Various HVDC configurations are highlighted in addition to having HVDC system as a means for power system transient stability improvement. Further, an overview of the four available DC breakers is presented indicating the challenges and advantages of each method. In chapter three, the VSC-HVDC system is modeled together with the inner current controllers and the outer controllers. Symmetrical optimum criteria (SOC) and the modulus optimum criteria (MOC) are mathematically derived and used for wider tuning of the DC voltage and the inner current controllers respectively. The VSC-HVDC system interconnected with wind power is also presented for the analysis of transient system stability. Comparison of the four available DC breakers is carried out in addition to the novel fast DC breaker developed in this thesis. Chapter four shows the simulation of the results and discussion while chapter five entails the conclusions and recommendations for future work aimed at improving the current research findings.

CHAPTER TWO

LITERATURE REVIEW

2.1 Wind energy

Wind energy is available in abundance but it is random and sporadic in nature and its integration to the conventional power grid is rather challenging. Though with these shortcomings, wind power has more advantages than disadvantages and therefore has continued to receive more attention from researchers and other stakeholders. Globally, wind energy generation is certainly number two after hydro power generation as a source of renewable energy. The harnessing and integration of wind power into the AC power grid always brings challenges that affect system transient stability and security. The wind characteristics should be critically analyzed and possible shortcomings addressed before a decision to integrate it to a conventional grid is arrived at otherwise, it may be a source of system instability under contingencies. Wind integration studies have advanced from whether it is possible to add wind generation to focusing on how it will be done, at what time and at what cost (Decesaro & Porter, 2009). This means that wind penetration to the grid is a reality and the critical thing is how it will be integrated to the grid including the power control measures, technical expertise and the cost associated. Research has also shown that, wind energy generation is relatively cheaper and freely available in most parts of the world compared to other sources of renewable energy generation and hence the reason for its popularity. It is noted that, wind power generation can provide the power deficit, reduce the cost of power per unit consumed and maintain the desired energy reserve. This will also stabilize the power system especially during the peak loads. However, concerns have been raised as to how much wind power should be integrated to the grid while maintaining the power system transient stability and security. Many countries especially the developing ones have received and continue to receive many proposals to set up wind farms to generate power and sell it to the monopolistic power utilities. However, most of the developing countries have weak network that goes off so often under the slightest system fault. It is therefore important that before any large scale generation of wind power is allowed, adequate

stability analysis of the existing network is carried out otherwise very low wind power integration levels can be realized. Many wind power plants do not deliver the amount of wind power initially scheduled due to many factors not put into consideration during the design and stability analysis of the existing power system. The most critical factors being the existing system stability, point of connection to the power grid, transmission technology and its controls and types of the wind turbines technology.

Further, it is important to study new aspects that the integration of wind power brings to the conventional system, including the aspects of the transient stability and the maximum amount of wind power that can be utilized to a given system (Chen &. Liu, 2010). Previous studies indicate that greater wind penetration is possible with better system control, good government policies and enhanced network. In addition, the extent to which the wind power can be integrated into the power system without affecting the overall stable operation depends on the technology available to mitigate the possible negative impacts such as loss of generation, voltage flicker, and voltage and power variations due to variation in speed of the wind design (Mutha & Arthi, 2012).

The importance of renewable energy sources amid rising environmental concerns has led to the rapid development of wind turbine generator (WTG) technology and large wind power plants (WPP). Due to the technological development in semiconductor devices, the sizes of turbines have continued to increase in sizes for economic reasons. Globally, the focus has shifted to the huge potential of off-shore wind energy though the onshore wind energy continues to be harnessed due to its easier and flexible transmission system. The harvesting of off-shore wind power has also been proved to be less prone to disturbance basically because there are no obstructions to wind flow and its transmission is based on underground system that is more reliable than overhead system. A total of 1471MW off-shore wind power generation, all in European seas, have been installed by the end of 2008, with 357MW of off-shore WPP installed in the year 2008 (EWEA, 2009). As per the reference scenario of EWEA, by 2030, the off shore WPP is expected to contribute 120 GW out of 300GW of installed wind power generation (EWEA, 2011).

Currently, developing countries have a huge energy capacity deficit whereby at peak loads, most large power consumers are in operation, there is insufficient power generation necessary to meet the users demand and any significant power reserves for

emergencies. For instance, in Kenya, we largely depend on power import from Uganda during the dry season because over 50% of the power generation is hydro related. However, the trend of power generation in Kenya has now shifted towards renewable generation especially wind, solar and geothermal power. Currently, the installed power capacity in Kenya is 2300MW against a maximum demand of around 1800MW. Due to diversifications of energy sources, the installed capacity in Kenya is likely to go up thus necessitating the government to aggressively connect as many customers as possible in addition to encouraging investors to put up more industries so that the power supply can match the demand otherwise, excess generation without demand can led to higher cost of power.

Due to persistent drought, globally, many countries are shifting away from overdependence on hydro-power sources and are thus diversifying search for alternative sources of green energy generation such as wind, geothermal and solar energy. Research has shown that for electricity generation from wind, then, the wind speed must be more than 5 or 6 m/s to facilitate the running of the wind turbines. Figure 2.1 shows different generation of renewable energy per unit cost.

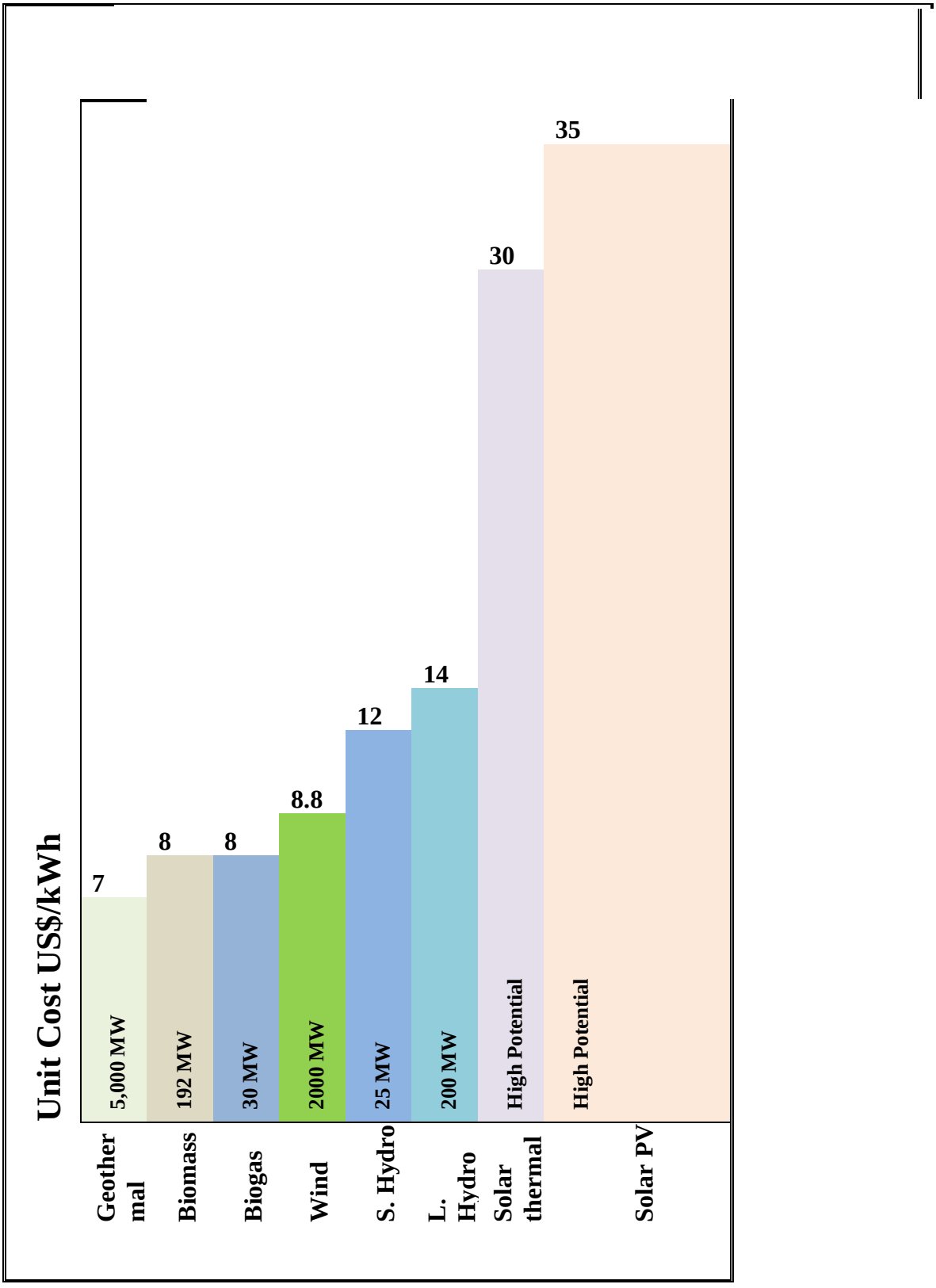

Figure 2.1: Comparison of generation cost for various renewable energy sources

Wind speed and wind power are governed by a third order relationship as given by equation (2.1).

$$P_{wt} = \frac{\rho}{2} C_p(\lambda, \theta) A_r V^3 \quad (2.1)$$

The actual relationship between wind speed and wind power turbine output of a wind turbine is defined by the wind turbine power curve, defining the amount of power generated by the wind turbine P_{wt} at wind speed (Van Kuik, G.A.M., 2007). Where ρ is the density of air in (Kg/m^3); C_p is the power coefficient of the wind turbine; λ is the tip speed ratio between the turbine blade tip speed $v_t\,(m/s)$ and the upstream rotor wind speed (Vm/s); θ is the blade pitch angle in degrees, A_r is the swept area of the turbine rotor blades (m^2).

Normally, the wind turbines control their $\lambda, \theta \; and \; C_p$ in order to maintain the rated electric power generation at higher wind speeds and prevent mechanical overloading of the turbines moving components and structure. The maximum power coefficient of the ideal wind turbine rotor is 16/27. This is known as the lanchester-betz-joukowsky limit (Van Kuik, G.A.M., 2007). Given that it is only feasible to maximize the C_p for a limited range of wind speeds, the design and control of C_p and the wind turbine are such that the conversion efficiency is highest at the wind speed range where the most energy can be captured.

There are four generator type concepts that have been developed to date. These are, (1) the wind turbine with fixed speed wind turbine with induction generator (type A), (2) variable speed with variable rotor resistance (type B), (3) variable speed with doubly-fed induction generator (type C), (4) direct drive turbine with permanent magnet generator (type D)(Polinder, VanderPilj, DeVilder &. Tavner, 2006; Eriksson ,2001). Currently, type C is widely used compared to other type of wind turbine generator due to its advantages of having unlimited variable speed. It involves a multi-stage gearbox connected to a doubly-fed induction generator and a power electronic converter connected to the turbine's rotor winding, with a rating equal to of the rated power of the generator. Therefore, the generator output is governed by the pitch angle of the wind turbines blades.

2.2 Effects of wind energy integration on power transient stability

Ordinarily, wind power improves system transient stability only to a certain integration levels. As more and more wind power is integrated to a power grid, the transient stability reduces consequently leading to partial or full system blackout. Besides, wind power plays a crucial role in system stability because it has better management for reactive and active power. Wind farms have the potential to absorb and supply reactive power from time to time based on demand. Researchers such as Eping, Stenzel, Pöller and Müller, (2007) focused on transient stability issues and analysed the impact of various aspects like location of wind farms, connection points and distributed generation. The points of linking wind farms to a conventional grid have various implications on the stability of the power system thus necessitating the analysis of the existing network and its ability to accommodate wind power.

The generator technology has a considerable impact on power system transient stability. For instance, Doubly-Fed Induction Generators (DFIGs) technology improves transient stability margins, when being equipped with low voltage ride-through capability, reactive current boosting and ideally with fast voltage control (Eping, et al., 2007). In terms of connection point, the integration of wind farms into sub-transmission and

distribution systems have negative impact on the transient stability, because the reactive contribution is highly limited due to reactive losses in sub-transmission and distribution systems. However, the above challenges can be overcome by ensuring that there are minimal losses on the sub-transmission and distribution systems through the installation of automatic voltage regulators and capacitive elements at the identified weak locations along the transmission power line. Conventional generation with wind farms based on Squirrel Cage Induction Generators (SCIG) have low wind power absorption capacity in addition to reduced transient stability. Therefore, careful selection of the wind turbines technology is an important factor for large wind power integration.

The effects of wind farms of different sizes on the Egyptian power system are investigated in (El-Sayed, & Moussa, 2008). The wind farms for the Egyptian system were aggregated into equivalent wind generator models for ease of analysis. The aggregation of the wind farms is done with the intention of reducing the simulation time while retaining the original parameter characteristics. This is important for validation purposes and for comparing the actual behaviour of the wind farms against the aggregated equivalent wind turbine models without losing its original performance. Power system dynamics simulation software is used to study the impact of increasing wind turbine penetration on system performance. The study for the Egyptian power system was also carried out considering different contingencies such as transmission line outages, loss of generation units and finally a combination loss of generation and transmission lines. The result indicate that the Egyptian system with a total installed capacity of 20400MW has only 900MW of wind power penetration an indication that the Egyptian system can accommodate only 4.4% of wind power. This is a very low absorption level compared to other developed countries that have greater wind penetration levels.

Jauch, Sørensen, Norheim and Rasmussen (2007) looked at the effect of wind power on the transient fault behaviour of the Nordic power system. The Nordic power system is the interconnected power system for countries such as Norway, Sweden, Finland and

Denmark. Here, the wind turbines installed in Eastern Denmark were used to investigate the impact of wind power integration on the Nordic power system. The models developed were simulated and yielded information such as how the faults impact on the wind turbines and how the response of the wind turbines influences the post fault behaviour of the Nordic power system. This information is important in determining how much wind power can be integrated to a conventional power grid and still maintain system stability under the influence of the uncertainty such as short-circuit faults. It is therefore important to analyse the power system behaviour with wind power integration before and after the fault. This will give candid information based on the power system stability.

2.3 Technological advancement of HV transmission

With the recent developments in semiconductors and control equipment, the HVAC and LCC-HVDC systems are gradually being replaced by the relatively newer transmission system based on VSC-HVDC. This system has numerous advantages and is currently widely applied for transmission of power over long distances at high DC voltages. Most of the wind farms are located far away at the coast and underground power cables are laid on the sea for long distance transmission of the wind power generated. Some of the advantages of using this technology are short-circuit current reduction under system faults, less land utilization for power line construction, independent control of active and reactive power. This makes the VSC-HVDC transmission system as the most suitable mode of power transmission over long distances. With such feasible characteristics, it is no doubt that the future long distance transmission and distribution system will be based on this superior technology. Further, VSC-HVDC technology makes good use of the more advanced semiconductor technology based on insulated gate bipolar transistor (IGBT) with fast switching speeds as an alternative for thyristors which have slow switching speed and low power losses. The converters utilize voltage source converters and operate at high switching frequencies (1-2 kHz) using the sinusoidal PWM

technique. This technology is commercially available as HVDC Light (Eriksson, 2001). IET and HVDC Plus (power link universal system) (Schettler, Huang & Christl, 2000).

2.3.1 High voltage DC transmission

The first electric power commercially generated by Thomas Elva Edison was based on DC technology. However, the impossibility of transmitting DC power over longer distances at lower voltages contributed to high power losses and the need shifted towards AC transmission systems as discussed in (Bajracharaya, 2008)The appearance and availability of transformers and the increased importance of single phase and three-phase induction motors in industries were other factors that made AC transmissions dominant. Also, the technical personnel had advanced knowledge in AC transmission compared to the relatively newer HVDC system that was still in the early stages of development. In addition, many electrical and electronic devices used in offices, schools, industries, hazardous installations and at home relied fully on AC system thus making AC transmission system the only monopoly semiconductor technology of choice.

Though AC transmission was popular during the early days, HVDC systems have over time evolved to be a technology of choice and are fast overtaking AC transmission systems. This is due to recent developments of the semiconductor technology that enables large power transmission over long distance with enhanced independent control of active and reactive powers. The land constraint has made HVDC system of transmission to be globally accepted because its wayleaves trace requirements for power line construction is minimal in comparison to AC mode of power transmission. HVDC transmission is the most preferred mode of power transmission over long distance and finds many applications such as in Power transmission via underground cables, bulk-power transmission over long-distance, unsynchronized AC-system connection and power system stability improvement. Further, HVDC system finds application in urban centers where there is high load concentration thus reducing the incidences of faults associated

with overhead system of transmission in addition to improved aesthetic. HVDC systems are more reliable and efficient for large power transmission over long distances.

2.3.2 Types of HVDC transmission technologies

There are currently two technologies of HVDC power transmission: the LCC-HVDC and VSC-HVDC transmission (Paulinder, 2003). The line commutated converter based HVDC is also known as classical HVDC. It is currently a widely used DC transmission system. It uses thyristor based converters and its turning off need the current flowing through them to be zero while the switching frequency is maintained at 50Hz or 60 Hz. This results in production of low order harmonics thus necessitating larger filters for filtering out the generated harmonics and prevents high frequency components from entering the AC system and the transformers through a diversion to the ground. These harmonics are source of poor power quality and should be eliminated by use of high pass filters. The issue of harmonics is challenging and affects the power stability and efficiency of the electrical power transmission.

LCC-HVDC consumes reactive power due to the lagging current generated by the delayed firing of the converter switches. This reactive power demand is a disadvantage to the surrounding AC network. The reactive power supply is achieved by installing shunt capacitors or Static Var Compensators (SVC) near the load points. Though AC system has been dominant transmission system for electrical power, classical HVDC systems has overtaken it and below are advantages associated with classical HVDC system (Arrillaga, 1998)

i. No limits for electrical power transmission distance for both overhead lines and submarine/underground cables.
ii. Fast and accurate control of power flow which improves the power system stability.

iii. Direction of power flow can be changed quickly by simply changing the current direction.

iv. An HVDC link does not increase the short-circuit power at the point of connection. This implies that it will not be necessary to change other equipment in the existing network from the viewpoint of short-circuit power.

v. HVDC can carry more power for a given size of conductor as compared to the AC system, which implies that when transmitting the same amount of active power, the need for right-of-ways (RoWs) is less for an HVDC than for an AC connection.

vi. Power can be transmitted between two AC systems operating at different nominal frequencies or at the same frequency without being synchronized.

Classical HVDC finds many applications as shown below (Woodford, 1998).

i. Used in point to point electrical power interconnections between asynchronous AC power networks.

ii. Delivery of electrical power from large energy sources over long distance.

iii. Import of power into congested load areas, where it is not possible to build new generations to meet the load demand. Underground DC cable transmission is usually used in such application.

iv. Increasing the capacity of existing AC transmission by DC transmission, which eliminates the need of new transmission right of way (RoW).

v. Power flow control. In AC networks the desired power flow control can be difficult to accomplish. Power marketers and system operators may require the power flow control capability provided by HVDC transmission.

The relatively newer VSC-HVDC system is the transmission technology based on voltage source converters and PWM. This system has improved operational characteristics compared to LCC-HVDC system thus enjoying many advantages and applications as will be seen later in this thesis. VSC-HVDC transmission uses the converters installed with antiparallel diodes working on a high frequency PWM

switching. As a result of high frequency harmonics generated by the very fast PWM switching, the filter sizes used are smaller as compared to LCC-HVDC system. In this respect, VSC-HVDC is a better choice to LCC-HVDC. Moreover, unlike classical HVDC, VSC-HVDC system does not need reactive power Provision for its operation since it has the ability to generate its own reactive power without additional reactive power elements. VSC-HVDC system has the ability to independently control its active and reactive power with ease as compared to LCC-HVDC system. This avoids additional costs for reactive power supply equipment, thus making this technology cost effective and more reliable. Additionally, the quality of power transmitted and received at the end terminal is of high quality and reliable. Further benefits of VSC-HVDC transmission systems are given in (Wu & Blaabjerg, 2013).

Since the first invention of VSC-HVDC in 1997 (Asplund, Eriksson & Svensson, 1997), major developments in the field of DC power transmission technology has been made. One of the major contributions by VSC-HVDC system is the ability to transmit large amount of wind power over long distance based on DC technology. Wind power is viable and competitive source of renewable energy. In 2008, total installed capacity of wind power plant (WPP) was 120.8 GW in the world and out of this nearly 66 GW has been installed in Europe, mostly onshore WPP's (GWEC, 2008). However, the high cost of land has made onshore sites for WPP unfavorable thus necessitating the development of the offshore wind farms. By 2030, Europe expects to have installed 180GW of onshore wind energy and 120GW from offshore WPP giving a total wind power installed capacity at 300GW (Chaudhary, Teodorescu & Rodriguez, 2008). VSC-HVDC system is currently the most efficient and reliable mode for transmission of large amount of electrical power over long distances with improved controllability of active and reactive power.

Researches based on control schemes for the VSC-HVDC system have been analyzed in (Lindberg, 1995; Noroozian, Edris, Kidd, & Keri, 2003; Svensson , 1998; Lamont & Jovcic, 2006). Enhanced design of the controllers is an important task that empowers

VSC-HVDC system to control the active and reactive power independently, control the DC voltage, current and its frequency. VSC-HVDC system utilizes vector current control method for d-q current components because it is faster in control of DC voltage, active and reactive power than the direct power control method and thus adopted in this research. The inner current control loop is designed for a digital control implementation and for a dead-beat control of the converter current when the converter is connected to a very strong AC network (Lindberg. 1995). A deadbeat controller is normally a digital controller that places all the closed loop poles in the origin subsequently enabling the system to reach the set point faster. However, deadbeat controllers are uncommon control schemes and have some limitations because the overshoot generated is very high and the cost of generating the control signal to counter it is expensive. It can only be used in extreme circumstances of war to generate weapons systems.

A grid-connected VSC using a discrete vector current controller is investigated in (Svensson, 1998). The outer controllers generate the reference d-q components of currents. The current values are later fed into the faster inner current controller which gives d-q component voltage values that are injected into PWM generator and into the system. In (Wasserrab & Balzer, 2011), all the outer controllers are implemented by a PI controller where the difference between the reference values and the actual value is fed into the controller as the d-q reference currents. Incorrect controller tuning harmonics and poor quality power delivery. Further analytical model of the power control terminal of a VSC-HVDC system is analyzed in (Durrant, Werner & Abbott, 2003; Zhang, Xu & Cai, 2001; Ottosson & Rudberg, 2008). From the analysis, short-circuit faults are the most common faults on transmission and distribution lines. In (Hafner, Hyttinen & Paajarvi, 2002) analysis of the effects of short-circuits currents in VSC-HVDC system is investigated with the objective of safeguarding its enhanced protection.

Faults on VSC-HVDC system have in many occasions damaged converters and the transmission system. To allow greater integration of wind power to AC grid, attention should be focused on the development of fast HVDC circuit breakers. The currently existing DC breakers are not fast enough to provide adequate protection for VSC-HVDC

systems. This exposes converters and transmission system to serious risks under short-circuits faults. It is particularly disastrous for DC faults that rely on AC breakers for isolation of the faulty section of the network. Despite the fact that HVDC breakers have their internal protection mechanism, it has been proven that it is not sufficient to interrupt the fault as quickly as possible, thus necessitating the design of a novel fast DC breaker. Additionally, the growth of multi-terminal HVDC systems and development of wind power that has intermittent characteristics justify better protection management of the VSC-HVDC system (Wasserrab & Balzer ,1011).

VSC-HVDC systems are highly vulnerable to DC short-circuit faults. The ability of the AC breakers to interrupt faults on the DC side is limited by the slow response of the breaker. In many instances, a fault on the DC side is not timely cleared by the AC breakers, consequently, leading to isolation of the whole network. This repeated operation reduces the useful life span of the AC breakers in addition to loss of revenue. One major advantage of AC breakers is that they have the ability to easily interrupt fault during the zero current crossing point, a sequence that is repeated twice every cycle though, the speed of fault interruption is slow. Fault interruption using DC breaker is challenging because it has no zero current crossing point, has small inductance on DC side of the system and the rate of rise of DC fault current is considerably high necessitating a very fast interruption technology not currently available in the market (Koldby &. Hyttinen ,2009)

Short-circuit faults in VSC-HVDC systems causes system transient instability, subsequently, decreasing the amount of wind power that can be integrated into a power grid. Due to slow reponse time by the currently availbale DC breakers, it is difficulty to adequately protect the conveter valves and the transmission network. Thus, this reseacrh provides development of a novel fast DC breaker and control a VSC-HVDC system with large integration of wind power for system transient stability improvement. DC circuit breakers for high voltage applications are not commercially and widely available today

(Franck, 2011), consequently, emphasizing on the need to develop fast DC breakers for protection of the VSC-HVDC system and transmission network.

2.3.3 Types of HVDC transmission configurations

There are numerous HVDC transmission schemes in power network. The selection of each of the scheme at planning stage depends on the operational requirements, flexibility of demand, reliability issue and cost (Paulinder, 2003). It also depends on the technical expertise desired to run the transmission system and sensitivity of the load. Therefore, correct selection of the HVDC transmission system is an important stage in ensuring that the configuration chosen meets the desired objective with the highest degree of efficiency and reliability. Below are the most common HVDC configurations:

i. Monopolar: In this configuration, two converters are connected by a single line pole and either a positive or negative DC voltage is used for power transmission. Figure 2.2 shows one insulated conductor with the return path for current being the ground (Arrillaga, 1998). Normally, most of the HVDC installations start as a monopolar transmission and latter develop to more reliable schemes such as bipolar, multi-terminal or homopolar. This scheme is effective for long distance DC transmission and is the cheapest among the available transmission configurations. The disadvantage with monopolar scheme is that under the influence of fault or during planned maintenance, the whole system has to be switched off and isolated leading to total outage. This causes loss of revenue to both the power utility and the electricity consumers. Due to inability to supply power during both planned and unplanned outages, the scheme is most suitable in low load density areas. Another major challenge with this configuration is that it cannot be used for sensitive loads such as hospitals and large industrial plants.

Figure 2.2: Monopolar HVDC Transmission system.

ii. Bipolar: The power transmission is carried out using two conductors of opposite polarity. It is a combination of two Monopolar systems thus improving the reliability of the system. This is a commonly used configuration for HVDC transmission system because it provides two sources of power supply and if one goes off the other pole provide the supply as a Monopolar system (Arrillaga, 1998). Therefore, there cannot be total power outage since consumers can be fed from the other pole. Also, during the planned maintenance, one of the poles is sufficient to supply power to consumers. Based on the above advantages, the configuration finds application such as for sensitive and large industrial loads. It is also noted that, this configuration has no return earth current because both poles operate at the same current level. Figure 2.3 shows the bipolar transmission scheme.

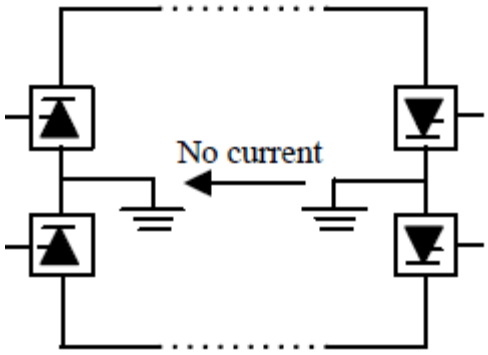

Figure 2.3: Bipolar HVDC transmission system.

iii. Back-to-back: This is a zero distance transmission and it is a common configuration for connecting two adjacent AC synchronous systems. The two converters are connected to each other without any need for a DC line. It is also applied when two transmission systems are of the same or different frequency and different control principles are interconnected. It is cheap to set up a back-to-back transmission system and it is mostly used as an interconnector between two or different countries that sell excess power to each other. Figure 2.4 shows a back-to-back HVDC transmission system. Such a system configuration can be found in Japan and South America (Graham, Menzies & Biledt ,2000).

Figure 2.4: Back-to-back HVDC transmission system.

Iv. Homopolar HVDC system: Two or more conductors have the negative polarity and can be operated with ground or a metallic return. When these two poles are operated in parallel, the homopolar configuration reduces the insulation cost though it has one disadvantage of large earth return current because the two poles operate at different current levels. Large earth return current can damage the equipment and cause death to human beings and animals when it passes through any part of the body or the equipment. It is therefore important that the return earth current is kept within levels not likely to damage the electrical and electronic equipment. Figure 2.5 shows the homopolar HVDC transmission system (Sano & Takasaki, 2012).

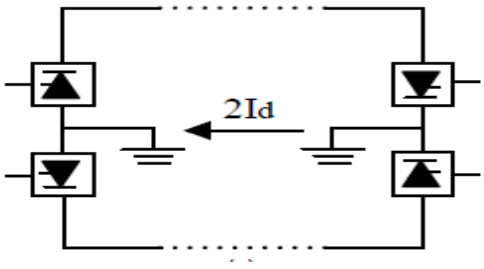

Figure 2.5: Homopolar HVDC transmission system.

V. Multi-terminal HVDC system: Three or more HVDC converter stations are geographically separated and interconnected through the overhead transmission lines or

the underground cables in either mainland or the sea. This system finds many applications such as in large power transmission and for critical loads like hospitals etc. The system is either parallel where the converters are connected to the same voltage or series multi-terminal system where one or more converters are in series in one or both poles (Damsky, Imam& Premerlani, 1979, April).

The parallel multi-terminal connection is shown in figure 2.6 while that for the series multi-terminal connection is shown in figure 2.7 respectively.

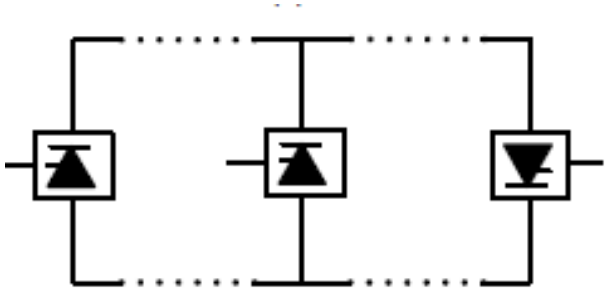

Figure 2.6: Parallel multi-terminal HVDC transmission system.

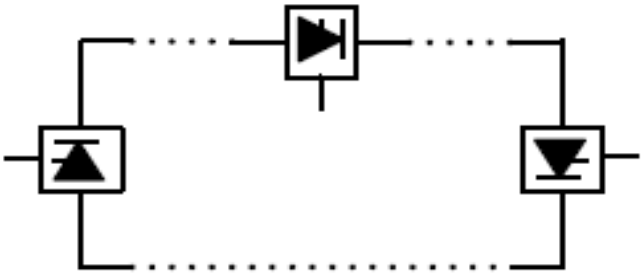

Figure 2.7: Series multi-terminal HVDC transmission system.

2.4 Power System Stability Improvement Strategies

Power system stability is the ability of the power system to remain in a state of equilibrium under normal operating conditions and to regain an acceptable state of equilibrium after being subjected to any form of a disturbance (Kundur, Balu & Lauby 1994; Kundur, et al. 2004). The power system stability depends on the initial operating

condition; system stability, distance of fault from the generation point and the nature of the disturbance among many other factors. Normally, under steady-state operating conditions, the mechanical torque input and electromechanical torque output from the generators are balanced however, under the influence of disturbance, the system stability is affected. To correct the situation, the synchronizing and damping torque must be positive for power system stability to be sustained consequently leading to the steady-state condition where the mechanical torque input and electromechanical torque output are balanced (Kudur, et al., 1994; Kundur, et al., 2004)

The Power system stability is majorly grouped into three groups namely; voltage stability, rotor angle stability and frequency stability Kudur, et al., 1994; Kundur, et al., 2004; Pavella, Ernst & Ruiz-Vega, 2012).Figure 2.8 shows the classification of power system stability.

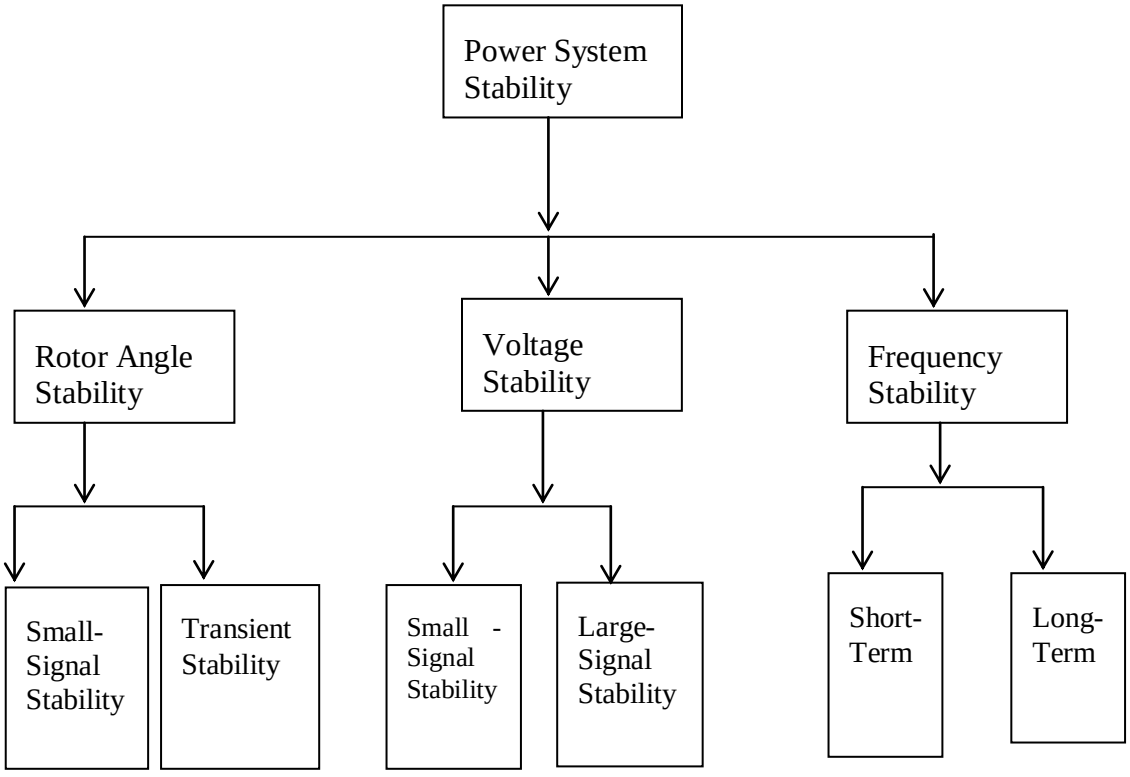

Figure 2.8: Classification of power system stability.

Globally, power system stability is an issue of concern to many power utilities and numerous strategies have been proposed by various researchers. The two most common strategies used are based on transmission level solutions and at the generation level solutions. The former is achieved through the use of flexible alternating transmission systems (FACTS) and high voltage direct current (HVDC) transmission control and the latter is achieved through the use of Power System Stabilizers (PSS), automatic voltage regulators (AVR) and governor controls (Hausler, 1999). Figure 2.9 shows the various strategies for power system stability improvement. This research emphasized on aspect of power system stability improvement at transmission level based on improved VSC-HVDC system.

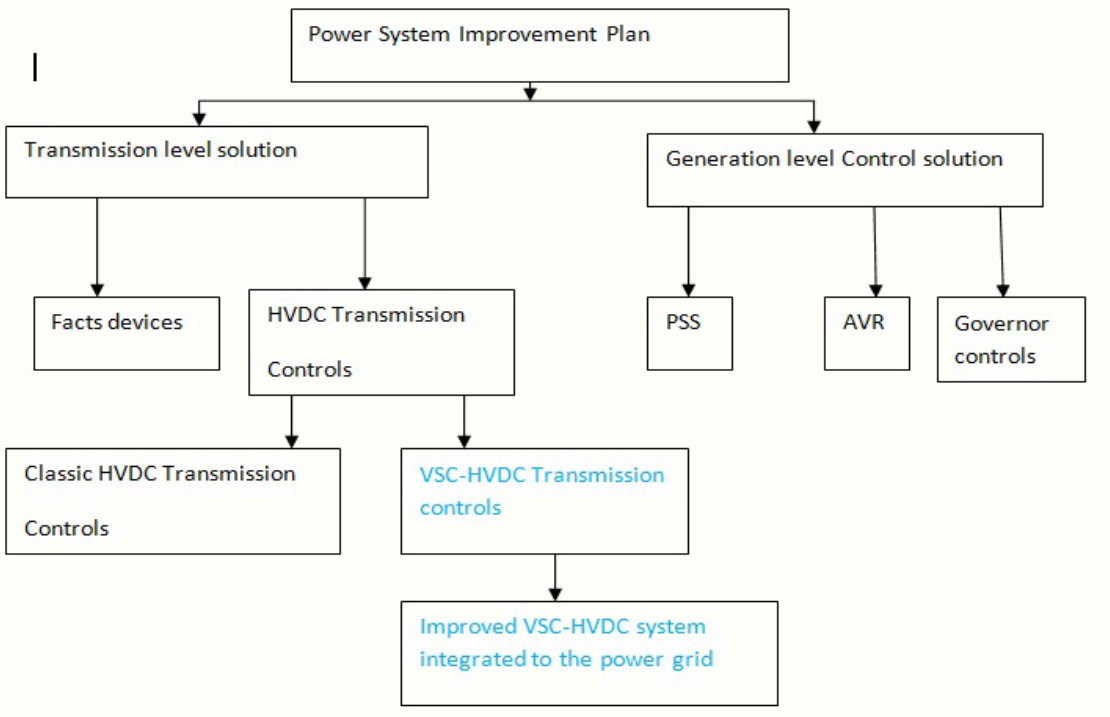

Figure 2.9: Power system Transient stability improvement strategies.

Many power utilities use PSSs and AVRs as excitation controllers at generation and transmission levels to enhance power system stability. However, due to limited capacity

and large system voltage variations introduced during disturbances upon utilizing them, they have become insufficient to create system wide influence (Abido, 2009) though they are still in use in old generation systems, they have proved incapable of controlling the voltage efficiently and reliably and are being replaced by fast and efficient control solutions. Such solutions are based on FACTS devices and HVDC controls at the transmission level. Globally the demand for power exceeds the supply thereby, stressing the existing generation, transmission and distribution systems. The conventional generation is insufficient to meet the power demand and maintain energy reserve. This has led to expensive energy diesel fired thermal power generation causing the cost of power to be expensive and production cost to be costly. For companies to break even, the cost of power is factored in the production of goods and services and passed to the consumers subsequently, affecting negatively the purchasing power of both the lower end consumers and the middle class. As such, independent power producers (IPP) and power utilities are diversifying into other methods of energy generation such as wind power. Though most wind farms are located far away from the load centers, the cost of power per unit consumed is relatively cheaper than other energy sources. This has motivated both power utilities and IPP to invest in large-scale wind power generation. A contractual agreement between the IPP and power utility is entered into and wind power is integrated to the national power grid at an agreed rate per unit.

FACTS is defined by the Institute of Electrical and Electronic Engineering (IEEE) as a power Electronic based system and other static equipment that provide control of one or more AC transmission system parameters to enhance controllability and increase power transfer capability (Bahrman, & Johnson, 2007). There are two groups of FACTS devices. The first group employs conventional thyristor-switched capacitors and reactors, and quadrature tap changing transformers. This includes the static var compensator (SVC), the thyristor-controlled series capacitor (TCSC), and the thyristor-controlled phase shifter (TCPS). The second group utilizes gate turn-off (GTO) thyristor-switched converters as voltage source converters (VSCs). This group contains static synchronous

compensator (STATCOM), the static synchronous series compensator (SSSC), the unified power flow controller (UPFC), and the interline power flow controller (IPFC) (Povh, 1998). FACTS devices have been mainly used for solving various power system steady-state control problems such as voltage regulation, power flow control, and transfer capability enhancement (Hingorani, 1991). As a supplementary function, damping the inter-area modes and enhancing power system stability using FACTS controllers have been extensively studied and investigated in (Molinas, Naess, Gullvik & Undeland, 2006). These regulatory tasks are accomplished through appropriate reactive power compensation, or by series capacitive compensation of line inductances, or by phase angle shifting.

Therefore, with the currently energy mix being injected into the conventional grid, power transmission improvement strategies based on PSS, AVR, HVAC, HVDC, and FACTS devices have not provided the best alternative solution for transient stability improvement. However, due to the technological development in semiconductor technology, a long distance transmission based on VSC-HVDC system with excellent control of active and reactive power is being adopted.

2.5 Importance of power system transient stability

When a power system is subjected to a physical disturbance in the initial operating condition and it is able to return to its initial operating condition or regaining equilibrium after dynamic motions of system variables, the ability of this system can be referred to as the power system stability based on the definition in (Al-Ismail & Abido, 2011, November). From this definition, power system stability is classified into three most important factors namely, rotor angle stability, frequency stability and voltage stability. Further, rotor angle stability is classified as small disturbance angle stability and large disturbance angle stability (Transient stability). In many instances, the breaker protecting the feeder trips on transient fault, however, on resetting the relay and closing the breaker it just holds without necessarily eliminating the fault permanently. This

sequence is repeated three times, then the fault sustain and the breaker cannot hold any more. These prompt the system controller and operation and maintenance engineer to sectionalize and physically locate and clear the fault. After fault clearance, it is now possible to reset the relay and close the breaker. Sometimes, the transient fault may be as a result of winds blowing and forcing tree branches to come into contact with conductors and returning to normal status when the wind goes. This can be a tricky situation because when the wind is calm, the breaker holds but when the weather is windy and rainy the breaker trips due to short-circuiting of the conductors. This is a confirmation that transient faults can be a nuisance until the actual fault is identified and resolved permanently.

Globally, the largest transmission system is based on alternating current (AC) due to its perceived advantages over the direct current (DC). In AC technology, two factors are critical in ensuring system stability. These are the system frequency and the voltage. During the normal operation of a power system, the Mechanical (Tm) and Electromagnetic Torques (Te) acting on each generator should be balanced and all the synchronous generators rotate at the same electrical speed in synchronization with the system frequency (so-called synchronism). Therefore, at any given time, during the generation and transmission of the electric energy, it is crucial to maintain the two torques at equilibrium otherwise the system will run out of synchronism. If the power system under large disturbances such as the short-circuit faults within the transmission lines is able to maintain the synchronism of generators then, this ability is referred to as the transient stability as defined in (NGET , 2013). Lack of transient stability results from inequality of the mechanical and electromagnetic torques thus causing blackout or total outage.

2.6 DC transmission systems based on LCC-HVDC and VSC-HVDC

The control system design and operation of HVDC based on line commutated converter (LCC) for power system stability improvement is discussed in detail in (Paulinder, 2003).

However, HVDC based on LCC has limitations particularly for long distance transmission and their inability to speedily and independently control active and reactive power. Thus, their applications have dwindled with the advent of the VSC-HVDC system. It is efficient in transmission of huge amount of electrical power for long distances with negligible losses thus finding application in power system transient stability. As discussed in (Bahrman & Johnson, 2007) the VSC-HVDC system often fails under severe short-circuit fault where the wear out failure of the VSCs that employs IGBTs and freewheeling diodes under field operation could be mitigated by scheduled maintenances based on lifetime prediction and condition monitoring. Preventive maintenance of the VSC does not in itself guarantee life time operation, nevertheless based on its life cycle, one is able to predict with some degree of certainty the time that the equipment is likely to fail and plan accordingly. However, serious faults such as short-circuit faults may be abrupt and unpredictable leading to catastrophic failure of the VSC-HVDC system. The advantages of VSC-HVDC systems are detailed in (Bahrman & Johnson, 2007;Al-Ismail & Abido, 2011)

VSC-HVDC system can carry more power for a given size of conductor as compared to the AC system. This implies that when transmitting the same amount of active power, the need for right-of-ways (RoWs) is less for a VSC-HVDC system than for an AC transmission. In VSC-HVDC transmission system reactive power is controlled at each terminal independent of one another. This reactive power control can be used for dynamic voltage regulation to support the interconnected AC systems under the influence of contingencies. This also helps to increase the overall system power transfer levels and improve system dynamic performance (Erickson, 2001). VSC-HVDC systems can be an attractive option to efficiently and timely relieve network constraints, thus reducing the need for building new expensive HVAC lines. Further, both HVDC and VSC-HVDC system provides the ability to transmit electrical power via underground cable system since it is safer and efficient than overhead system. Unless the cable insulation is damaged, the undergrounding system is maintenance free for its entire useful life time.

VSC-HVDC also provides mitigation of power quality disturbances through independent control of active and reactive power. The reactive power capabilities of the VSC-HVDC can be used to control the AC network voltage and thereby contribute to an enhanced power quality. Furthermore, quick response due to increased switching frequency, offers new levels of performance regarding power quality control such as flickers and harmonics. Power quality problems are issues of priority for owners of industrial plants, grid operators and for the public (Bollen, 2000).. For instance, low voltage may cause the machines to fail to start thus forcing the industrial consumers to use other alternatives sources of power supply such as the expensive diesel generators. This is a loss to both the utility power company and the consumers. To the contrally, high quality power increases transmission efficiency subsequently increasing revenue for the power utility and the consumers.

2.7 Layout of a typical VSC-HVDC system connected to a wind farm

Figure 2.10 shows the typical layout of a VSC-HVDC system for grid integration of onshore wind farms. The VSC on the rectifier side and inverter side consists of self-commutated IGBT to enable AC/DC power conversion. The DC capacitors on both sides are meant to maintain the balance between A/C and D/C power as the DC voltage sources while the AC transformers and series reactors are connected to the AC bus on both side of the VSC-HVDC system. The high frequency filters (HFFs) are needed to eliminate the high frequency components of AC harmonics generated by module cells (Bahrman & Johnson, 2007).

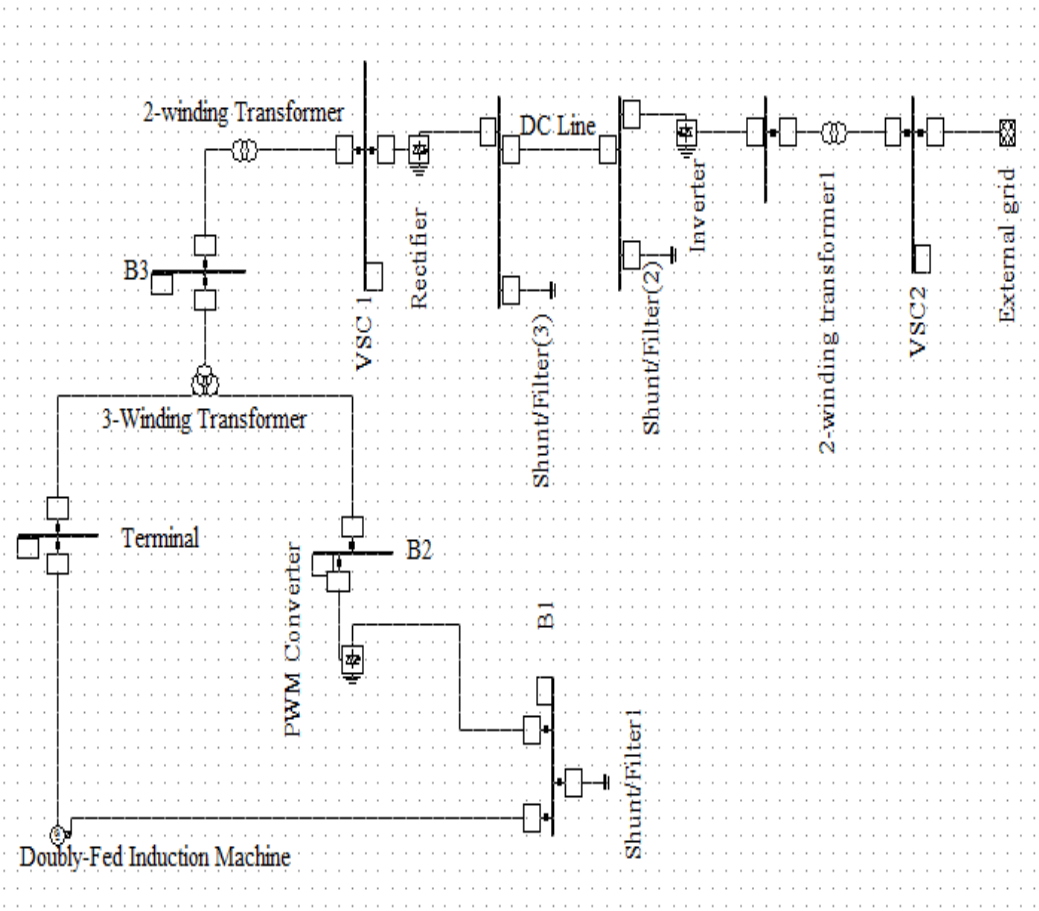

Figure 2.10: Layout of VSC-HVDC system connected to a wind farm.

It is important to have a reliable and efficient transmission system for control of active and reactive power. Such a system is based on VSC-HVDC and basically involves the control and the transfer of the scheduled power. Moreover, the VSC controls are often used to provide ancillary services, such as to improve the dynamics of AC grids.

There are different control strategies found in literatures based on the control of VSC-HVDC system. One such method for control of VSC-HVDC is known as direct power control (DPC) method; it is based on the instantaneous active and reactive power control loops (Shire, 2009) In this method, there is no internal current control loops and there is no PWM modulator block, because the converter switching states are selected by a

switching table based on the instantaneous errors between the commanded and the estimated values of active and reactive power (Shire, 2009) It uses the estimated virtual flux vector in its control loop. DPC operate by balancing the converter voltage magnitude with that of the system voltage and when the former is greater than the latter, the reactive power is injected in the AC system; if it is smaller, reactive power is absorbed by the converter respectively. DPC has disadvantages such as variable switching frequency and necessity of fast conversion and computation and therefore its use is uncommon. Other fast control method for VSC-HVDC has recently been adopted such as vector control that utilizes the modeling of the three-phase systems by use of d-q transformations. The method uses sinusoidal PWM converters because of its accuracy and reliability. The control method is best suited for independent control of active and reactive power for AC applications. One of the major advantages of vector control is that vectors of AC currents and voltage occurs as constant vectors in steady state and hence static errors in the control system are easily avoided by use of PI controllers. On the other hand, the vector control strategy has excellent dynamic performance and inherent protection against over-currents (Shire, 2009). Due to these unique characteristics, the vector current control scheme is globally utilized. In vector current control strategy, the input currents to the rectifier and the output currents from the inverter are measured and compared with the reference current values and the error signal is fed to the controllers to produce switching signals to the converters. In this thesis, the control system for VSC-HVDC transmission system is developed based on vector control strategy.

VSC-HVDC system is the most convenient and reliable mode of power transmission compared to LCC-HVDC and the HVAC system due to its inherent ability to independently control the active and reactive power through vector current control method. It also has better control of the DC voltage through regulation of the active and reactive power.

Doubly fed induction generator (DFIG) based wind turbines are utilized due to their inherent ability to control voltage and reactive power. Further, DFIG operate over wide

range of speeds with excellent control of active and reactive power. However, most of the onshore and offshore wind farms are located far away from the load centers thus making the traditional power transmission method uneconomical and not feasible. In (Preitl & Precup, 1999). wind power has emerged as one of the most dominant renewable sources of energy with immense growth potential across the globe. Actually, the global wind energy capacity has increased rapidly and is the fastest growing renewable energy sources globally. The wind energy is largely harnessed from the offshore wind farms where wind is strong, large available sea areas, has high wind speed, and is less turbulent. Further, in the offshore, there is little human activity taking place and thus the noise produced by the wind turbines have no impact on human beings and unlike the onshore wind farms that produce some noise impacting negatively on the community living nearby. Wind power transmission cannot go unchallenged especially where underground cables in the sea get damaged, the cost and process of repair is expensive and time consuming compared to overhead transmission for the case of onshore wind farms. These losses are aggravated if the total cost of lost revenue by the power utility company and the power consumers are factored in. It is therefore important that the underground cables are carefully safeguarded against damage from both internal and external sources. As previously mentioned in this thesis, transmission of wind energy using conventional system is cost effective for distances less than 100km (Rezek, et al., 2001, June).). However, for distance exceeding 100km, the conventional system (HVAC) may start experiencing challenges such as those stated in (Xu & Fan, 2012, September). These challenges can be overcome by use of VSC-HVDC system as shown in figure 2.10.

2.8 Components of the VSC-HVDC controller

As shown in figure 2.11, a VSC-HVDC system consists of various components such as transformers, phase reactor, AC filter, DC capacitors, converters and the DC transmission line. These components are important in a VSC scheme based on the role each contributes towards realizing an independent control of active and reactive power

between the power grids and the converters. Generally, not all the elements required for both steady-state and dynamic analyses are shown in figure 2.11. Some of these elements are obviously known to be part of the semiconductor devices such as air conditioning system. Figure 2.11 shows the components of a VSC-HVDC scheme (Cigre, 2004).)

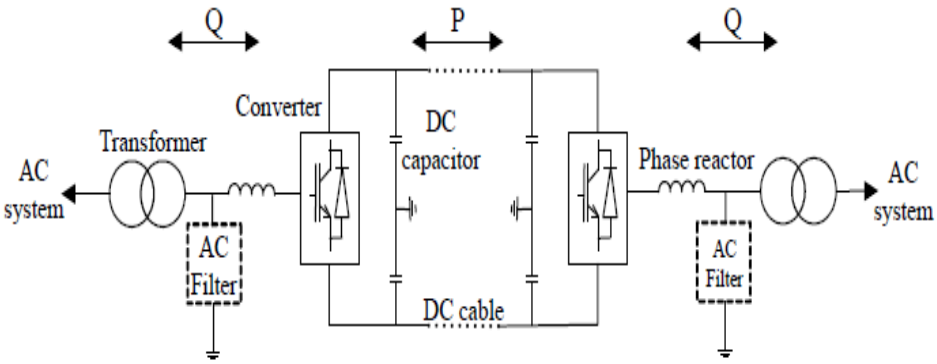

Figure 2.11: VSC-HVDC control system.

2.8.1 Transformers

Three-phase transformers are used in VSC-HVDC system and their primary function is to step up or to step down the voltages. It is an important element because it converts voltages to levels suitable for converters and other semiconductor devices. Though transformers are critical elements in VSC-HVDC system, they have higher power losses as a result of harmonic content of the current and are subjected to high vibration levels caused by saturation of the core due to small DC current components (Cigre, 2004).). It is therefore important that three-phase transformers are specifically designed and appropriately selected for VSC-HVDC system and by so doing and by the virtue of the AC filter installed between the converter and the three-phase transformer, the harmonic contents are easily eliminated thereby safeguarding the converter and the AC system. Also, voltages from the three-phase transformers can be either high or low an indication of something is not right and since there are no moving parts in transformers, very little

intervention is necessary. However, in such scenarios, the tap charger can be tapped up or down to either increase or lower the reactive power thus correcting the voltage to the desired levels.

2.8.2 Converter

A converter is a very important element in a VSC-HVDC system. Converters are used as rectifiers and inverters where the AC voltage is converted to DC and vice versa. The purpose of converting voltage to DC is to enable high efficient transmission of power with minimal losses. This type of configuration is mostly used for sensitive loads because of its enhanced reliability.

2.8.3 AC Filter

VSC-HVDC system employs insulated gate bipolar transistor (IGBT) due to their high switching speed necessary to protect the converter. The high switching speed generates harmonics that are detrimental to the converters thus the need for the high pass filter (HPF). The HPF also mitigates against high frequency components from entering the transformer and because of the high switching speed of the IGBT, the VSC-HVDC requires smaller filter or no filter at all is needed to compensate any reactive power as compared to the slow switching insulated gate bipolar thyristors that require large filtering elements.

2.8.4 Phase reactor

The phase reactors are used on the AC side basically to control the active and reactive power flow through control of the current. Phase reactor normally has large reactance and small resistance aimed at controlling both the real and reactive power. It also functions as an AC filter to prevent high frequency harmonics contents generated by high switching speed of the IGBT from entering both the converter and the AC side.

2.8.5 DC capacitors

DC capacitors are the storage element for the VSC-HVDC system. The VSC-HVDC system voltage is controlled by charging or discharging of the capacitor based on the needs of the converter at that time. When a capacitor discharges, the voltage reduces to zero and if there is no element to charge the DC capacitor, the system can collapse thus negatively affecting the operation of the VSC-HVDC system.

2.9 Types of DC circuit breakers.

DC breakers utilizing IGBTs have fast switching speed compared to other DC breakers incorporating thyristors. Currently, there are four types of DC breakers available (Kostoulas, Sitokonstantinou, Idris, Sterling & Sayed, 2015) namely:

i. The electromechanical resonance DC breaker,
ii. The solid-state breaker,
iii. The hybrid DC breaker,
iv. The new design of solid-state breakers.

The electromechanical breakers are basically an extension of the AC breakers and are huge, weighty and slow in operation. Further, all the DC breakers do not have the naturally occurring current zero crossing point necessitating the use of resonant circuit during fault. This inability to provide the zero current point makes it difficult for the DC breaker to interrupt fault.

2.9.1 Electromechanical resonance DC circuit breaker

The electromechanical resonance CB is classified into passive and active resonance. The former is an old technology and was initially developed for CSC-HVDC systems (Cigre, 2004).). Figure 2.12 shows a simplified diagram of an electromechanical HVDC passive resonance circuit breaker.

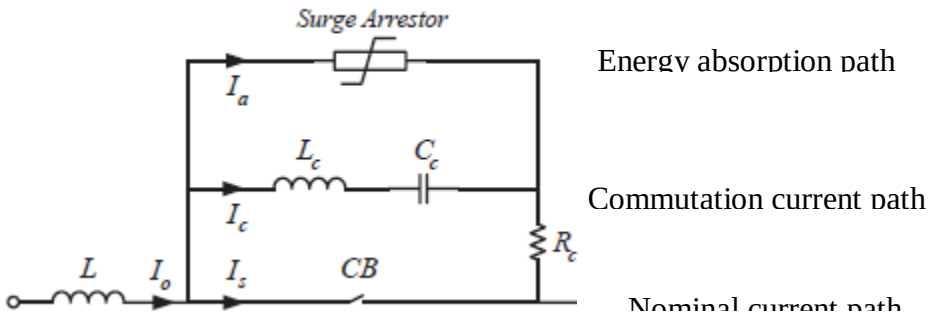

Figure 2.12: Electromechanical HVDC passive resonance CB.

The nominal current path is usually where the DC current(I_s) passes through and the switch (CB) is the circuit breaker that is closed during the normal operation while the commutation path consists of a series resonant circuit with an inductor and a capacitor. This kind of arrangement creates the inverse current condition that forces the current to cross zero point in an ideal condition for current interruption while the energy absorption path consists of a surge arrestor (Kostoulas et al., 2015). The energy generated during fault is quickly absorbed and dissipated as heat thus enabling the resumption of the normal CB operation. This ability to speedily dissipate the energy is based on the amount of energy absorbed and the rating of the element dissipating the energy as heat into the atmosphere. When an interruption is required, current oscillation can occur between the nominal and the commutation path at the natural frequency $(1/LC)$ (Kostoulas et al., 2015). If the amplitude of the oscillating current is larger than that of the input current then, zero current crossing occurs through the trip relay sending a signal to the CB to interrupt the current in the nominal path. This follows the flow of Current (Io) and charging the capacitor to its rated capacity. If the capacitor voltage exceeds a given value, which is chosen to be the voltage capability of the DC breaker, the energy absorption path (surge arrestor) will act resulting to current decrease thereby providing an ideal zero point for current interruption. Electromechanical HVDC circuit

breakers have been in use for many years and are available up to 500 kV, 5 kA with a fault-clearing time of the order of 60-100ms (Kostoulas et al., 2015).

For the purpose of understanding the interruption process it is necessary to analyze the current equation during the process. The differential equation during fault interruption can be written as shown below:

$$L_c \frac{d^2 i_s}{dt^2} + \left(R_C + \frac{\partial_{u_{arc}}}{\partial_{i_s}}\right)\frac{d_{i_s}}{dt} + \frac{1}{C_s} i_s = \frac{I_o}{C_c} \tag{2.2}$$

$$i_s = I_O\left(1 + e^{\frac{1}{2L}\left(R_C + \frac{\partial_{u_{arc}}}{d_{i_s}}\right)t} \mathrm{Sin}\omega_c t\right) \tag{2.3}$$

Where $\omega_c = \sqrt{\left(\frac{1}{L_C C_c}\right)}$. If $R_C + \frac{\partial_{u_{arc}}}{d_{i_s}} < 0;$ then, i_s will oscillate with increasing amplitude. The first zero crossing of current will be enough for the breaker to interrupt the fault being the ideal fault break off point for the DC breaker.

The other classification of electromechanical DC breaker is based on active resonance CB also known as two stage interruption method (Mokhberdoran, Carvalho, Leite & Silva , 2012). The only notable difference with active resonance CB is that the resistor is used as an energy absorption mechanism as opposed to the surge arrestor in passive resonance CB. Surge arrestors are not as rugged as resistors when subjected to frequent short-circuit faults thus, are not long lasting and reliable. They are costly as compared to resistors and their rate of energy absorption under short-circuit fault is slow thus resulting into slow dissipation of the energy absorbed. This slowness in energy absorption also slows down the rate of fault current clearance and can damage the converters and the transmission network.

2.9.2 Solid State circuit breakers

The SSCB have ultra-switching speed and are the best for fault interruption in DC circuit. Research on the development of SSCB has been ongoing and some new ideas are noted in ((Kostoulas et al., 2015; Sano & Takasaki, 2012). There are two topologies of SSCB discussed in the literature, namely, CB paralleling a surge arrestor and CB with a freewheeling diode (Mokhberdoran et al., 2012). Figure 2.13 shows a CB paralleling a surge arrestor.

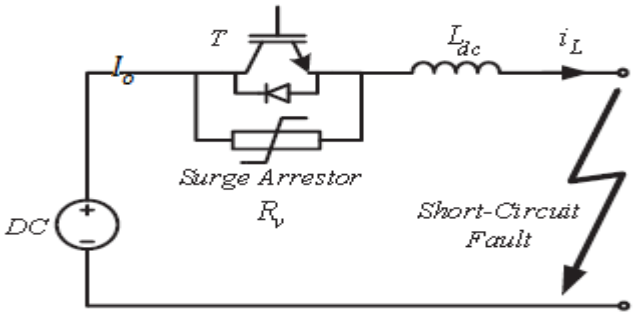

Figure 2.13: CB paralleling a surge arrestor (Mokhberdoran et al., 2012)..

SSCBs employing a parallel surge arrestor utilize an IGBT for quick switching operation during fault. In addition, under normal operation, current flows from the DC source to the load through the IGBT. However, when a fault is detected, the IGBT switches off preventing any current flow through it. Under this condition, the load-current commutates to the surge arrestor. Also, the surge voltage across the IGBT is limited to clamping voltage of the surge arrestor, which is assumed as $V_{dc} + V_{mag}$. It is also assumed that the impedance of the fault point is small. When IGBT turns off at time $t = 0$;

V_{margin} is applied voltage while I_o is the peak current of L_{dc}, so the inductor current can be calculated as follows:

$$i_L = I_O - \frac{V_{mag}}{L_{dc}} t \quad (2.4)$$

Where I_O is the amplitude of the fault current at $t = 0$. The time to turn off the fault current T_{open} is derived as follows:

$$T_{open} = \frac{L_{dc}}{V_{mag}} I_o \quad (2.5)$$

Therefore, the total energy the DC breaker can dissipate to the surge arrestor can be given by:

$$W_R = \left(\frac{V_{dc}}{V_{margin}} + 1\right)\frac{1}{2} L_{dc} I^2 o \quad (2.6)$$

$V_{margin\ (V_{mag})}$ is usually much smaller than V_{dc} in high power applications in order to suppress the voltage across the IGBT and to reduce its conduction loss. In such a case, the term in the parenthesis of Equation (2.6) becomes large, and W_R is much greater than the stored energy in L_{dc} at t= 0. The energy dissipated is given by $\frac{1}{2} L_{dc} I_o^2$ and the more the energy in IGBT is suppressed, the more capacity the surge arrestor needs to accommodate and dissipate (Preitl & Precup, 1999).).

The other SSCB topology employs CB with freewheeling diode ((Mokhberdoran et al., 2012). The purpose of the diode is to bypass any reverse voltage impulse during the abnormal condition thereby protecting the IGBT against voltage spikes mostly known to damage the IGBT valves. This kind of arrangement where the CB employs a freewheeling diode reduces the energy absorbed in the SSCB without suppressing the surge voltage across the IGBT as shown in Equation (2.7). This is a confirmation that CB employing freewheeling diode is able to quickly dissipate the little energy absorbed

and swiftly dissipate it as heat thus providing the much needed fast DC breaker operation.

$$W_R = \frac{1}{2} L_{dc} I_o^2 \tag{2.7}$$

A circuit configuration of the solid-state DC circuit breakers using a freewheeling diode is shown in Figure 2.14 (Mokhberdoran et al., 2012).

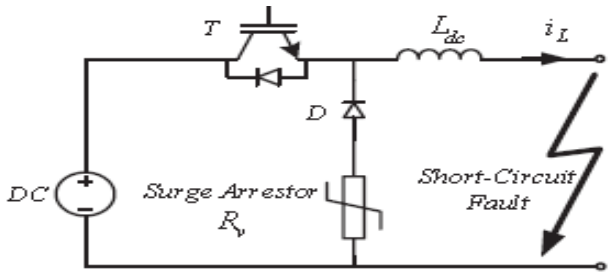

Figure 2.14: Solid-state DC breaker with freewheeling diode.

2.9.3 Hybrid DC breakers.

As the name suggests, hybrid DC breakers employ both mechanical switches and solid state devices for switching operation. The technology has two major advantages, notably low losses because of the mechanical switches utilized and the ultra-switching speed due to the application of solid state devices. This reduces the fault impact on the converter known to be mostly affected by the short-circuit faults. However, one major disadvantage with hybrid DC breakers is the utilization of many solid state devices thus making it relatively expensive compared to other DC breakers. The application of hybrid DC breakers continues to attract a lot of attention from stakeholders and researchers such as recently witnessed in (Shukla &. Demetriades, 2015). Further, ABB and ALSTOM have developed Hybrid HVDC CB prototypes with some considerable improvements based on recent research [Shukla &. Demetriades 2015; Adapa, 2012) Figure 2.15 below shows a circuit diagram of a hybrid DC breaker courtesy of ABB (Callavik, . Blomberg,. Häfner &. Jacobson, 2012).

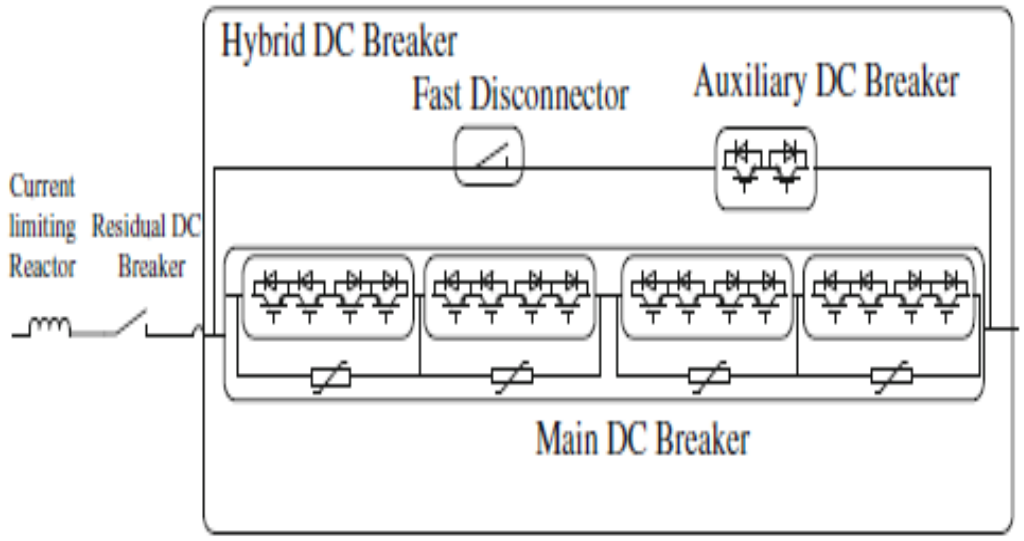

Figure 2.15: ABB Hybrid DC breaker.

Under normal operation, the current will only flow through the ultra-fast disconnector (UFD) and the load commutation switch while the current in the main breaker remains zero (Tang, 2010). Once the DC fault is detected by the relays, the interruption command is sent to the CB. The UFD switch opens and the load commutator switch (auxiliary DC breaker) switches off and commutates the current into the main breaker. The opening of the UFD creates a physical isolation, protecting the LCS from the voltage drop when the main breaker interrupts the current (Adapa, 2012).

2.9.4 The new solid-state DC breaker

The new solid-state DC circuit breaker was first developed by (Negari, 2015). Several topologies have been developed based on the solid-state devices or a combination of solid state devices and mechanical switches [63-(Callavik, Blomberg,. Häfner &. Jacobson, 2012). The reaction time upon detection of a fault depends on the type of the DC breakers selected, the absorption and the heat dissipation elements. The speedy operation of the DC breakers is critical in isolation of the faulty network thus allowing only the healthy network to continue with the operation. The converter would be able to

continue with its normal operation as soon as the fault is cleared (Eriksson, Backman & Halen, 2014),. Notably, the main challenge with new solid-state DC Circuit Breaker is the absorption of the energy generated during the fault. The response time should be reduced to protect the converter and the transmission network from imminent failure under severe short-circuit faults.

Normally DC breakers have challenges in fault interruption because they do not have the naturally occurring current zero point like it happens with the AC breakers. Many of these breakers have been known to rely on resonant circuit to create zero current crossing point and also use the surge arrestors to absorb the energy generated at the time of fault ((Kostoulas et al., 2015); Mokhberdoran, Carvalho, Leite & Silva, 2014) and (Wang & Beddard, 2014) . The new DC breaker utilizes the mutual inductance instead of surge arrestors to absorb the energy and dissipate it to the resistive element as heat. The use of mutual inductance eliminates the need for surge arrestors because any abnormal condition (sudden impulse) in either current or voltage can be suppressed by the high pass filter. Under normal operation, the current flowing through R_2 is insignificant and the resistor will only operates under short-circuit fault.

Also, a diode is included in the circuit to bypass any reverse voltage impulse thus protecting the IGBT from voltage spikes. This new solid-state DC breaker developed in 2015 shown in figure 2.16, has the ability to clear the fault in 5ms (Negari, 2015)

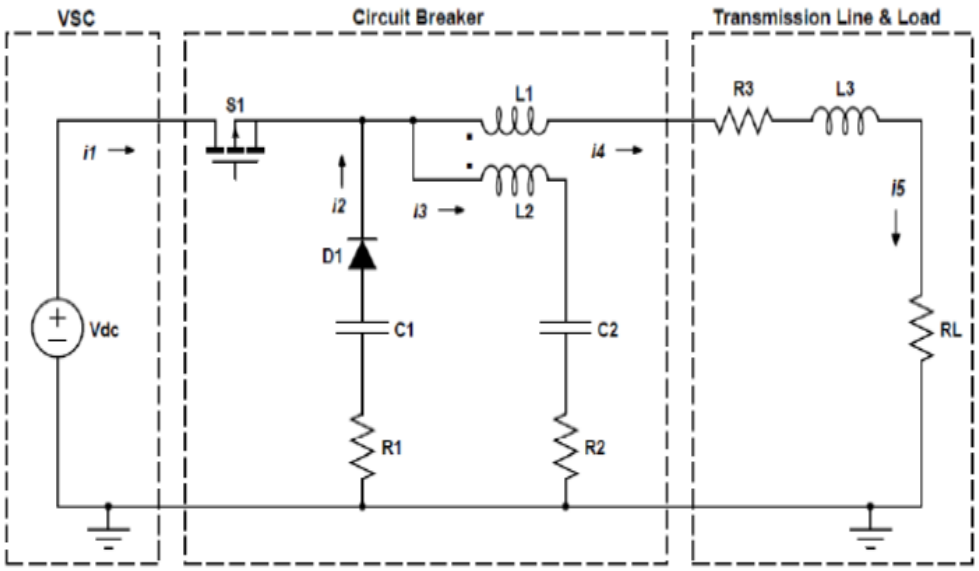

Figure 2.16: The new solid state DC circuit breaker.

2.9.5 Comparison of the DC breakers technologies

The characteristics of the four types of DC breakers are summarized into five categories, namely(Magnusson, Saers, Liljestrand, & Engdahl, 2014)

i. Current interruption time
ii. Power losses
iii. Voltage rating
iv. Current rating.
v. Cost

Table 2.1shows the relationships of the four types of the DC breaker (Magnusson et al., 2014).

Table 2.1: Comparison of DC breakers characteristics.

DC breaker type	Interruption time	% of the VSC station power losses.	Voltage rating	Current rating	**Cost (USD)**
Electromechanical	60ms	0.001%	550kv	5KA	**4,450**
Solid state	40ms	30%	800kv	5KA	**300**
Hybrid	2-30ms	0.1%	320kv	9KA	**54,544**
New solid state	5ms	30%	800kv	5KA	**60,000**

From table 2.1, it is apparent that among the currently available DC breakers, the new solid-state DC breaker has many advantages compared to other types of DC breakers in terms of the speed of interruption, the high voltage transmission and-currentrating. The high voltage across the inductor allows overvoltage which is a good ingredient for fast demagnetization process thus limiting the peak current to considerably low levels. These characteristics further limit the damage that can be exposed to converters valves under short-circuit faults. Despite the DC breaker having many advantages, it has shortcomings such as the highest VSC station power losses and is vulnerable to reverse voltage spikes generated at the time of current disruption that take place during the zero-current crossing point. The novel fast DC breaker overcomes the above challenges by providing double protection for the IGBT thus inhibiting the voltage spikes and the high

current magnitude generated during the fault. This causes huge power loss during the on-state conduction process because the resistance of the new solid state DC breakers is negligibly small. Though the cost of the new solid state DC breakers seems prohibitive, in contrally, it is not because the rapid switching operation of the IGBT provides excellent protection against the internal converter faults and the short-circuit faults thus reducing the down time.

2.10 Challenges in HVDC circuit breaker design.

As earlier mentioned, the current zero crossing for DC current has to be artificially created to forcefully interrupt the current at the occurrence of the fault. This is the most ideal point for current interruption. Such a DC breaker design is shown by (Sano & Takasaki, 2012)in figure 2.17.

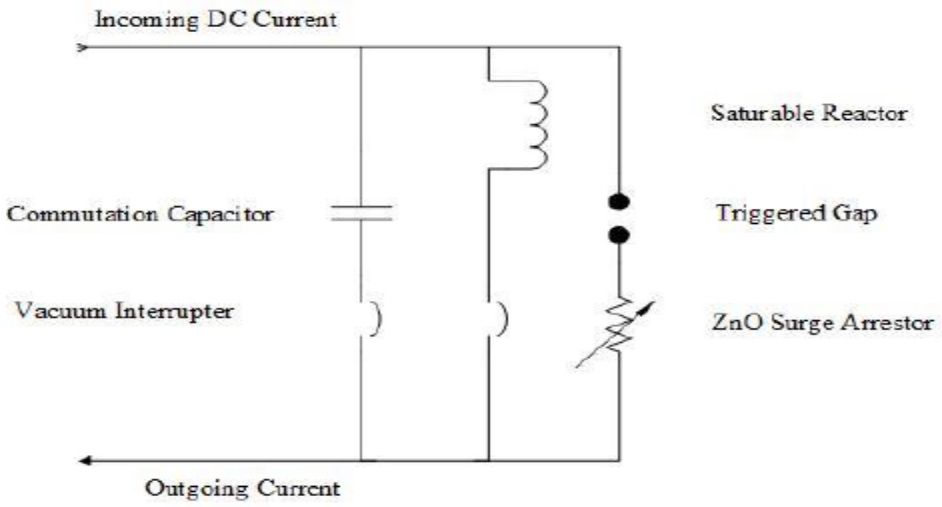

Figure 2.17: DC circuit breaker with resonant feature.

Under fault condition, the DC breaker receives a signal from a relay notifying it that there is a fault. This results into opening of the DC breaker and discharging the stored energy into the inductor through the triggered gap. Normally, to create the zero crossing condition in DC systems, the DC breaker must provide counter voltage greater than the

system voltage. One of the solutions recommended is to provide counter voltage in DC breakers by use of metal oxide varistors (MOV) (Kostoulas et al., 2015). One notable disadvantage with MOV is that it is slow in forcing the current to cross to zero point and other fast method such as the one using solid state breakers with freewheeling diode are adopted. The energy absorbed by the inductor is dissipated to the surge arrestor and converted into heat. The surge arrestor is the absorbing agent for energy stored on the line while the resonant circuit creates the much needed-current zero crossing point. The inductive reactance assists in maintaining the rate of current change $\frac{di}{dt}$ at a controlled level and the high pass filter circuit regulates the recovery voltage (Damsky, Imam & Premerlani, 1979; Davidson,. Whitehouse, Barker, Dupraz &. Grieshaber, 2015). In the event of short-circuit fault, HVDC breakers have short interruption time thus resulting to high $\frac{di}{dt}$ that is detrimental to the converters and the valves. The surge arrestor has shortcomings such as the energy stored in it deteriorates its life span while the solid state valves are sensitive to reverse voltage spikes caused by switching transients. The above challenges can be overcome by designing a fast DC breaker that incorporates passive components as opposed to Zinc oxide arrestors which has low life span and is not affected if it absorbs more energy. The currently available DC breaker has a fault clearing time of 5ms (Damsky, et al. 1979). There is need to develop a fast acting DC breaker to enhance protection of the VSC-HVDC converters and transmission system. In this thesis, the novel design of a fast DC breaker is an improvement of CB discussed in section 2.9.4. The novel DC breaker is shown in figure 3.6 where additional commutation circuit and freewheeling diode is included on both sides of the IGBT. This arrangement reduces the amount of energy absorbed during short-circuit fault and quickly dissipate the energy. The fast absorption and dissipation of the energy emitted during faults allows the developed DC breaker to quickly clear the fault on the system in less than 5ms.

A quick and effective DC breaker is necessary to enable protection of the VSC-HVDC system especially against the DC circuit's faults that can cause the collapse of the whole network when protected by AC breakers. DC breakers have the potential to isolate the faulty section of the DC circuits and quickly restore normal operation.

The total clearing time of a DC circuit breaker (DC-CB) is the time from fault initiation to complete interruption of current flow. This total operating time is divided into two sections: the detection time period and the interruption time period. The detection time period is by default shorter to commensurate with the levels of overcurrent. The higher the current, the faster the detection time for the fault while the interruption time period is the "action" period in which the device forcibly opens the path of overcurrent flow reducing it to zero. Therefore, the total interruption period is the same as the arc quenching period from the start of interruption to the time when the current reduces to zero. Figure 2.18 illustrates the total clearing time of a protection device.

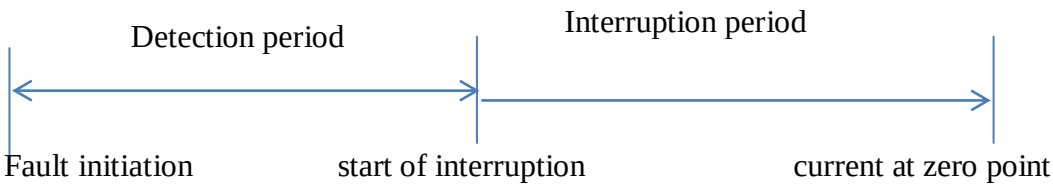

Figure 2.18: Time periods in the clearing cycle of a DC breaker.

2.11 Summary

In this chapter, VSC-HVDC system and types of HVDC topologies with their merits and demerits have been presented. Power system stability improvement strategies are discussed with special focus to transmission level solutions based on FACTS and HVDC system. The importance of wind farm connected to VSC-HVDC system is also discussed. Four types of DC breakers were discussed in detail and reasons why they are not able to adequately provide protection to VSC valves and transmission system against short-circuit faults are given. Further, shortcomings of the existing four types of DC breakers are discussed.

CHAPTER THREE

RESEARCH METHODOLOGY

3.1 Introduction

In this chapter, wind farm with VSC-HVDC power transmission system are modeled and transient stability improvement analyzed using time domain simulations. Further, three configurations are compared to find out the level of wind power integration and transient stability improvement of the power system under short-circuit fault, these are: (i) Conventional generation alone (ii) Conventional generation with the modeled wind farm (iii) Conventional generation with wind farm connected via VSC-HVDC system. In each of the configuration, a short-circuit fault is initiated along the transmission line and time domain simulation for various parameters are graphically presented on the same scale to find out the critical clearing time. Tuning of the controllers based on Symmetrical Optimum Criteria and Modulus Optimum Criteria is carried out to test the performance of the developed controller performance. Finally, a novel DC breaker is developed in this research with a fault clearing time of 1ms. The design involves double protection for the IGBT. It has the RC circuit and the diode to bypass any reverse voltage impulse during the abnormal condition thereby protecting the IGBT against voltage spikes mostly known to damage the IGBT valves. This kind of topology where the CB employ freewheeling diode, quickly dissipate the little energy absorbed because of its small energy storage capacity and swiftly dissipate it as heat providing the fastest fault response time without compromising the system transient stability.

3.2 Modeling of VSC-HVDC system control with wind power injection

3.2.1 VSC-HVDC mathematical modeling

The vector control strategy for VSC-HVDC starts from the mathematical modeling of VSC-HVDC system in rotating dq-reference frame. The voltage source converter can be represented as shown in (Schettler, et al.. 2000). by a controlled voltage source for the AC side in figure 3.1 (a) and a current source for the DC side in figure 3.1 (b).

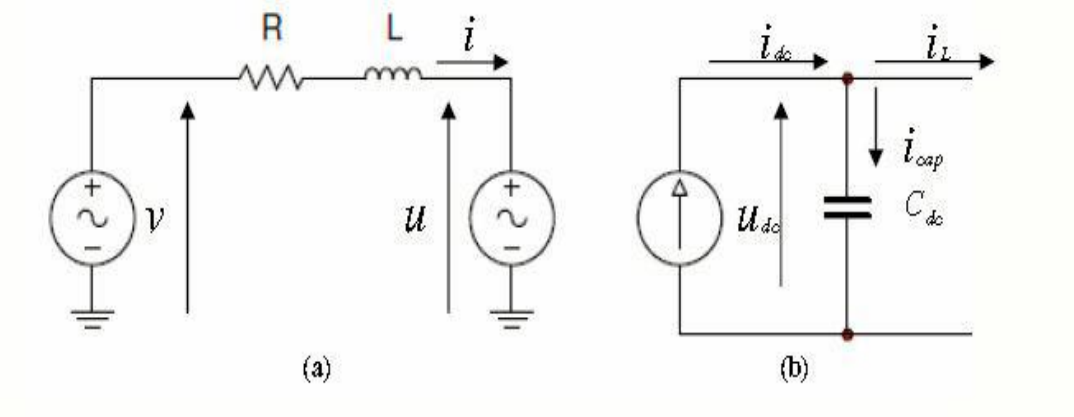

Figure 3.1: Two equivalent circuits of VSC-HVDC station.

Therefore, we can represent the converter and grid interaction by the two equivalent circuits in figure 3.1. Applying Kirchhoff's voltage law across the reactor and the resistor, the following equation holds true.

$$L\frac{di_{abc}}{dt} = \overrightarrow{v_{abc}} - \overrightarrow{u_{abc}} - \overrightarrow{R_{i_{abc}}} \tag{3.1}$$

Where v_{abc} is the grid AC voltage in abc reference frame; u_{abc} is the converter AC side output voltage in abc reference frame; i_{abc} is the AC current through the reactor in abc

reference frame ;R is the reactor resistance and L is the reactor inductance. Then, applying the coordinate transformation technique known as Clark transformation (see appendix D.1), the time varying three-phase quantities are transformed to fixed vectors in a two coordinates (α, β) system.

$$\begin{bmatrix} x_\alpha \\ x_\beta \end{bmatrix} = \frac{2}{3}\begin{bmatrix} 1 & cos\frac{2\pi}{3} & cos\frac{4\pi}{3} \\ 0 & sin\frac{2\pi}{3} & sin\frac{4\pi}{3} \end{bmatrix}\begin{bmatrix} x_a \\ x_b \\ x_c \end{bmatrix} \tag{3.2}$$

This Clark transformation gives the advantage of dimension order reduction. Hence,

$$L\frac{di_{\alpha\beta}}{dt} = \overrightarrow{V_{\alpha\beta}} - \overrightarrow{U_{\alpha\beta}} - \overrightarrow{Ri_{\alpha\beta}} \tag{3.3}$$

By using transformation angle from the system phase measurement at the PLL the electrical quantities are further transformed from the $(\alpha\beta)$ stationary coordinate system quantities to a rotational dq-reference frame equivalent quantities by applying the following Park transformation which can also be obtained from appendix D.2.

$$\begin{bmatrix} I_d \\ I_q \end{bmatrix} = \begin{pmatrix} cos\{\theta\} & sin\{\theta\} \\ -sin\{\theta\} & cos\{\theta\} \end{pmatrix}\begin{bmatrix} I_\alpha \\ I_\beta \end{bmatrix} \tag{3.4}$$

Where,

I_d and I_q are rotating reference frame quantities

I_α and I_β are orthogonal stationary reference frame quantities

θ is the rotation angle

Hence, equation (3.3) is transformed to,

$$L\frac{di_{dq}}{dt} = \overrightarrow{V_{dq}} - \overrightarrow{U_{dq}} - \overrightarrow{(R + j\omega l)\imath_{dq}} \tag{3.5}$$

Where the term $j_{\omega l}$; represent the time derivative of the rotating reference frame. Re-arranging equation (3.5) into real and imaginary components gives equations (3.6) and (3.7) that show the relationship between the converter voltages and input currents in rotating dq reference frame.

$$L\frac{di_d}{dt} = V_d - U_{dconv} - R_{id} + jwi_q \tag{3.6}$$

$$L\frac{di_q}{dt} = V_q - U_{qconv} - R_{iq} - jwi_d \tag{3.7}$$

Similarly, applying Kirchhoff's current law on the output side of the DC circuit of figure 3.1 yields the following equation;

$$i_{dc} = C\frac{du_{dc}}{dt} + i_L \tag{3.8}$$

Where; i_{dc} is the converter output DC current; i_L is the DC current through the DC link; C_{dc} is the DC capacitance. Thus, equations (3.6), (3.7) and (3.8) complete the mathematical modeling of VSC-HVDC system. The developed VSC-HVDC is shown in figure 3.2.

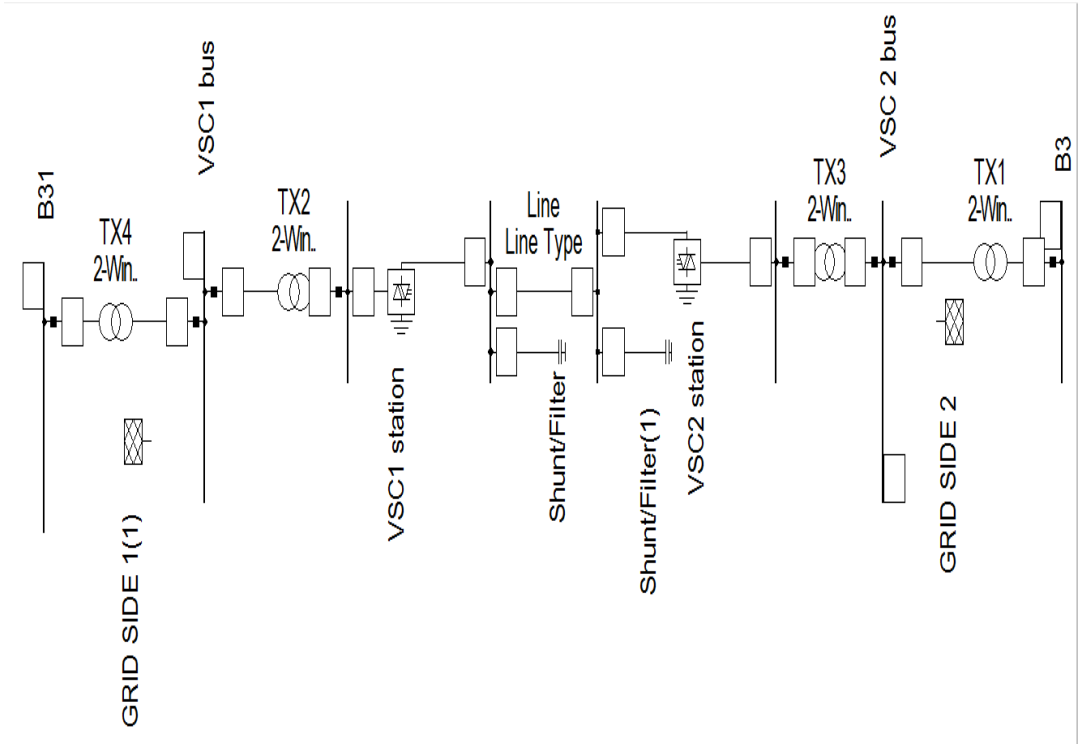

Figure 3.2: Developed model of VSC-HVDC power transmission system.

3.2.2 Vector current control principle

Vector current control is the most dominant current control method for VSC-HVDC system. It is based on manipulation of the three-phase alternating currents in a rotating dq-reference frame through an inner current control loop to achieve desired active and reactive power flows independent of each other (Svensson, 1998).. The inner current control loop normally decouples the current component into d-axis current and q-axis current components. The d-current component is normally used to control active power or direct voltage while the q-current component controls reactive power or alternating voltage. The major disadvantage with vector current control is the low-frequency resonance which can interfere with the fast inner current control loop, thereby limiting the VSC-HVDC performance. Further, the effectiveness of the VSC-HVDC internal protection ability is compromised by the low frequency resonance and can cause

duplication of faults and eventual total system breakdown. Figure 3.3 shows the vector current control principle (Bajracharya, 2008).

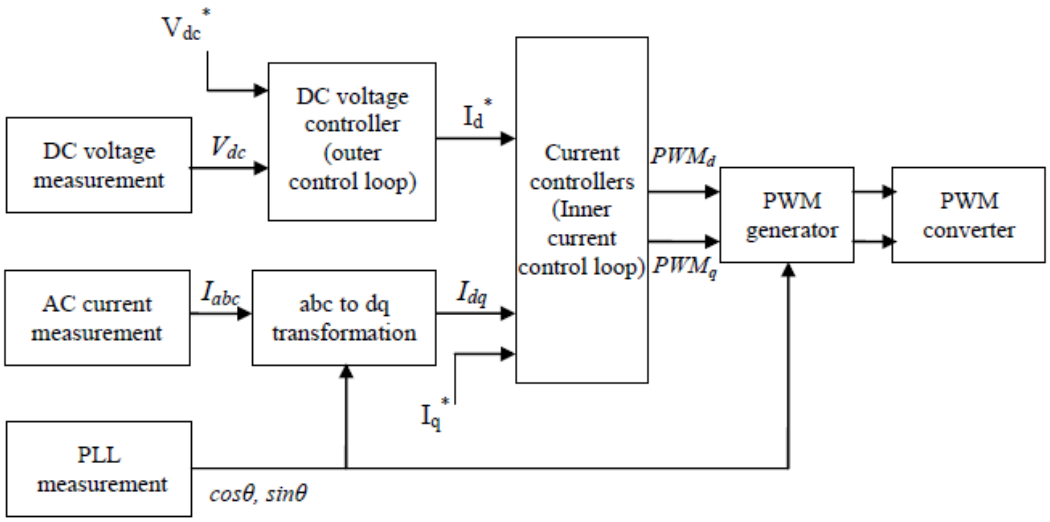

Figure 3.3: Vector control principle.

Based on vector current control in HVDC systems, the active power is transmitted over the DC link or links, whereas the reactive power is only exchangeable on the AC side of the grids. Various control strategies can be selected for each converter based on the desired applications. For instance, one converter can be selected to control DC voltage and reactive power while the other converter selected to control active and reactive power respectively. This kind of implementation that involves independent control of active and reactive power in HVDC system is achieved through a commonly known control principle based on vector current control. Using synchronously rotating dq-reference frame, independent control of active and reactive power can be attained. Figure 3.4 shows Stationary *abc* and αβ reference frames. The dq-coordinates are transformed into two vectors in the stationery αβ reference frame and using Clark transformation we get equation (3.9);

$$\begin{bmatrix} x_\alpha(t) \\ x_\alpha(t) \end{bmatrix} = \begin{bmatrix} \frac{\sqrt{2}}{3} & -\frac{1}{\sqrt{6}} & -\frac{1}{\sqrt{6}} \\ 0 & \frac{1}{\sqrt{2}} & -\frac{1}{\sqrt{2}} \end{bmatrix} \begin{bmatrix} x_a(t) \\ x_b(t) \\ x_c(t) \end{bmatrix} \quad (3.9)$$

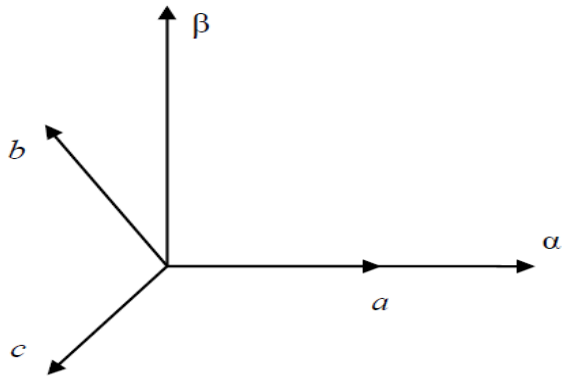

Figure 3.4: Stationary abc and αβ reference frames.

Using a Park transformation in appendix D.2, the transformation from *αβ* frame to *dq* can be written as:

$$x_{dq} = x_{\alpha\beta} e^{-j\theta} \quad (3.10)$$

The vectors $x_\alpha(t)$ and $x_\beta(t)$ in figure 3.4 are rotating with the angular frequency $\omega(t)$, which is the angular frequency of the grid voltage in rad/s (Malesani, Rossetto, Tenti, Tomasin. Since the inner current controller is the dominant part of the vector control, an equivalent circuit representing the VSC is analyzed in figure 3.5 to further derive mathematically and show exactly how the vector current control is used to independently control active and reactive power. Based on Kirchhoff's voltage law, applied across the phase reactor (L_f, R_f), it is shown how active and reactive power is independently controlled through differential equations.

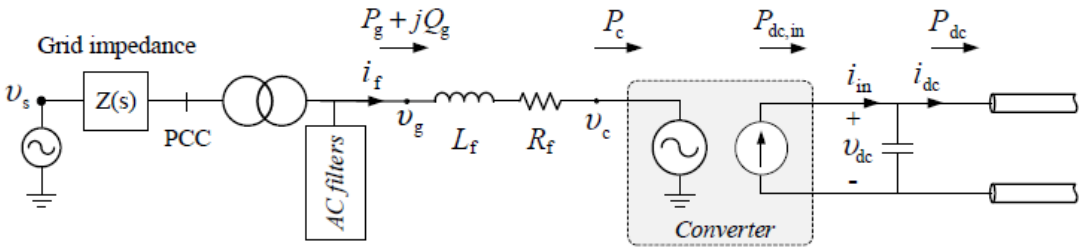

Figure 3.5: Equivalent model of the Voltage source converter.

$$v_g^{(abc)} - v_c^{(abc)} = L_f \frac{di_f^{(abc)}}{dt} + R_f i_f^{(abc)} \tag{3.11}$$

By applying Clarke's transformation described in the Appendix D.1, equation (3.11) can be expressed in the fixed □□□-coordinate system;

$$\vec{v}_g^{(\alpha\beta)} - \vec{v}_c^{(\alpha\beta)} = L_f \frac{d\vec{i}_f^{(\alpha\beta)}}{dt} + R_f \vec{i}_f^{(\alpha\beta)} \tag{3.12}$$

By applying the Park transformation and using the Appendix D.2, the PLL of the VSC is synchronized with the voltage vector □$\vec{v}_g^{(dq)}$ to gives the voltage and-current vectors in equations (3.13)-(3.15) respectively.

$$\vec{v}_g^{(\alpha\beta)} = \vec{v}_g^{(dq)} e^{j\theta_g} \tag{3.13}$$

$$\vec{v}_c^{(\alpha\beta)} = \vec{v}_c^{(dq)} e^{j\theta_g} \tag{3.14}$$

$$\vec{i}_f^{(\alpha\beta)} = \vec{i}_f^{(dq)} e^{j\theta_g} \tag{3.15}$$

Equation (3.12) can thus be transformed into rotating dq-reference frame:

$$\vec{v}_g^{(dq)} e^{j\theta_g} - \vec{v}_c^{(dq)} e^{j\theta_g} = L_f \frac{d[\vec{i}_f^{(dq)} e^{j\theta_g}]}{dt} + R_f \vec{i}_f^{(dq)} e^{j\theta_g} \quad \Rightarrow$$

$$\vec{v}_g^{(dq)} e^{j\theta_g} - \vec{v}_c^{(dq)} e^{j\theta_g} = J \frac{d\theta_g}{dt} L_f \vec{i}_f^{(dq)} e^{j\theta_g} + L_f e^{j\theta_g} \frac{d\vec{i}_f^{(dq)}}{dt} + R_f \vec{i}_f^{(dq)} e^{j\theta_g} \implies$$

Where, based on transformation on D.6,

$$L_f \frac{d[\vec{i}_f^{(dq)} e^{j\theta_g}]}{dt} = J \frac{d\theta_g}{dt} L_f \vec{i}_f^{(dq)} e^{j\theta_g} + L_f e^{j\theta_g} \frac{d\vec{i}_f^{(dq)}}{dt} \tag{3.16}$$

$$\vec{v}_g^{(dq)} e^{j\theta_g} - \vec{v}_c^{(dq)} e^{j\theta_g} = J\omega_g L_f \vec{i}_f^{(dq)} e^{j\theta_g} + L_f e^{j\theta_g} \frac{d\vec{i}_f^{(dq)}}{dt} + R_f \vec{i}_f^{(dq)} e^{j\theta_g} \tag{3.17}$$

Where ω_g is the angular frequency of the *dq*-rotating frame. Usually, the variations in ω_g (*t*) are very small over time and therefore considered constant. Under this condition and eliminating the term $e^{j\theta_g}$, equation (3.17) can be re-written as;

$$L_f \frac{d\vec{i}_f^{(dq)}}{dt} = -R_f \vec{i}_f^{(dq)} - j\omega_g L_f \vec{i}_f^{(dq)} + \vec{v}_g^{(dq)} - \vec{v}_c^{(dq)} \tag{3.18}$$

Equation (3.18) can further be expanded into real and imaginary pars to yield equations (3.19) and (3.20) respectively.

$$L_f \frac{di_f^d}{dt} = -R_f i_f^d - \omega_g L_f i_f^q + v_g^d - v_c^d \tag{3.19}$$

$$L_f \frac{di_f^q}{dt} = -R_f i_f^q - \omega_g L_f i_f^d + v_g^q - v_c^q \tag{3.20}$$

Equations (3.19) and (3.20) are cross-coupled first-order subsystems, with the cross-coupling being initiated by the terms $-\omega_g L_f i_f^q$ and $\omega_g L_f i_f^d$; the complex power s_g, is calculated as shown;

$$s_g = \vec{v}_g^{(dq)}\left[\vec{i}_f^{(dq)}\right] = \left[v_g^d + jv_g^q\right]\left[i_f^d - ji_f^q\right]$$
$$= \left(v_g^d i_f^d + v_g^q i_f^q\right) + j\left(v_g^q i_f^d - v_g^d i_f^q\right) \quad (3.21)$$

Separating real and imaginary part of equation (3.21) gives active and reactive power as shown in equations (3.22) and (3.23) respectively.

$$P_g = v_g^d i_f^d + v_g^q i_f^q \quad (3.22)$$

$$Q_g = v_g^q i_f^d - v_g^d i_f^q \quad (3.23)$$

Considering that the PLL performs the synchronization by aligning the *d*-axis of the *dq*-rotating frame to the vector $-\vec{v}_g^{(dq)}$, the *q*-component of the latter will be zero in steady-state condition, thus;

$$\vec{v}_g^{(dq)} = v_g^d \quad (3.24)$$

Applying equation (3.24) to equations (3.22) and (3.23) gives;

$$P_g = v_g^d i_f^d \quad (3.25)$$

$$Q_g = -v_g^d i_f^q \quad (3.26)$$

The objective of the vector current control is to independently control active and reactive power. Thus, equation (3.25) shows that active power can only be controlled via the d-current component of the current i_f^d while equation (3.26) shows that reactive power can only be controlled with the current q component of the current i_f^q.

3.2.3 Modeling the inner current controller

The inner current controller is placed between the outer controllers and the PWM generator and normally, the inner current loop is also referred to as vector current control (Schauder & Mehta, 1993). Its response time is very fast compared to the outer controllers to ensure system stability. In this thesis, the current loop is modeled considering constant DC bus voltage because the voltage control loop is much slower than the inner current control loop. According to (Schauder & Mehta, 1993), the inner current control is implemented in a dq-coordinate system. The phase locked loop (PLL), which provides the reference angle of the dq-transform, normally enables the d-axis to be aligned with the voltage vector at the point of common coupling (PCC). In order to achieve an independent control of real and reactive power (Schauder & Mehta, 1993), the inner current control loop should have two PI regulators each for the d-axis current and q-axis currents. These controllers transform the error current from the comparison to a voltage signal which is used by PWM generator for switching the converter. The inner current controller design model is built in PowerFactory software as shown in figure 3.6. The controller utilized is the proportional and integral controllers (PI controllers) and basically they are PQ controllers which improve the system steady-state performance by adding the type of the system by one. As a result of the dq-transformations produced by the DC vectors, the PI is able to reduce the steady state error signal to zero.

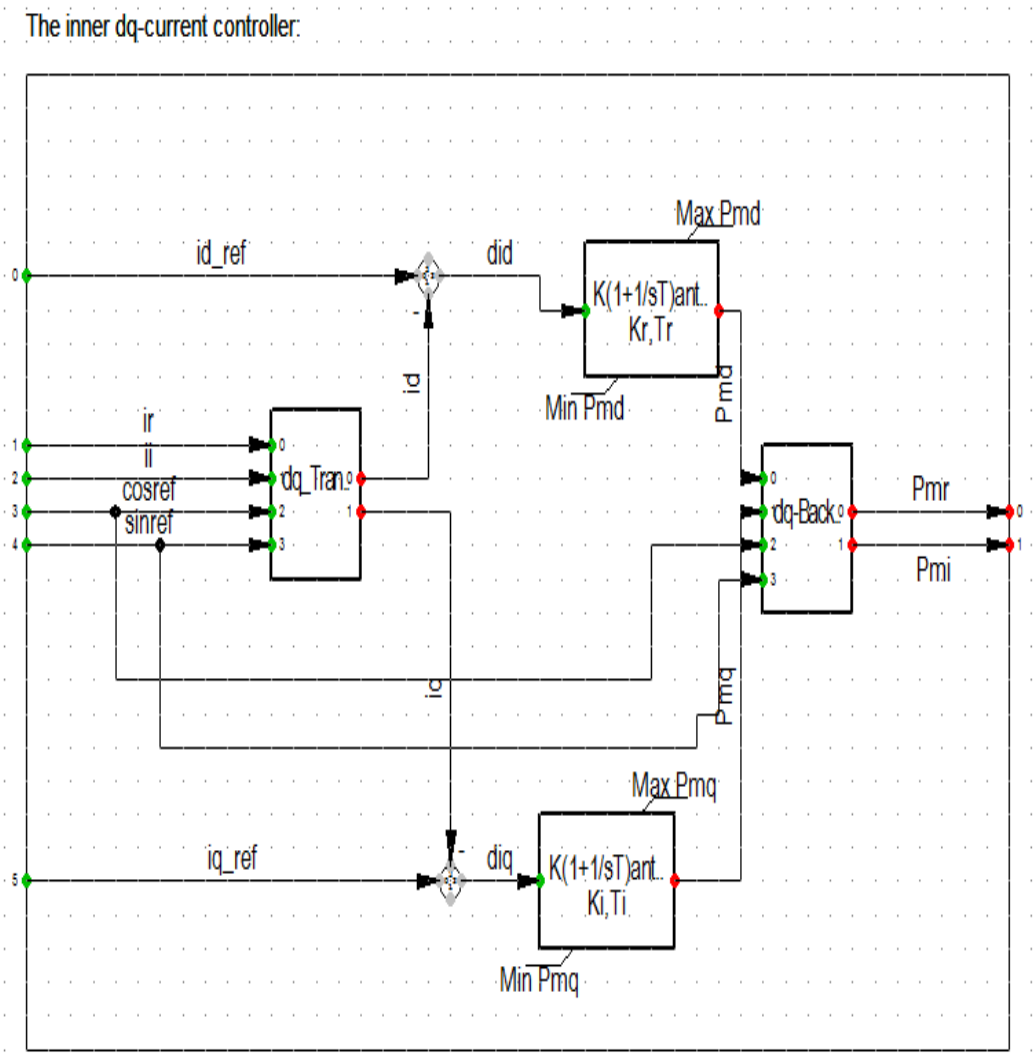

Figure 3.6: The inner current controller design model built in PowerFactory.

High frequency is normally chosen to reduce the size of the filters required to eliminate the harmonics generated at the switching time and during the faults. The elimination of the harmonics ensures quality of power supply is enhanced in addition to lengthening the life span of the transmission and semiconductor devices.

3.2.4 Modeling of the wind farm

Doubly-fed Induction Generators (DFIGs) are the most commonly used wind turbines with diverse ratings. DFIG has the advantages of variable speed operation and ability to control active and reactive power and is very sensitive to grid disturbances, particularly to voltage dips. A sudden drop in the grid voltage causes over voltages and over currents in the rotor windings that can destroy the converter if no internal and external protection mechanisms are put in place. In this research, an IEEE 9-bus is used where one of the synchronous generators namely G3 is replaced with an equivalent wind farm of 108.8MVA. Normally, the wind farm consists of DFIG, PWM converter, 3 winding transformer, and shunt/filter and series reactor. The modeled wind farm is shown in figure 3.7 while figure 3.8 shows G3 replaced with a wind farm connected to an IEEE 9-bus system.

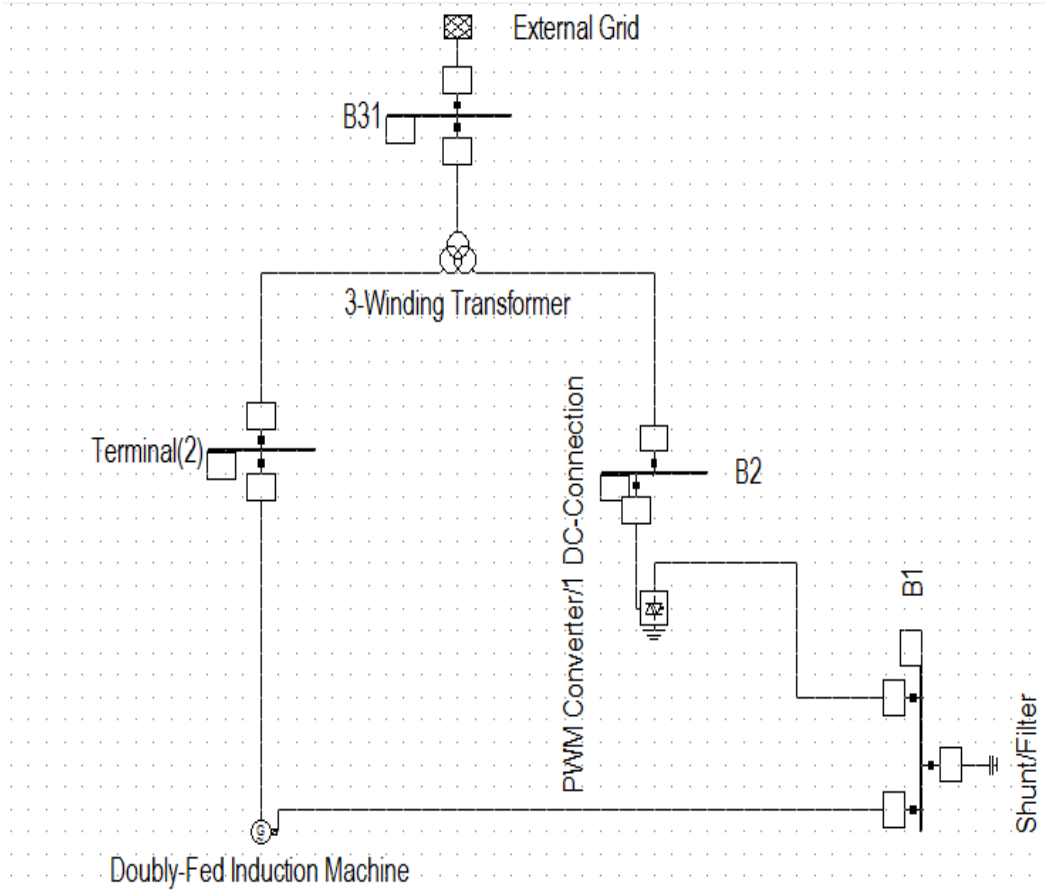

Figure 3.7: Developed wind farm model.

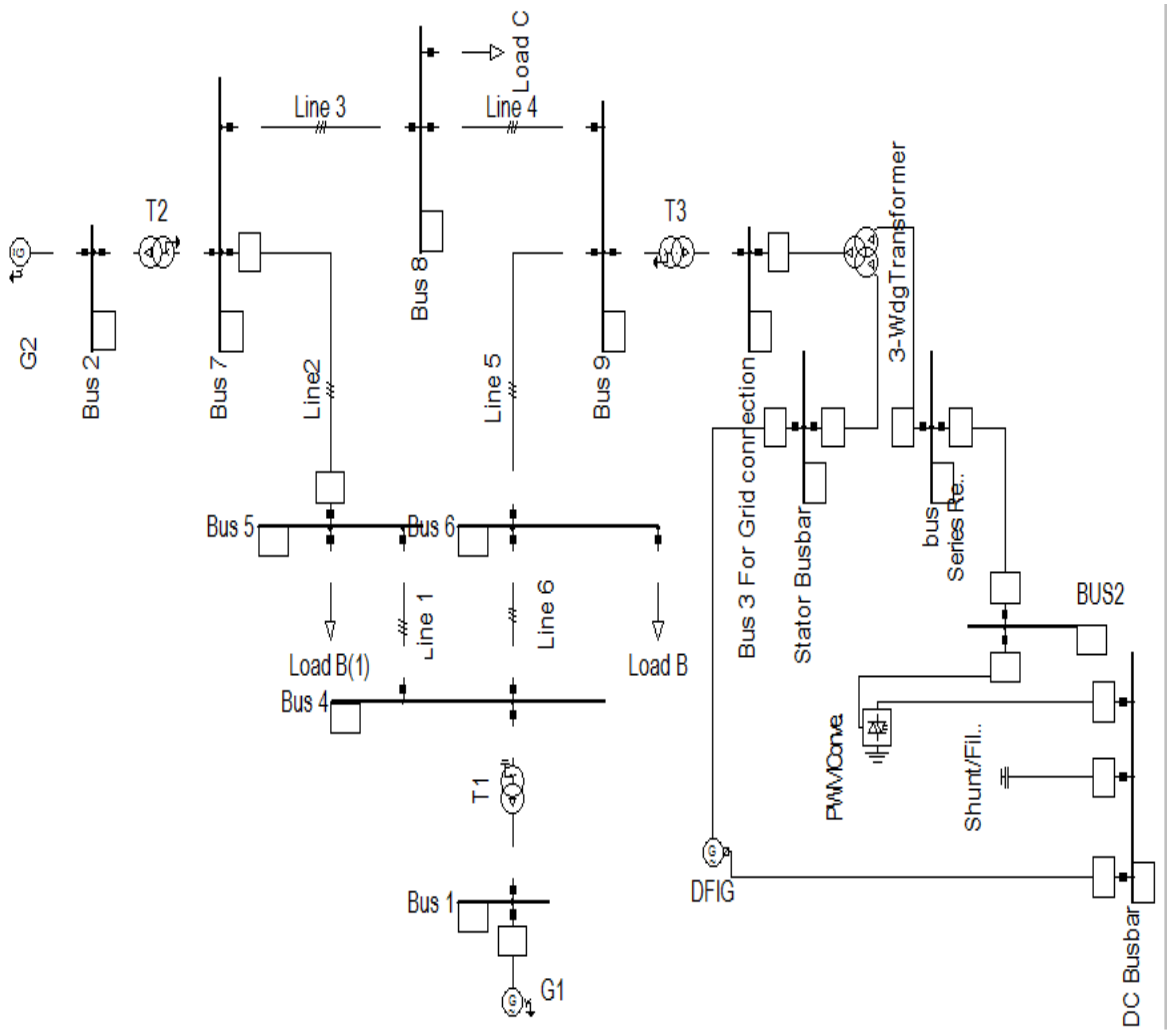

Figure 3.8: An IEEE 9-Bus system connected to a wind farm equivalent to 21% of the total power generation.

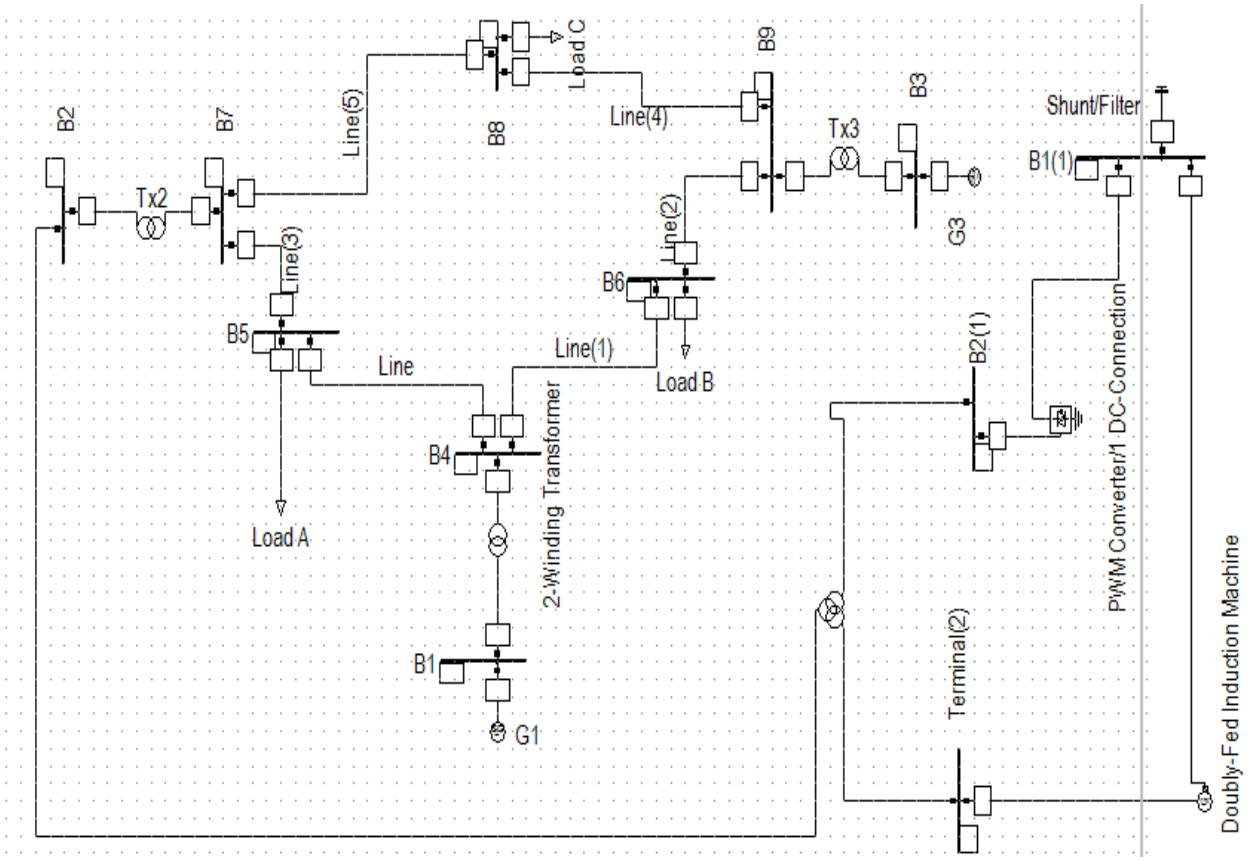

Figure 3.9: An IEEE 9-Bus system connected to a wind farm equivalent to 34% of the total generation.

3.3 Modeling the VSC outer controllers

VSC-HVDC control system consists of inner current controller controlling the AC and the outer controllers comprising of DC voltage controller, frequency controller active and reactive power controller (Padiyar &. Prabhu, 2004; Du, Sannino & Bollen, 2005; Liu, Xu, Gao, 2002; Suzuki, Nakajima, Konishi & Nakamura, 1992; Lindberg, 1995). The AC references are supplied by the outer controllers. In this thesis, only three outer controllers are discussed. These are the Active power controller, Reactive power controller and the DC voltage controllers. Generally, a two terminal-HVDC system has a rectifier and an inverter. The rectifier station converts AC to DC voltage and operates as a power control mode to control active power drawn from the AC grid and at the same

time control the reactive power compensated to the grid. It also has the capability to control AC grid voltage directly. The inverter station has the responsibility of ensuring that the DC link voltage is maintained at the desired specific level otherwise the active power flow balance between the two converters may result into system being unstable. The outer controllers need to be properly tuned so as to damp the system oscillations and attain system stability. The outer controllers generate the reference d-component currents and q-component currents. In (Liying &. Ertugrul, 2010), all the outer controllers are implemented by a PI controller where the difference between the reference value and the actual value is fed into the controller as the d-q reference currents.

3.3.1 Active and reactive power controllers

The objective of PQ controllers is to regularly regulate the active and reactive power exchange between the converters and the grid. The reactive power balance in a grid largely relies on the voltage levels on the grid and any deviation will lead to system instability. The active and reactive powers are calculated from the grid and compared with the reference values and the error signal is made to pass through PI regulator. The PI controllers create the rotating reference d and q current components which are fed to the inner current controllers (Cole & Belmans, 2011). Figure 3.9 shows the active and reactive power controller design model.

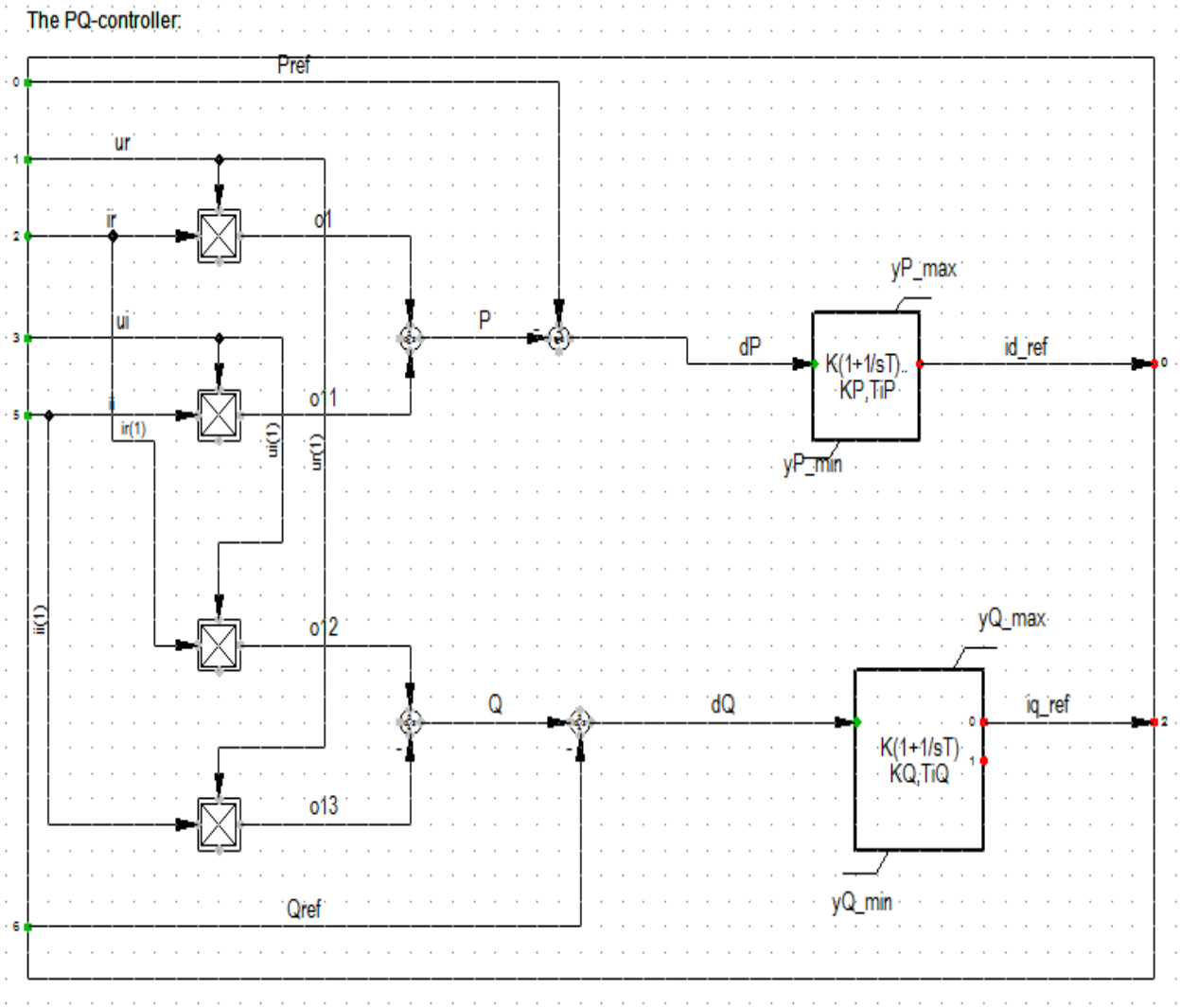

Figure 3.10 Active and Reactive power controller design model built in PowerFactory.

In VSC-HVDC system, every converter can be selected to independently control its reactive power injection into the power system. Similarly, only one converter is selected at a time to independently control the active power and the DC voltage respectively. In (Liying &. Ertugrul, 2010),, the converter selected to control the DC voltage is called the slack converter because it usually compensates the losses in the DC network and therefore has a similar function as a slack node in an AC grid. The outer control loop of

the VSC converter controls the active and reactive power. The PI controller used for the active and reactive power controller has the same structure as the PI controller with proportional gain and time constant. In (Elansari, Finney &. Edrah, 2015), the author states that there is no general rule for tuning the controllers and the common approach by many researchers is based on trial and error method until the controller parameters selected meet the desired performance.

3.3.2 DC voltage controller

DC voltage controller is responsible with controlling the active and reactive powers between the converters. In VSC-HVDC system, the DC voltage control is implemented through the integration of the inner current loop and the outer control loop. The two loops must work concurrently for power flow balance between the converters and subsequently between the grids. As previously mentioned, the inner current controller should be fast enough in order to get the best system response. Based on (Hassan, Vanfretti & Wei, 2014), the DC voltage controller has four parts, namely;

i. The PI controller $K_p(1+\frac{1}{sT_i})$

ii. The inner current controller, $(\frac{1}{1+sT_{eq}})$

iii. The system, $\frac{3}{2}\frac{1}{CS}\frac{Vd}{Vdc}$

iv. The measurement circuit is the feedback loop $\frac{1}{1+sT_s}$.

Where T_s is the sampling time of the inner current controller. In order to derive the DC voltage control loop, some assumptions are made. Assuming a lossless converter, the power input to the converter is equal to the power output of the converter. Therefore, based on this assumption, the two equations hold true:

$$P = \frac{3}{2}V_d i_d \tag{3.27}$$

$$Q = -\frac{3}{2}V_d i_q \tag{3.28}$$

Equations (3.27) and (3.28) indicate that, the active power is dependent on d-axis current while the reactive power is dependent on q-axis current. Similarly, the DC Power is given by;

$$P_{dc} = V_{dc} i_{dc} \tag{3.29}$$

Equating the active power equation (3.27) with the DC power equation (3.29) yields equation (3.30).

$$\frac{3}{2}V_d i_d = V_{dc} i_{dc} \tag{3.30}$$

Rearranging equation (3.30) gives equation (3.31);

$$i_{dc} = \frac{3V_d i_d}{2V_{dc}} \tag{3.31}$$

Applying the Kirchhoff's current law at the node on the dc of figure 3.1 and any unbalance between AC and DC power causes change in voltage over the DC link capacitors as given by equation (3.32);

$$C_{dc}\frac{d}{dt}U_{dc} = i_{dc} - i_L \tag{3.32}$$

Where i_{dc} is the current on the DC side of the converter, i_L is the current from the DC link, C_{dc} is the DC capacitance, U_{dc} is the voltage on the DC side of the converter, C_{dc} is the capacitance on the DC side of the converter .

Inserting equation (3.31) to equation (3.32) yields equation (3.33);

$$C_{dc}\frac{d}{dt}U_{dc} = \frac{3V_d i_d}{2V_{dc}} - i_l \tag{3.33}$$

Rearranging equation (3.33) and making U_{dc} the subject of the formula gives,

$$U_{dc} = \frac{3V_d i_d}{2C_{dc}\frac{d}{dt}V_{dc}} - i_L \tag{3.34}$$

Noting that, if $f(t) = 1, then\ F(S) = \frac{1}{S}$, this is called Laplace transformation of 1. Then, taking the Laplace transformation of equation (3.34) and solving for U_{dc} in equation (3.34), we get;

$$U_{dc} = \frac{1}{S}\left(\frac{3}{2C}\frac{V_d i_d}{V_{dc}} - i_L\right) \tag{3.35}$$

The resulting block diagram of the DC voltage controller loop is shown in figure 3.11. The disturbance introduced by i_L can be eliminated by introducing a compensation term $\left(\frac{2}{3}\frac{V_{dc}}{V_d} i_L\right)$ before the converter (Singh, 2015).

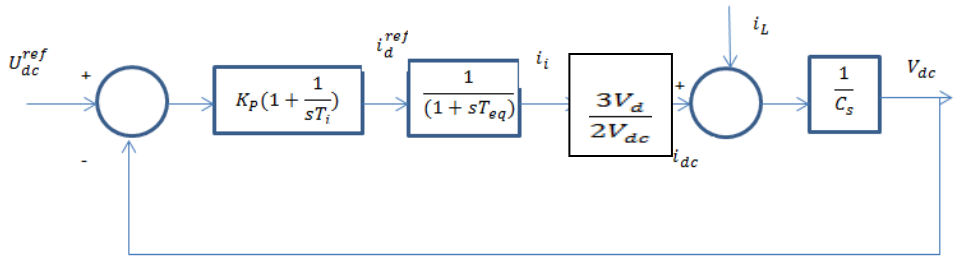

Figure 3.11: DC voltage control loop in dq axes.

Comparing the active and reactive power controller with the DC voltage controller, one unique observation is that both utilize PI controllers for control of the active and reactive power. DC voltage variations in a power system affect the Reactive power balance between the converters and the grid, consequently, the voltage has to be maintained at a reasonable tolerance levels otherwise any large deviation can cause the power system to collapse. Figure 3.12 shows the developed DC voltage controller model in PowerFactory software. It uses the PI controller and if it detects the system voltage drop it immediately request for more reactive power from the system. Once the capacitors are fully charged, the voltage rises when the DC voltage reaches the prescribed set point in steady state condition when the active powers get balanced again and the same cycle is repeated when the voltage drops beyond the allowable tolerance.

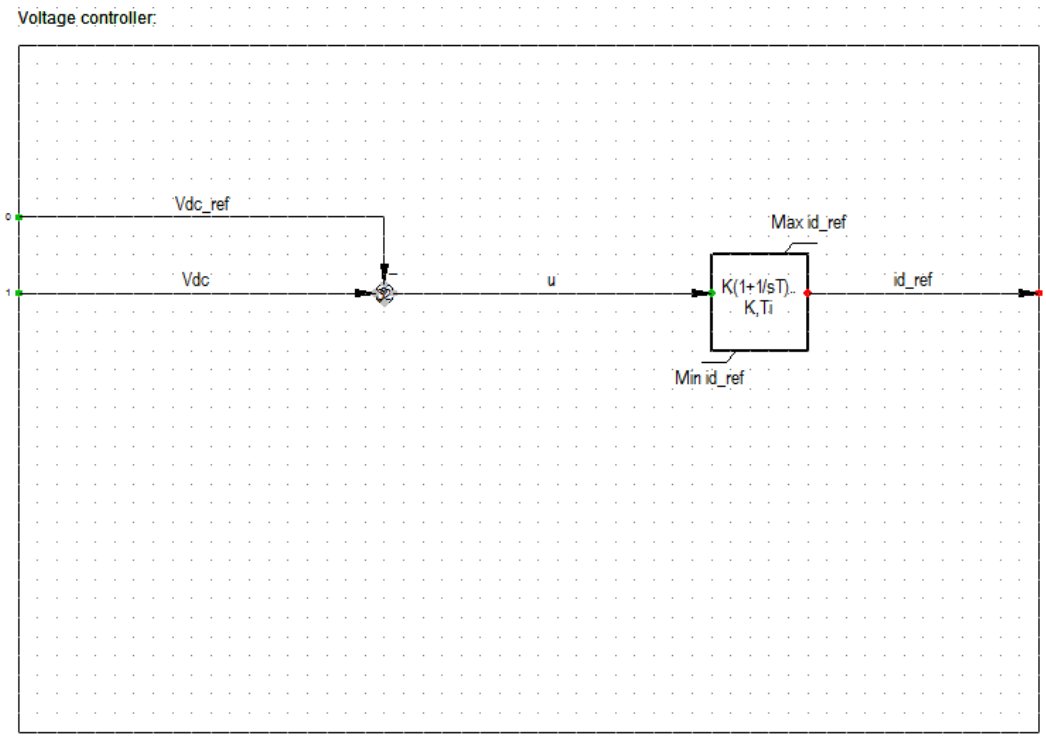

Figure 3.12: DC voltage controller model built in PowerFactory.

3.3.3 Tuning the DC voltage controller using the symmetrical optimum criterion

Tuning the DC voltage controller is a critical activity in maintaining the correct voltage values and reactive power at desired levels otherwise a slight change in DC voltage can lead to system instability. Based on SOC, controllers can be tuned to control the system response, overshoot, and phase margin and damping levels. These parameters affects the system stability subsequently, correct tuning of the controllers parameters by varying the symmetrical distance 'a' affects the system stability. Using pole placement where a>3, Symmetrical optimum technique can be extended to specify damping factor for the system as part of tuning procedure (Machaba, 2008). The controlled system has one dominant time constant and other minor time constant where the PI controller can be tuned using the Modulus Optimum Criteria however, when one of the poles is already near to the origin or at the origin itself, the pole shift does not change the situation significantly (Rezek, et al., 2001, June).The open loop transfer function of the voltage controller has two poles at the origin, thus an alternative criterion to tune the controllers in this condition is given by the Symmetrical Optimum Criteria. As shown in figure 3.11, DC voltage controller loop has a pole at the origin and thus the symmetrical optimum tuning is used in this study to design the DC voltage controller's parameters. Research has been carried out concerning the tuning of the DC voltage controller based on Symmetrical Optimum Tuning (Rezek, et al., 2001, June) and [96], indicating that:

$$T_i = a^2 T_{eq} \tag{3.36}$$

Where a- is the symmetrical distance between $\frac{1}{T_i}$ to the phase margin and $\frac{1}{T_{eq}}$ to phase margin.

T_i is the proportional time constant. It is also recommended that the symmetrical distance 'a' is between 2 and 4 (Machaba, 2008; Preitl & Precup, 1999), thus, the equivalent time delay T_{eq} due to the current control loop is given below.

$$T_{eq} = aT_a = a\frac{T_s}{2} = a\frac{1}{2f_s} = 2 \times \frac{1}{2\times5000} = 0.0002$$

Where f_s is the switching frequency.

$$T_a = \frac{1}{2f_s} \tag{3.37}$$

$\frac{1}{2f_s}$ is the inverse of the switching frequency.

If a= 3 then,

$$T_{eq} = 3 \times \frac{1}{2\times5000} = 0.0003$$

$$T_i = 3^2 \times 0.0003 = 0.0027$$

In this thesis, the parameters below were utilized based on the Symmetrical Optimum tuning

$$V_{dc} = 81.7Kv, V_d = 45Kv, C = 53.933\mu f.$$

For a= 2, the proportional gain becomes;

$$K_p = \frac{2}{3}\frac{V_{dc*C}}{aV_d T_{eq}} = 0.163$$

From figure 3.10, K is given by:

$$K = \frac{3}{2}\frac{K_P V_d}{Vdc} = 0.137$$

Now using the PI controller parameters, the overall closed loop transfer function for figure. 3.10, become,

$$G_{cl} = \frac{K+KT_i s}{K+KT_i s+TiCS^2+T_i T_{eq} CS^3} \quad (3.38)$$

$$G_{cl} = \frac{0.1347+1.078\times10^{-4}s}{0.1347+1.078\times10^{-4}\ s+4.315\times10^{-8}s^2+8.629\times10^{-12}s^3}$$

For a=3;

$$K_p = \frac{2}{3}\frac{81.7*53.933^{-6}}{3*45*0.0003} = 0.07253$$

$$K = \frac{3}{2}\frac{KpVd}{Vdc} = 0.05993$$

$$KT_{is} = 0.05993 \times 0.0027 = 1.6181 \times 10^{-4}$$

For a=4

$$Teq = 4 \times \frac{1}{2\times5000} = 0.0004$$

$Ti = 0.0064, Kp = 0.0408, K = 0.03371.$

Similarly, other parameters of the DC voltage controller for various values of symmetrical distance were calculated and graphically shown in figure 4.51.

3.4 Tuning of the inner current controller by modulus optimum criteria (MOC)

Tuning the inner current controller based on MOC is done with the aim of achieving fast system response and system stability towards the inner loop (60). This method is implemented when the controlled system has one dominant time constant and the other minor time constant. The dominant pole is cancelled by the controller zero to arrive at a standard transfer function. This method is selected because of its simplicity and fast response at tracking the reference value. Figure 3.13 shows the inner current control loop in dq axes whose open loop transfer function of the system is obtained through the modulus optimum criteria.

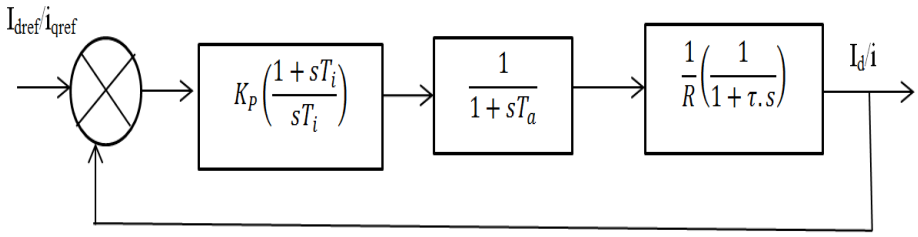

Figure 3.13: Inner current controller in dq axes.

$$G_{ol}(s) = K_p\left(\frac{1+sT_i}{sT_i}\right)\left(\frac{1}{1+sT_a}\right)\left(\frac{1}{R+sL}\right) \tag{3.39}$$

Based on MOC;

$$T_i = \tau = \frac{L}{R} \tag{3.40}$$

Eliminating the zero of the regulator and rearranging the time constant gives;

$$G_{ol}(s) = K_p\left(\frac{1+sT_i}{sT_i}\right)\left(\frac{1}{1+sT_a}\right)\left(\frac{1}{R}\right)\left(\frac{1}{1+sT_i}\right) \tag{3.41}$$

After cancelling the dominant pole and zero of the controller, we get a second order Closed Loop Transfer Function (CLTF) shown in equation (3.42).

$$G_{cl}(s) = \frac{{}^{K_P}/_{R}}{sT_i(1+sT_a) + {}^{K_P}/_{R}} \tag{3.42}$$

Further simplification of equation 3.42 gives;

$$G_{cl}(s) = \frac{\frac{K_p}{R}}{s^2T_iT_a + sT_i + \frac{K_p}{R}} \tag{3.43}$$

Equation (3.43) is re-arranged to yield a standard second order equation (3.44).

$$G_{cl}(s) = \frac{K_p/_{RT_iT_a}}{s^2 + \frac{s}{T_a} + \frac{K_p}{RT_iT_a}} \tag{3.44}$$

From equation (3.44), we get the undamped natural frequency as;

$$\omega_n = \sqrt{(\frac{K_p}{RT_iT_a})} \tag{3.45}$$

To get the damping ratio, equation (3.44) is compared with a standard second order equation below;

$$\frac{C(s)}{R(s)} = \frac{\omega_n^2}{S^2 + 2\xi\omega_n s + \omega_n^2} \tag{3.46}$$

From equations (3.44) and (3.46) we can relate them to get equation (3.47).

$$2\xi\omega_n = \frac{1}{T_a} \tag{3.47}$$

From equation (3.47) we can make the damping ratio as the subject of the formula.

$$2\xi\sqrt{\frac{K_P}{RT_iT_a}} = \frac{1}{T_a} \tag{3.48}$$

Squaring both sides of equation (3.48) gives equation (3.49).

$$4\xi^2\frac{K_p}{RT_iT_a} = \frac{1}{T_a^2} \tag{3.49}$$

Given the values of RT_iT_a and K_p; it is possible to calculate various values of the damping ratio. The power system can either be critically damped ($\xi = 1$), overdamped ($\xi > 1$), or underdamped ($0 < \xi < 1$) and it is the damping ratio that has great impact on the power system stability. Therefore, re-organizing equation (3.49) gives equation (3.50).

$$\xi = \frac{1}{2}\sqrt{\left\{\frac{RT_i}{K_pT_a}\right\}} \tag{3.50}$$

In this thesis;

R=0.20253 Ohms; L=12.9 mH; thus, $T_i = \frac{L}{R} = 0.063694\ S$

For a= 2;

$$T_a = \frac{T_{eq}}{2} = 0.0001s$$

Where T_a=Average time delay of the converter.

Rearranging equation (3.50) gives equation (3.51).

$$K_p = \frac{T_iR}{4\xi^2T_a} \tag{3.51}$$

$$K_p = \frac{T_i R}{4\xi^2 T_a} = \frac{0.063694 \times 0.20253}{4 \times 0.707^2 \times 0.0001} = 64.51$$

The final closed loop transfer function becomes;

$$G_{cl} = \frac{50.02 \times 10^6}{S^2 + 10^4 S + 50.02 \times 10^6}$$

Using the same procedure, $T_i, K_p \ and \ T_a$ are calculated for other values of symmetrical distance and step response for each is generated as shown in figure 4.43.

Four VSC-HVDC controllers were modeled. These were the inner current controller, DC voltage controller, active and reactive power controllers. In addition, VSC-HVDC transmission model, wind farm model and an IEEE 9-bus system were also modeled. The three models were connected together and time domain simulations carried out with an IEEE 9-bus system without wind farm, an IEEE 9-bus system with a wind farm model and finally an IEEE 9-bus system with wind farm connected through the developed model of VSC-HVDC transmission system.

For the first configuration where no wind farm was connected, a short-circuit fault was initiated along the transmission line and various data such as the rotor angle, DC voltage, active and reactive power were obtained through load flow calculation. The same process was repeated for the next two configurations and wind power was increased till the point where system stability could not be sustained. Later, the data obtained from the three configurations was coded and analyzed in Matlab software and graphically presented. The critical clearing time was used to find the longest time that the fault can be sustained without losing system transient stability. Figure 3.14 shows the VSC-HVDC system with wind farm connected to an IEEE 9-bus system.

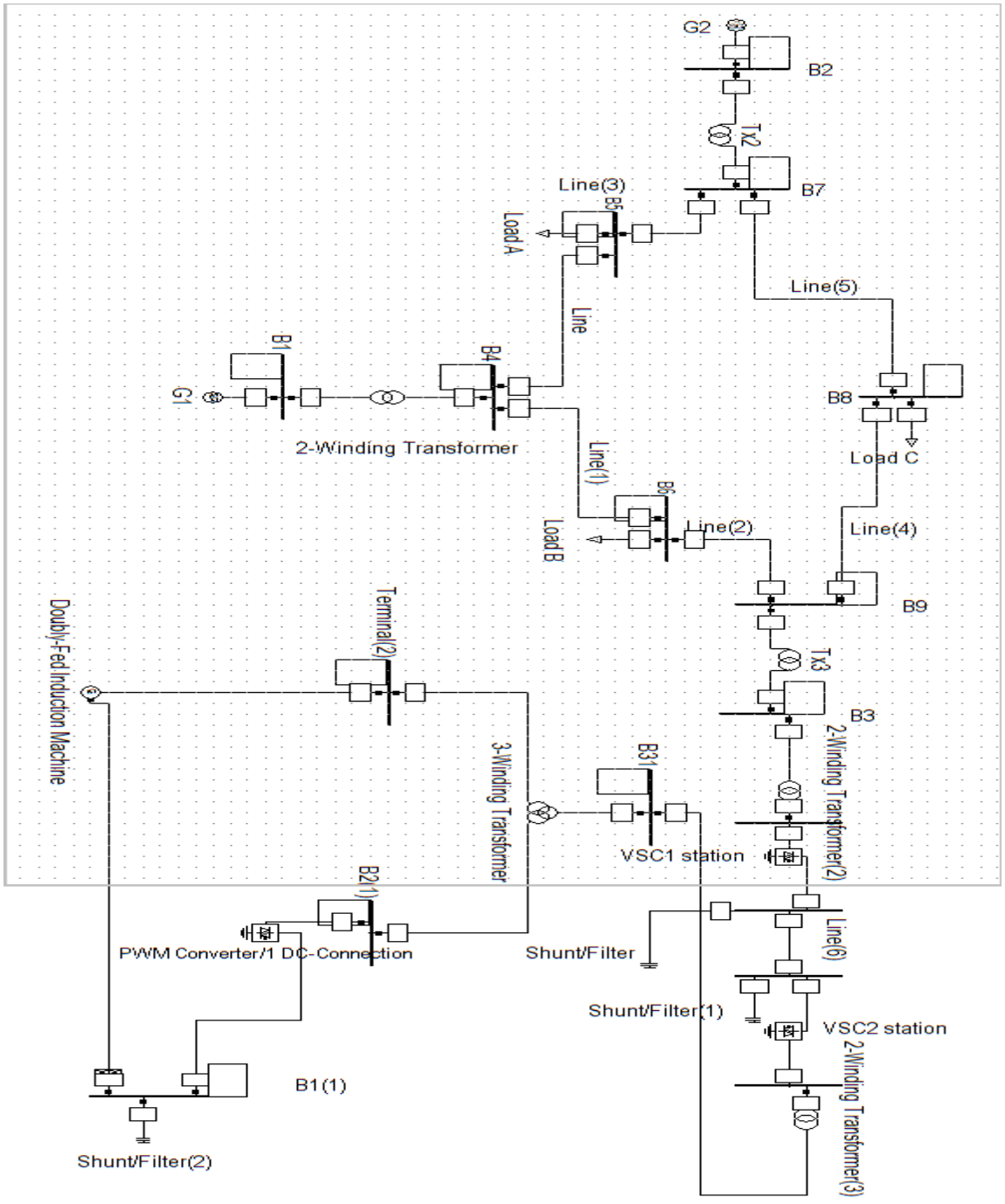

Figure 3.14: VSC-HVDC with wind farm connected to an IEEE 9-bus system.

3.5 Design and analysis of the proposed novel fast solid-state DC breaker

As earlier discussed, four types of DC circuit breakers have been developed over the years though not all are commercially available. As in (Negari, 2015) and (Eriksson, Backman & Halen, 2014), the latest developed DC circuit breaker has a fault clearing time of 5ms which is still not fast enough to provide enhanced protection of the converter valves and transmission network against short-circuit faults. Traditional DC circuit breakers such as the Electromechanical type relies on resonant circuit to force current to zero-crossing point at the time of fault clearance while others relies on charged capacitor bank that is discharged in an oscillatory behavior resulting to zero current crossing an ideal condition for fault interruption (Eriksson, Backman & Halen, 2014), During fault interruption, a lot of arc is generated by the AC breakers. The quenching media traditionally used are air, oil or the SF_6 gas however, under short-circuit faults. These traditional cooling media have proved ineffective in quenching the arc in DC circuit breakers. In electromechanical type of DC circuit breakers, the energy generated at the time of fault can be absorbed and dissipated by the Zno arrestors while the novel solid-state DC circuit breakers utilize the mutual inductances for absorption of the heat generated. To easily understand the modification introduced in the novel DC circuit breaker, it is important to present the existing fast design model as shown in figure 3.15.

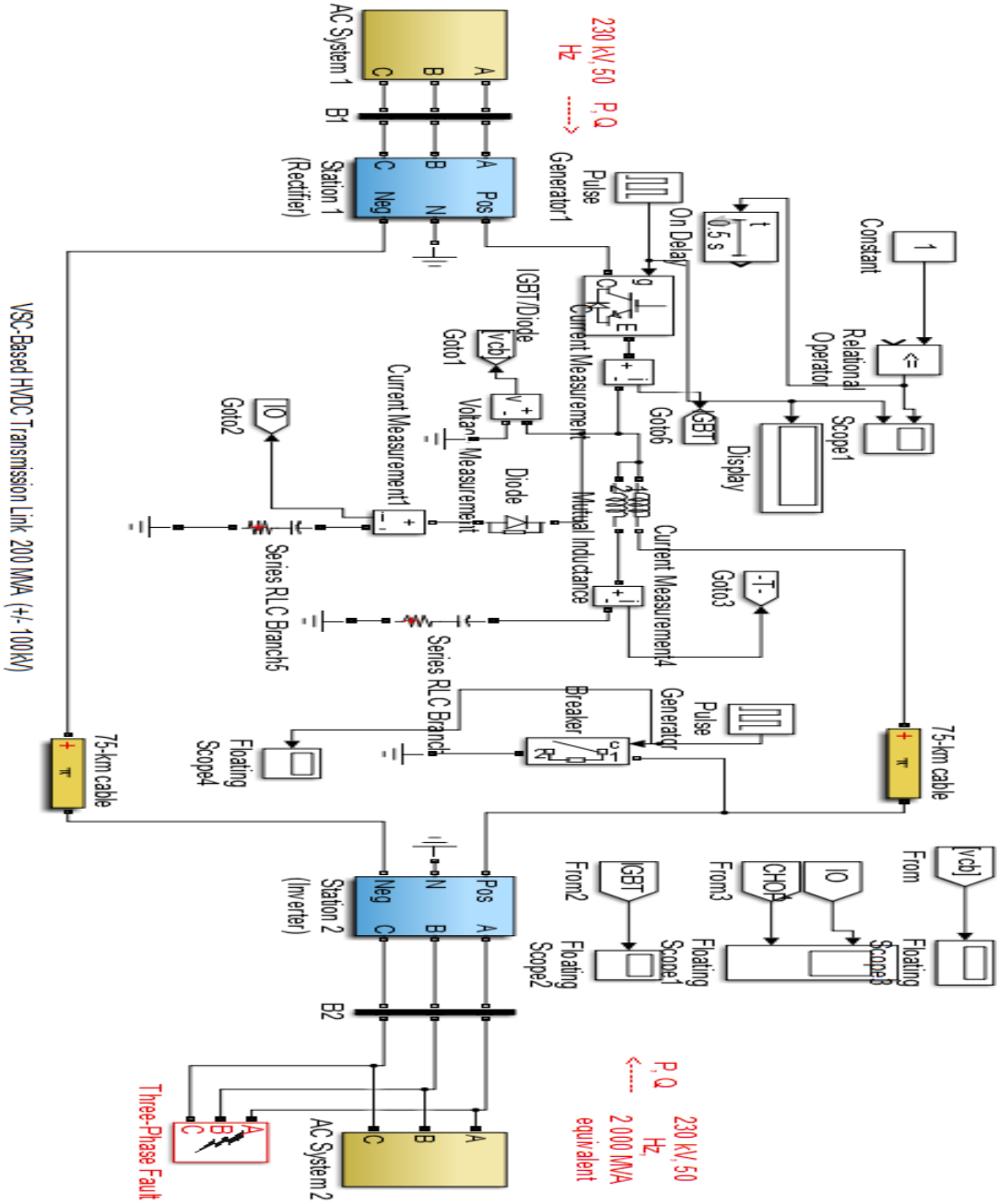

Figure 3.15 Existing VSC-HVDC Transmission systems with a DC circuit breaker.

As previously mentioned, the existing DC solid-state circuit breakers have slow response time, high power losses and partial protection of the IGBT. These challenges lead to delay in fault clearance thus triggering burning of the converter valves and interference of the transmission system subsequently triggering system blackout. To overcome these concerns, a model of VSC-HVDC system with a novel DC circuit breaker is developed in MATLAB with modifications on the timing circuit, IGBT protection, energy absorption and dissipation as shown in figure 3.16.

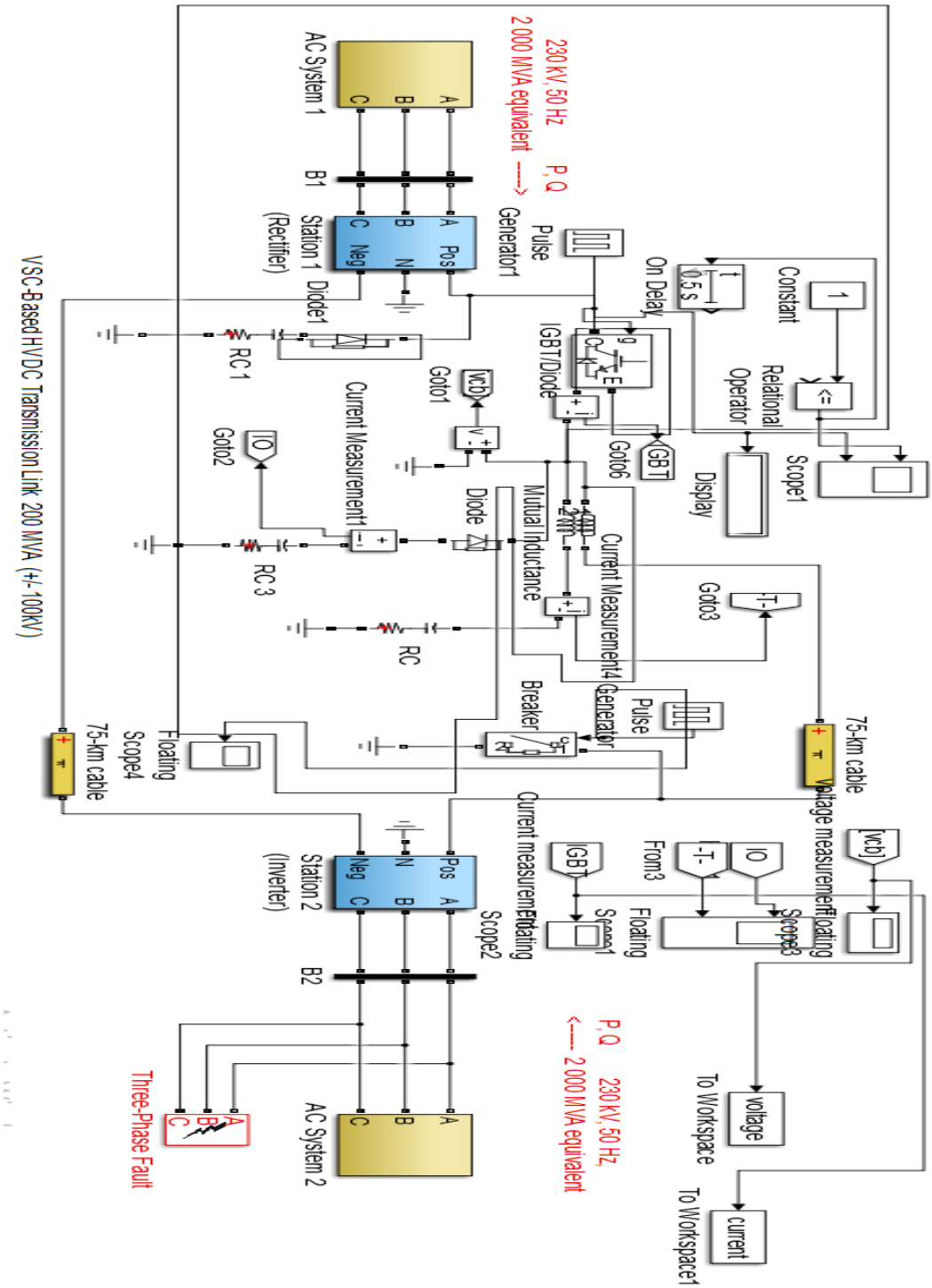

Figure 3.16: Modified VSC-HVDC Transmission system with a novel DC circuit breaker.

The novel fast DC circuit breaker proposed in this research is developed through the act of balancing the amount of energy absorbed and speedy dissipation of the same energy through mutual inductances. The new design ensures that the mutual inductance being the absorption media have little storage capacity for the energy generated under short-circuit fault and quickly dissipate it as heat. Thus, the RC circuits on both side of the novel DC circuit breaker guarantee full protection of the IGBT enabling it to function swiftly without any limitation. Further, the freewheeling diodes are included to protect the IGBT against overvoltage. Most DC breakers use Zinc oxide arrestors to damp and suppress the voltage across the IGBT however, short-circuit current in the range of 5KA can damage the IGBT thus the need to use resistive elements that are hardy, need no maintenance and are quick to absorb and dissipate the energy generated during faults. The use of mutual inductance and high pass filters RC with freewheeling diode on both sides of the IGBT shown in figure 3.16 eliminates the need for Zinc oxide arrestors. This makes the developed DC breaker reliable, efficient and fast compared to other available DC circuit breakers. Besides, Equation (2.7) illustrates that, the energy absorbed by the mutual inductance is less for a DC CB connected with the freewheeling diode (see figure 2.14) and thus adopted in this research. The figure 2.14 was modeled and inserted in the developed novel DC breaker in figure 3.16 that made it possible to quickly dissipate the heat thus allowing almost immediate DC breaker operation. This is critical because the greater the amount of energy absorbed, the longer it takes to dissipate it as heat thus negatively affecting the DC CB response time. Hence, this type of the DC circuit breaker topology was adopted in this research with some modifications aimed at reducing the breaker response time upon a fault occurrence. This enhanced design has reduced the DC breaker response time to 1ms as will be seen later in chapter four of the simulation of the results. This is a great stride from the previous available DC circuit breakers with a fault clearing time of 5ms (Negari, 2015) and (Eriksson, Backman & Halen, 2014),.

3.6 Summary

The mathematical models of the VSC-HVDC system and vector current control principle have been presented. As previously mentioned, VSC-HVDC system has four controllers which have been developed and built in PowerFactory software. Three configurations developed for the VSC-HVDC system with a wind farm connected to an IEEE 9-bus system are analyzed. The configurations involved analysis of the conventional system without wind power, with wind power alone and with wind power and the developed VSC-HVDC system. In each of the configuration, a short-circuit fault was created and data obtained analyzed and graphically presented as shown in chapter 4. The objective was to find out which among the three configurations can accommodate more wind power without losing transient stability. Further, a novel DC solid-state circuit breaker have been developed and compared with the currently available DC circuit breakers. The novel DC breaker provide full protection of the IGBT due to the presence of the freewheeling diode that safeguard it against voltage surges commonly known to damage the converter valves and the transmission system. It also includes a mutual inductance and RC circuit on both sides of the IGBT that is specifically designed to ensure that the generated energy during fault is almost instantaneously discharged. The novel DC circuit breaker designed in this research has a fault clearing time of 1ms, this is a great milestone in the development of a fast DC circuit breaker that safeguard the converter valves and the transmission system against short-circuit faults.

CHAPTER FOUR

RESULTS AND DISCUSSION

4.1 Introduction

This chapter presents the simulation results and discussion. Three scenarios were analyzed to assess the effects of power system transient stability under short-circuit faults as follows: (i) A conventional IEEE 9-bus system alone, (ii) A conventional IEEE 9-bus system with a wind farm, (iii) A conventional IEEE 9-bus system connected to an improved VSC-HVDC system and integrated with wind power. Further, tuning of the DC voltage controller, inner and outer controllers were carried out for the purpose of exploring larger values of symmetrical distance that will ensure good system response and maintain transient stability. In addition, a novel DC circuit breaker is designed and simulation results presented. The designed DC breaker has the ability to clear fault in 1ms thus providing a great milestone in the development of a fast DC breaker. The simulation results that follow are based on the three objectives of this thesis:

4.2 Effects of various levels of wind power integration on transient stability

A standard IEEE 9-bus system was used for analysis of the effects of wind power integration on power transient stability. Two scenarios were analysed, the first being the effects of transient stability with conventional generation alone while the second analysis involved the effects of transient stability of a power system with both the conventional generation and wind farm at different wind power penetration levels.

4.2.1 IEEE 9-bus system without wind farm integration.

The IEEE 9-bus system is not connected to a wind farm. In this case, the transient responses of active and reactive power were shown in figures 4.1 and 4.2 when a three-

phase short-circuit fault was created at line 3 near bus 7 at 1 s and cleared at 1.123 s. Figures 4.1 and 4.2 shows the characteristics for generator 1 when no wind power was added to the system.

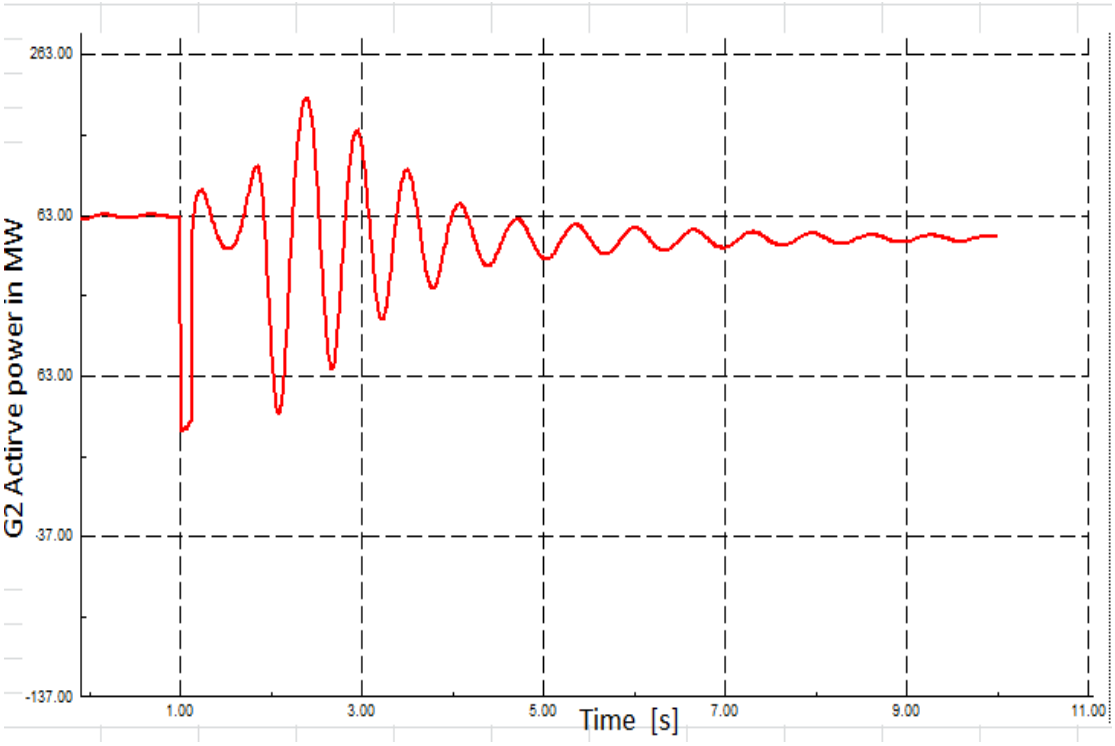

Figure 4.1: Characteristics of active power parameter for a fault at 1 s cleared at 1.123 s.

The system has no wind farm and in this scenario, the transient response of the active power when a short-circuit fault is initiated at 1s and cleared at 1.123 s is shown in figure 4.1. It clearly indicates that, the system has a critical clearing time of 0.123 s. The swing curves shows that the synchronous generator will remain stable if the fault is cleared at 0.123 s and any further delay after 0.123 s, the system will lose its transient stability.

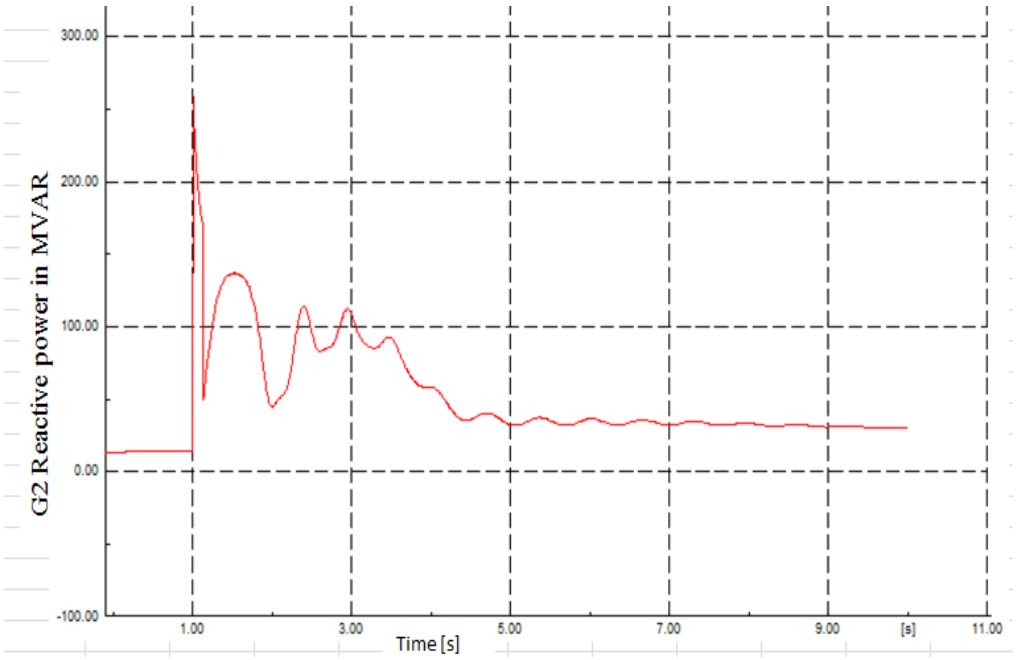

Figure 4.2: Characteristic of Reactive power parameter for a fault at 1 s cleared at 1.123 s.

Figure 4.2 represent the reactive power behaviour under three-phase short-circuit fault with a critical clearing time of 0.123 s.

4.2.2 An IEEE 9-bus system with wind farm integration

(1) With wind power integration at 22%

The figures 4.3 to 4.7 shows the various characteristics of G2 for a fault created at line 3 near bus 7 when G3 was replaced with an equivalent wind farm of 128MVA.

From table C.2,

Total MVA=$(G_1 + G_2 + G_3 = 567.5MVA)$;

$G_3 = \frac{128}{567.5} \times 100 = 22\%$. This means that an equivalent wind power plant of 22% penetration level was achieved.

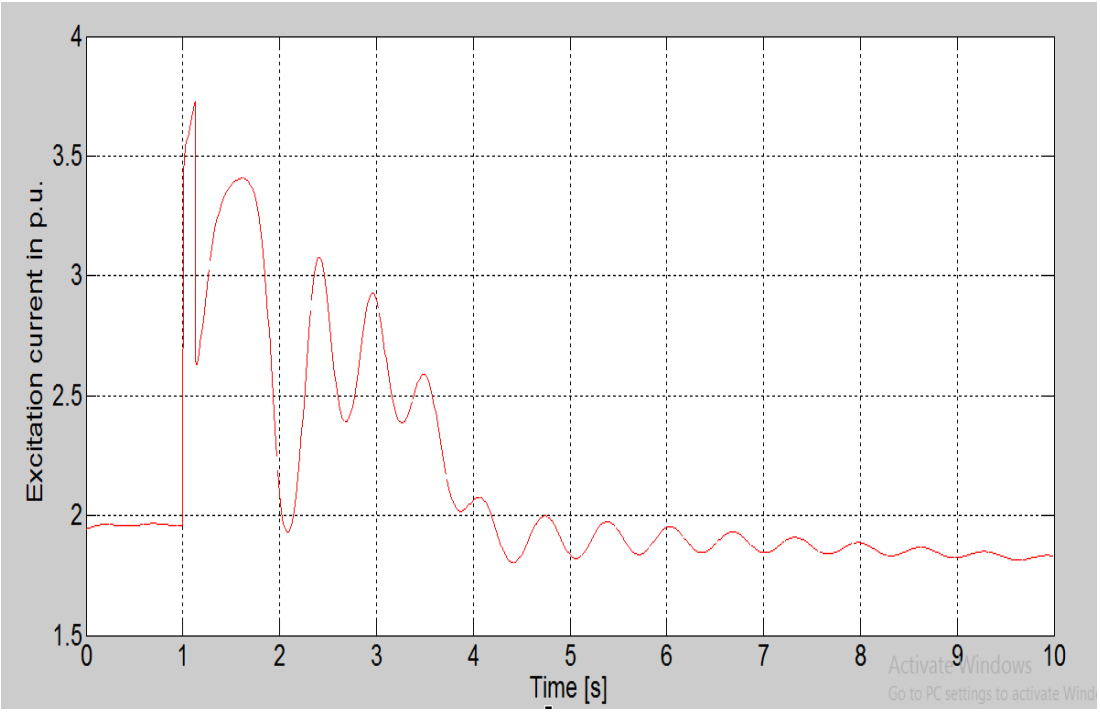

Figure 4.3: Characteristic of excitation current parameter for a fault at 1 s cleared at 1.129 s.

Figure 4.3 shows the excitation current behavior when a short-circuit fault was created at 1 s and cleared at 1.129 s. This is an indication that the system achieved a critical clearing time of 0.129 s and any time delay beyond 1.129 s will have resulted into system instability.

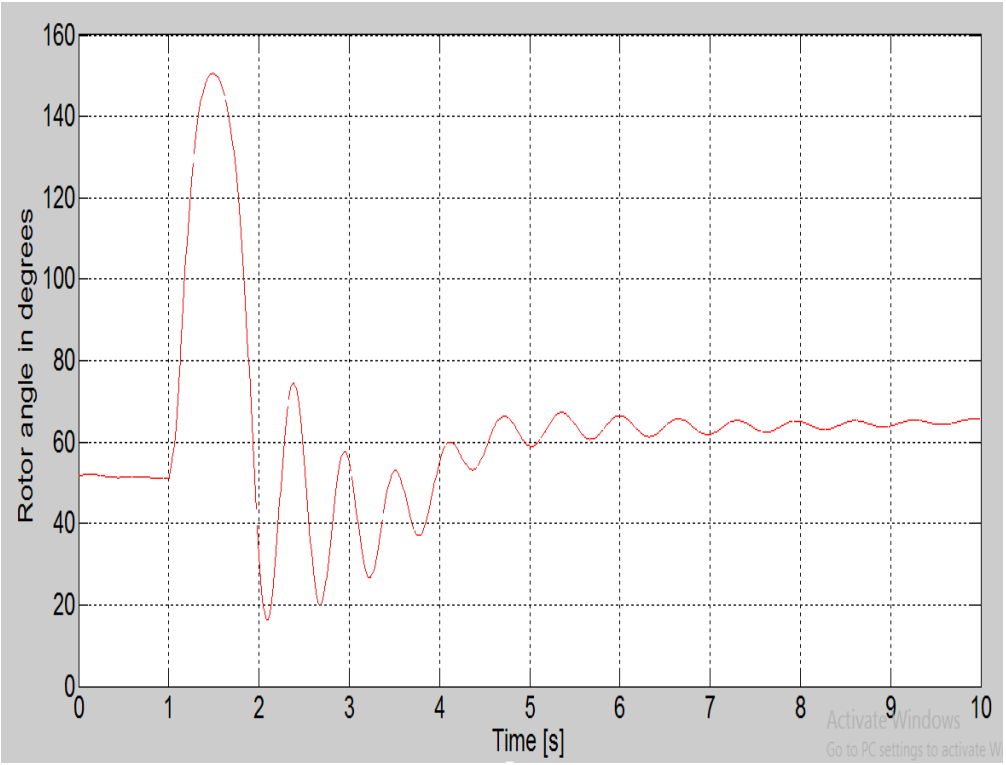

Figure 4.4: Characteristic of rotor angle parameter for a fault at 1 s cleared at 1.129 s.

Figure 4.4 show the effect of rotor angle for a system connected to a wind farm. The fault was created at 1s and cleared at 1.129 s when the oscillations died out. It is evident that the integration of wind power from doubly-fed induction generator (DFIG) increases the critical clearing time an indication that DFIG improves system transient stability.

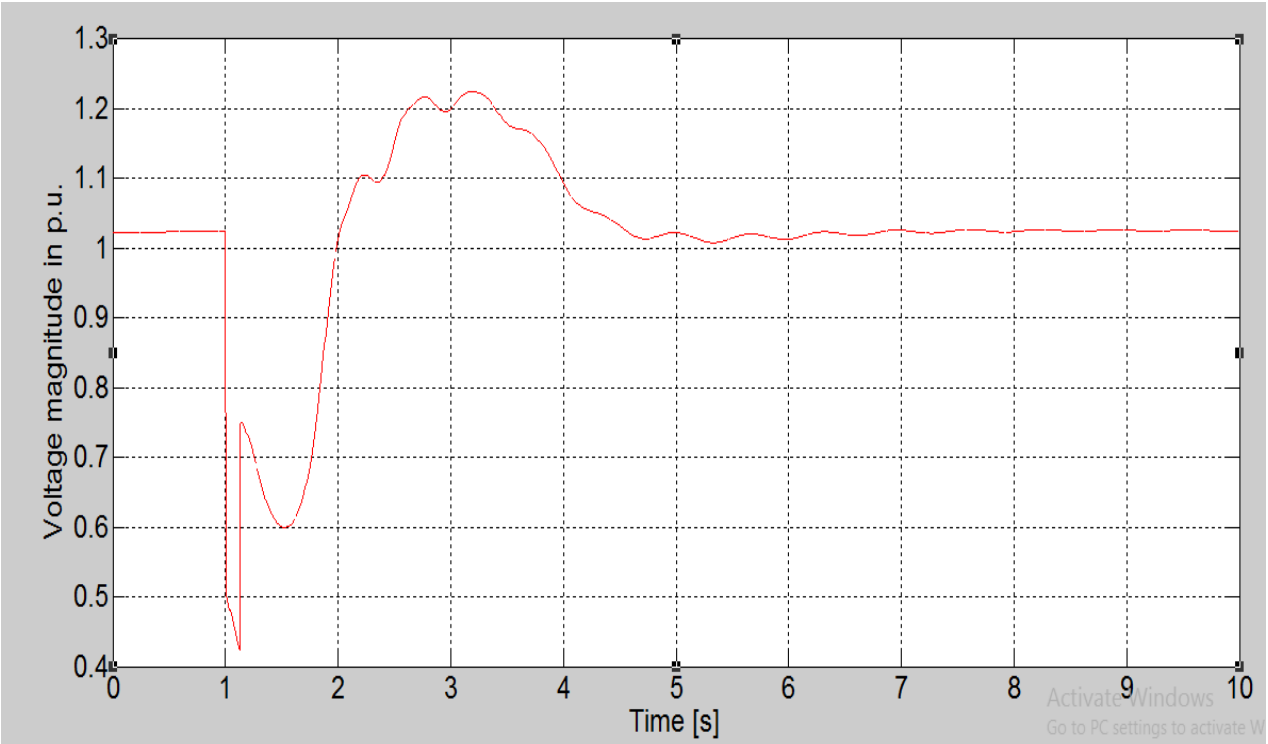

Figure 4.5: Characteristic of voltage magnitude parameter for a fault at 1 s cleared at 1.129 s.

Figure 4.5 show voltage magnitude characteristic with system attaining stability with a critical clearing time of 1.129 s. If fault clearing time was extended beyond 1.129 s, the system would have run out of synchronism resulting to continuous swing curves and indication of system instability.

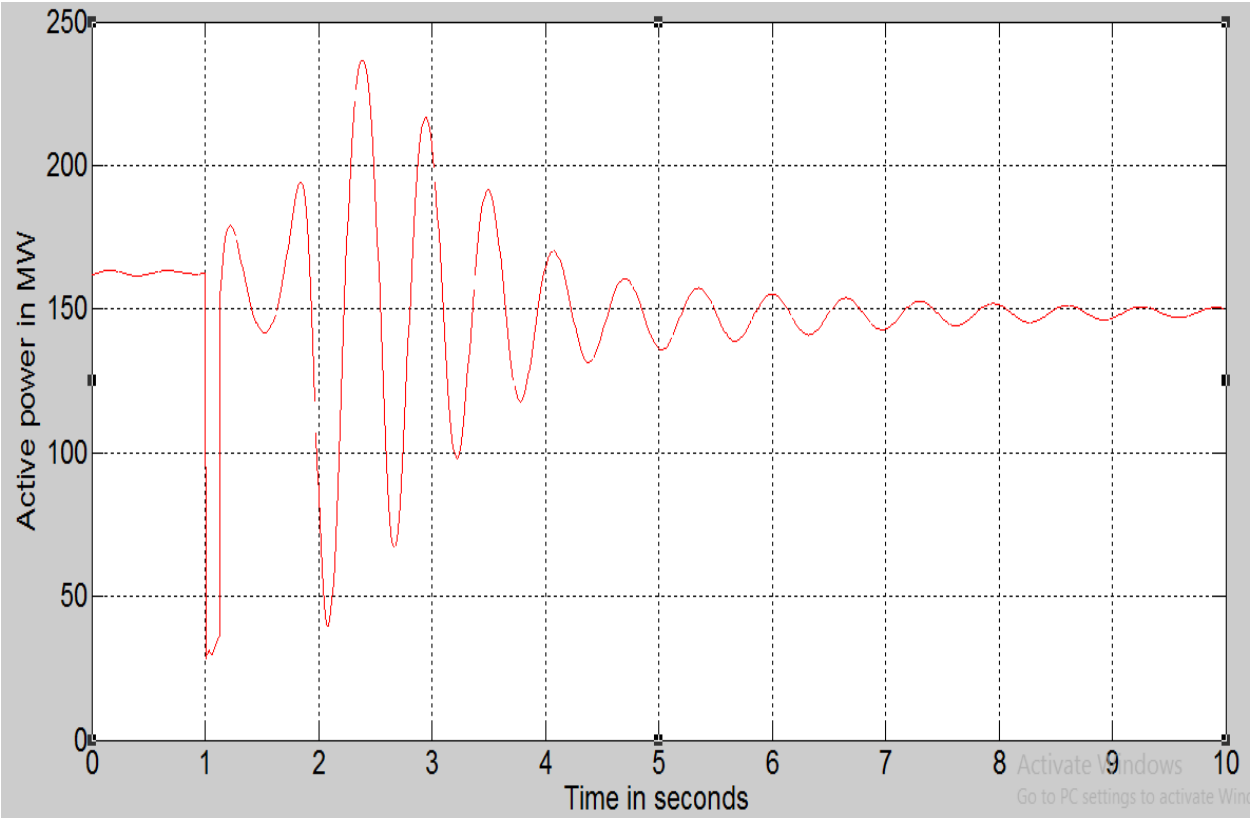

Figure 4.6: Active power for a fault created at 1 s and cleared at 1.129 s.

Figure 4.6 shows that the system stabilizes after attaining a critical clearing time of 0.129 s. Comparing the critical clearing time for figure 4.6 and figure 4.1, it clearly shows that figure 4.6 takes longer time to lose system transient stability compared to figure 4.1 that had a critical clearing time of 0.123 s. This further proves that wind farm with DFIG takes longer time to lose stability under short-circuit fault compared to conventional synchronous induction generator.

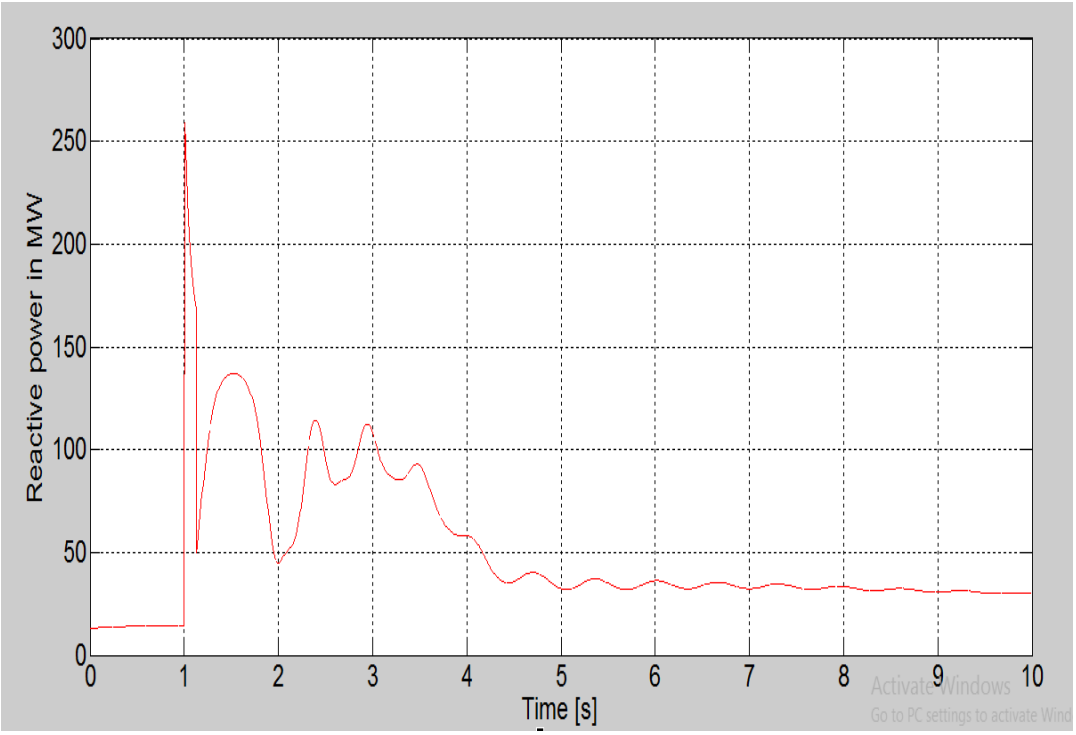

Figure 4.7: Reactive power for a fault created at 1 s and cleared at 1.129 s.

Figure 4.7 shows that the system stabilized at 1.129 s with a critical clearing time of 0.129 s. Compared to figure 4.1 whose system attained a clearing time of 0.123 s, the system with wind power in figure 4.7 increased the transient stability from 0.123 s to 0.129 s.

(11) With wind power integration at 34%

Figures 4.8 to 4.12 shows the various characteristics of G1 for a fault created at line 3 near bus 7 when G2 was replaced with an equivalent wind farm of 192MVA. From table C.2,

Total MVA=$(G_1 + G_2 + G_3 = 567.5MVA)$;

$G_2 = \frac{192}{567.5} \times 100 = 34\%$. This means that an equivalent wind power plant of 34% penetration level was achieved.

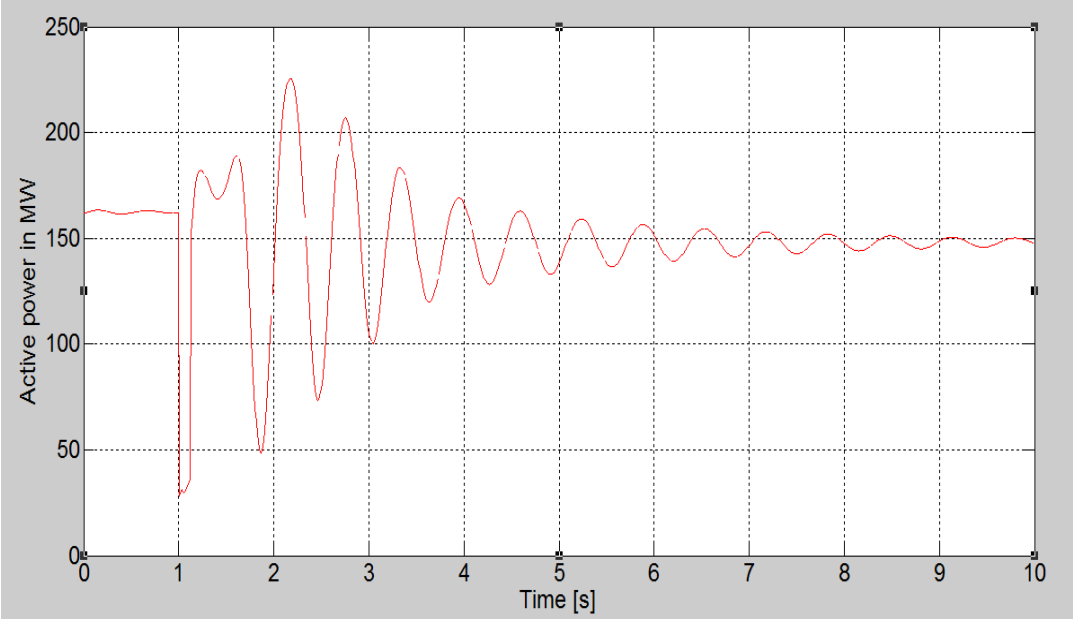

Figure 4.8: Active power for a fault created at 1 s and cleared at 1.127 s.

Figure 4.8 shows the characteristic of the active power at 34% of wind power integration. The system without wind power shown in figure 4.1 attained a critical clearing time of 0.123 s while that in figure 4.6 with wind power integration at 22% had a critical clearing time of 0.129 s compared to figure 4.10 with a critical clearing time of

0.127 s. This is an indication that wind power integration to a conventional system can only be possible to a certain level with increased system transient stability and any further integration of the wind power reduces the system transient Stability.

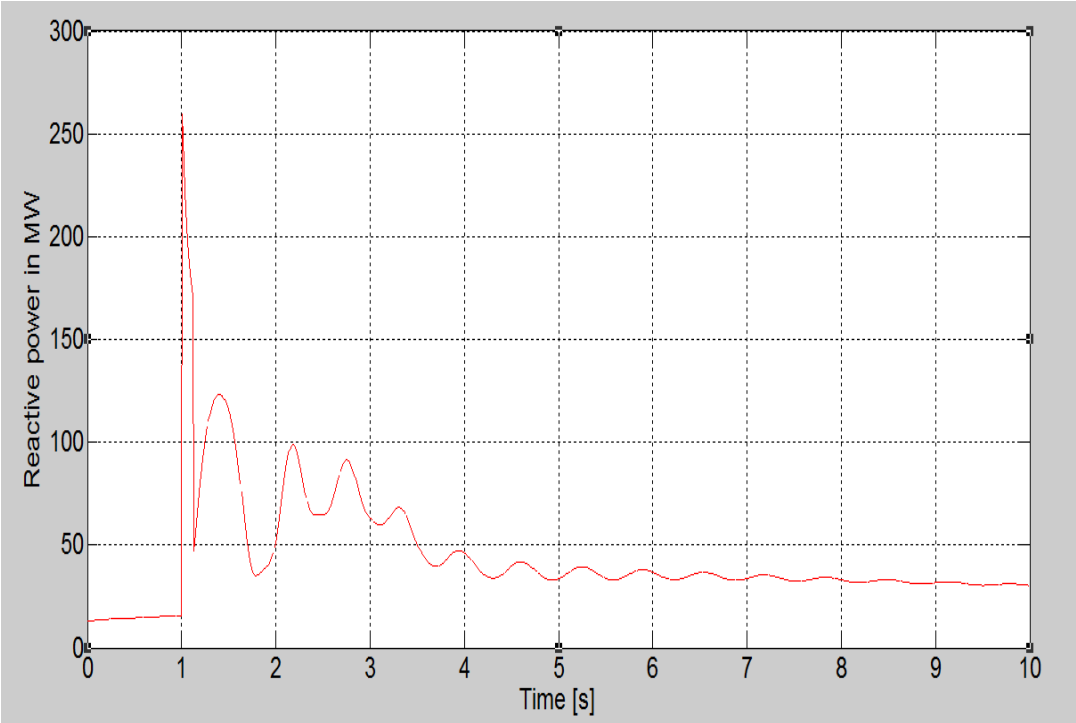

Figure 4.9: Reactive power for a fault created at 1 s and cleared at 1.127 s.

Figure 4.9 shows the characteristic of the reactive power at 34% of wind power integration. The system achieved a critical clearing time of 0.127 s. Figure 4.7 shows a system with 22% wind power integration with a critical clearing time of 0.129 s. This clearly shows that the critical clearing time reduced from 0.129 s to 0.127 s respectively subsequently reducing the transient stability period for the system.

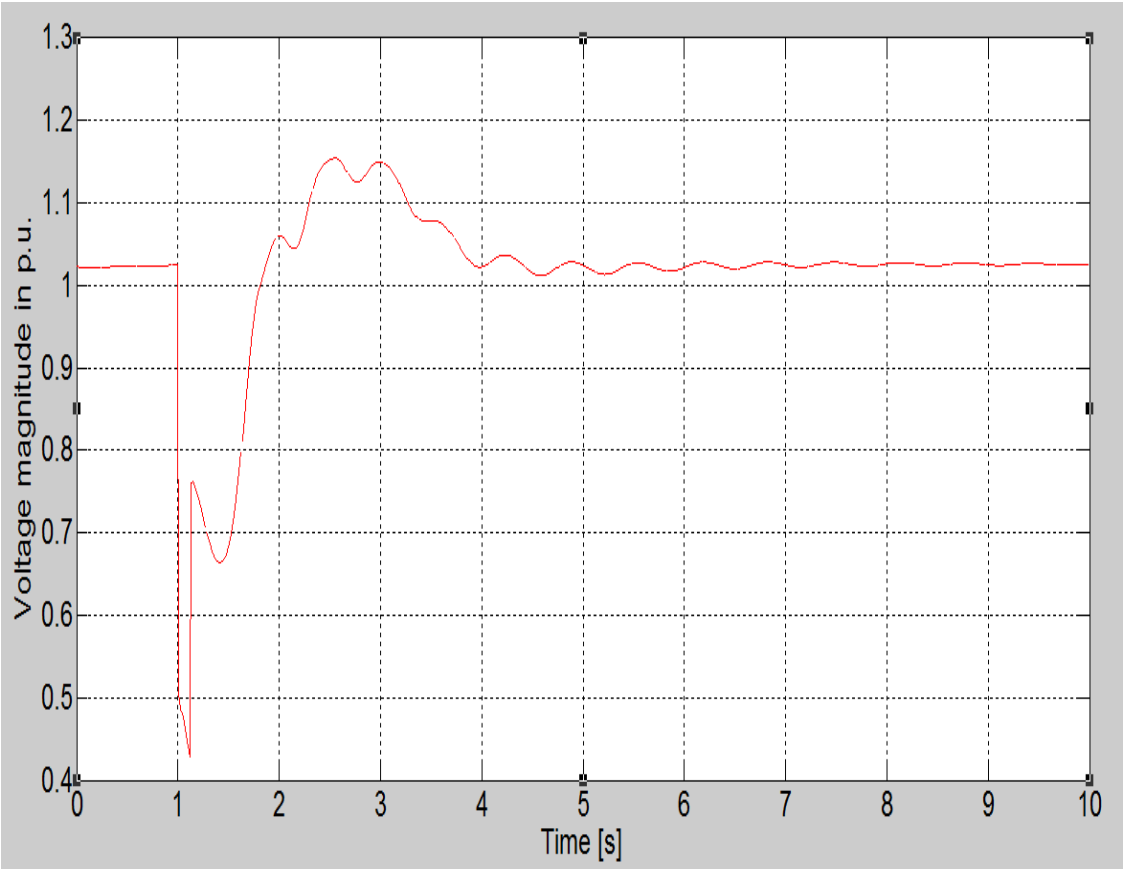

Figure 4.10: Voltage magnitude for a fault created at 1 s and cleared at 1.127 s.

Figure 4.10 shows the characteristic of voltage magnitude at 34% of wind power integration. The system achieved a critical clearing time of 0.127 s. This shows reduced critical clearing time compared to system with 22% wind power integration.

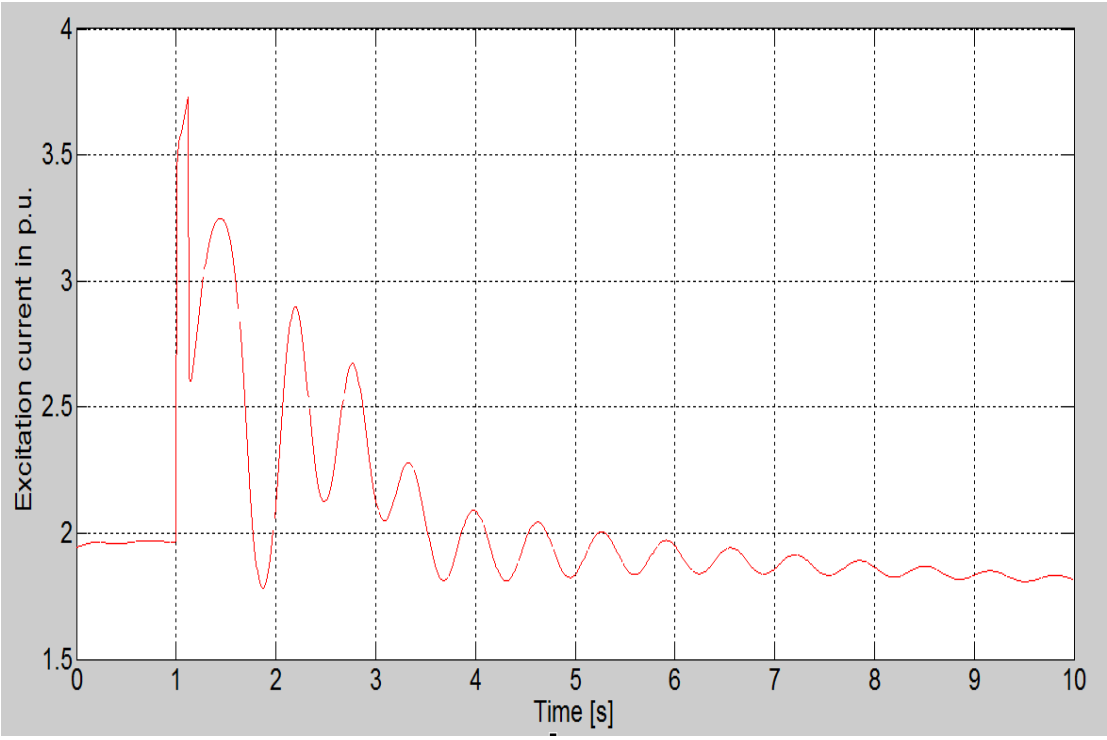
Excitation current in p.u.
Time [s]
4
3.5
3
2.5
2
1.5
0
1
2
3
4
5
6
7
8
9
10

Figure 4.11: Excitation current for a fault created at 1 s and cleared at 1.127 s

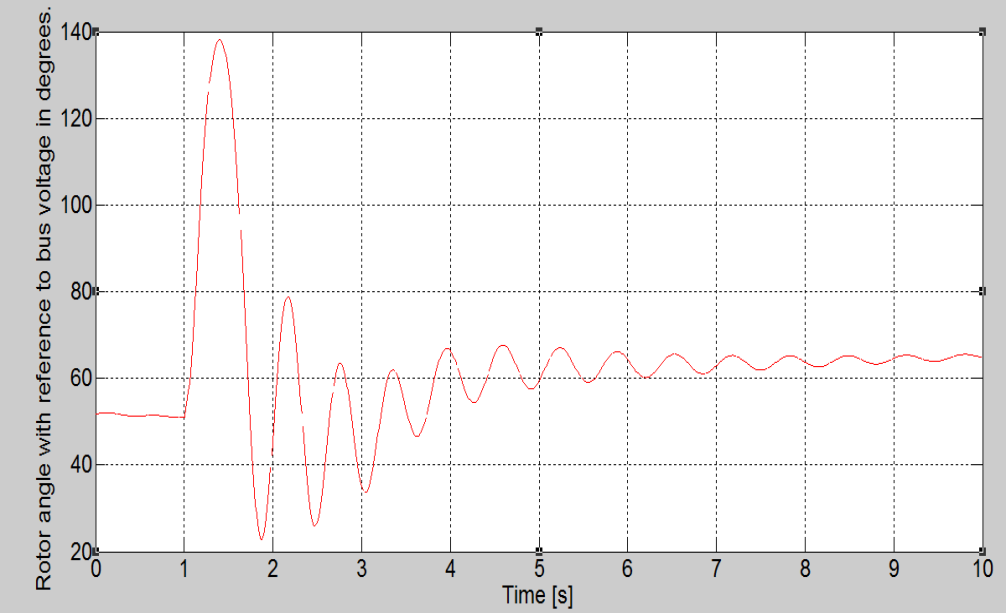

Figure 4.12: Rotor angle for a fault created at 1 s and cleared at 1.127 s.

Figures 4.11 and 4.12 shows the characteristics of excitation current and rotor angle with reference to bus voltage at 34% wind power integration. The system stabilized at 1.127 s with a critical clearing time of 0.127 s while the critical clearing time for figures 4.3 and 4.4 with 22% of wind power integration had a critical clearing time of 0.129 s. The system with 22% wind power integration shows increased critical clearing time and transient stability while the system with 34% recorded reduced critical clearing time to 0.127 s. Therefore, wind farm enhances the transient stability thus allowing greater wind power integration, however, as the amount of wind power to the grid is increased, the transient stability improves to a certain level before it start reducing.

4.3 Performance of the Proposed VSC-HVDC System with Various Control Strategies.

In this thesis, two control strategies were selected for each converter to analyze the grid performance both under normal conditions and under faults. The developed VSC-HVDC

controllers were implemented using DigSilent Power Factory software and subjected to a three-phase to ground fault to analyze the controller's performance ability to respond to such disturbance and restore the system to stability.

4.3.1 Active power direction reversal

The modeled VSC-HVDC controller is tested to analyze its effectiveness in regard to the active power variation on other parameters of interest. The active power reversal with Active and Reactive (PQ) power controller occurred at 3 s and 5 s respectively on grid side 2. The active power is reversed from -1 P.u. to 1 P.u. for grid side 2 while that for grid side 1 is unchanged as shown in figure 4.13.

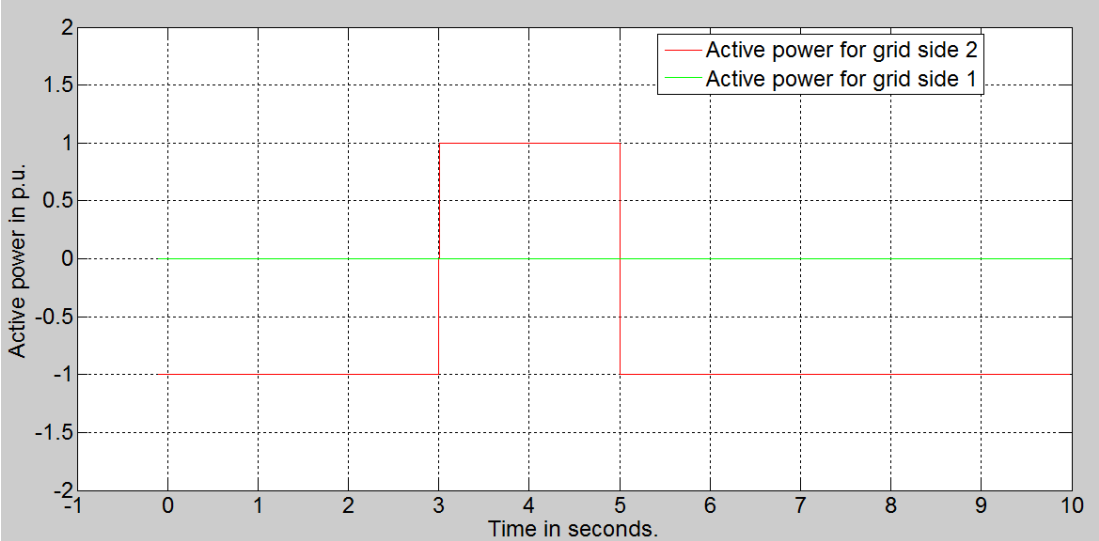

Figure 4.13: Active and Reactive Power controller.

Figure 4.13 shows a system with PQ controller. The short-circuit fault on grid side 2 affected the active power on this grid only while the active power controller on grid side 1 remained unaffected. This is an indication of independent control of active and reactive power by the PQ controller.

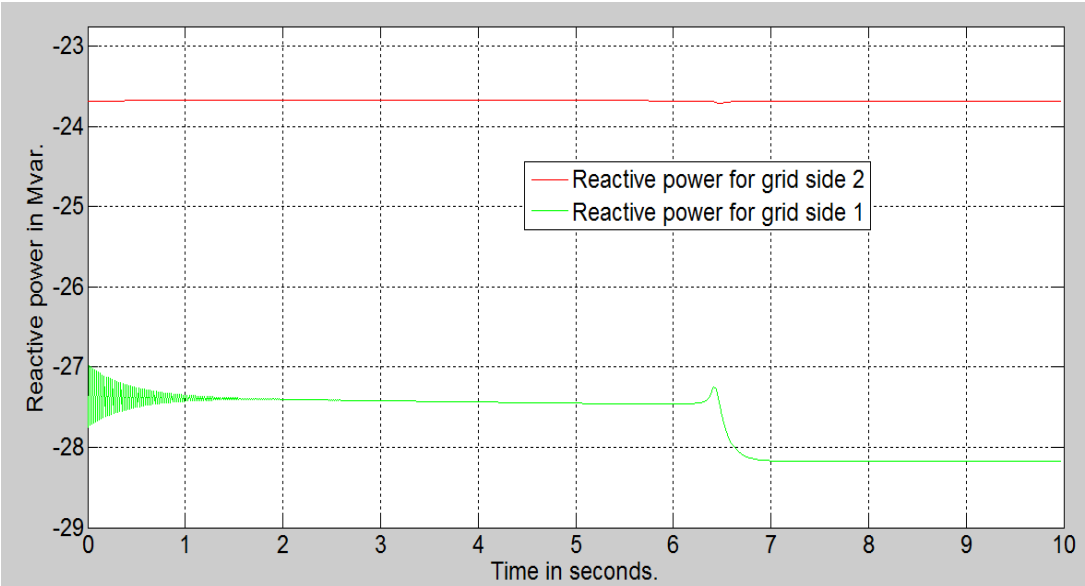

Figure 4.14: Reactive power in Mvar.

Figure 4.14 shows that the reactive power changes at the two grids are slightly small except for some transients; it therefore means that the reactive power control is independent of the active power.

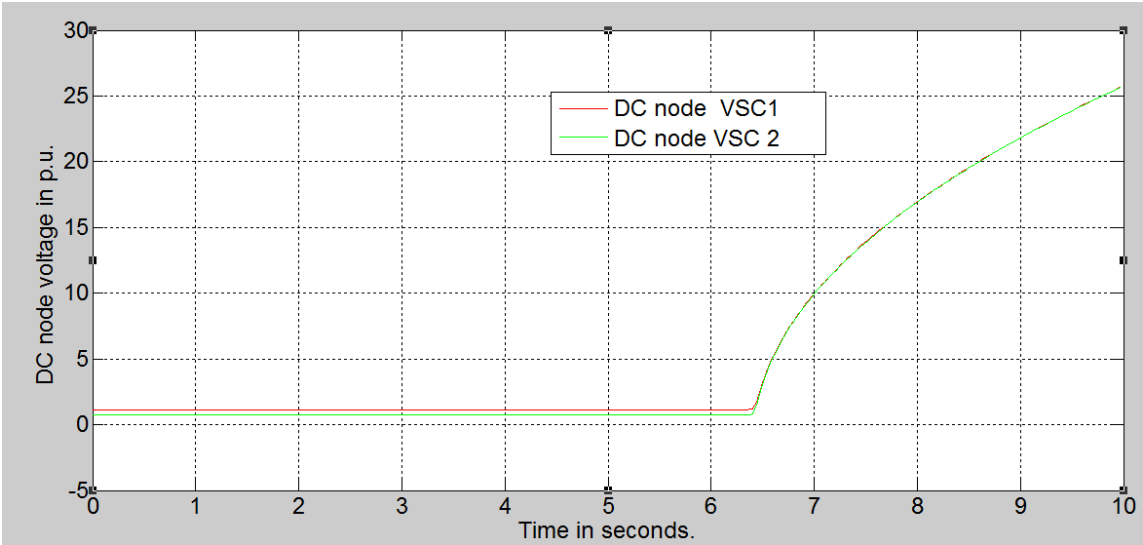

Figure 4.15: DC node voltage in p.u.

Figure 4.15 shows that the DC link bus voltages are at the desired value of 1pu and are thus not affected by the parameter event between 3s and 5s, respectively.

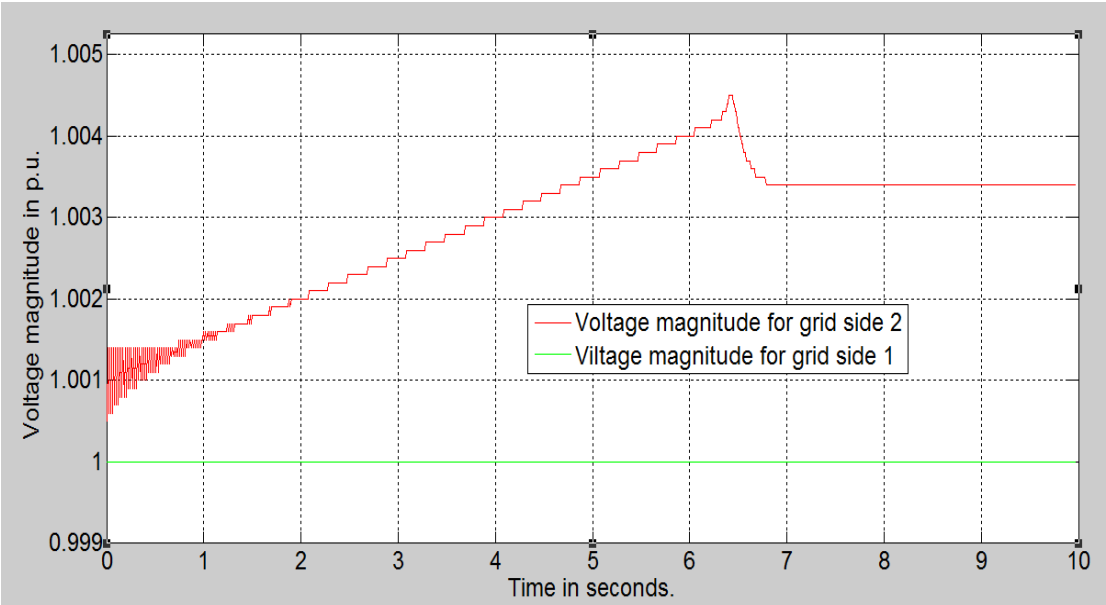

Figure 4.16: VSC voltage in p.u.

Figure 4.16 shows a slight change in voltage for VSC-2 (grid side 2) because the occurrence of the short-circuit fault is near this bus while VSC 1 (grid side 1) has no voltage variation. This behavior shows that a change in voltage has greater impact on reactive power changes than the active power.

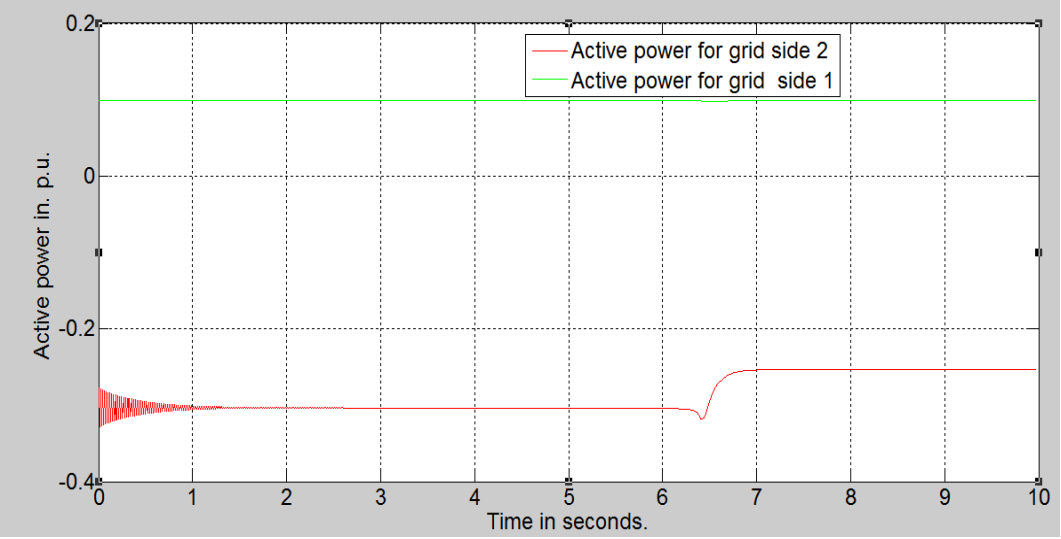

Figure 4.17: Active power controller.

Figure 4.17 shows active power reversal as ordered by the PQ controller. This proves that active power is independently controlled by the two grids. A variation of active power in one grid has no impact on the other grid.

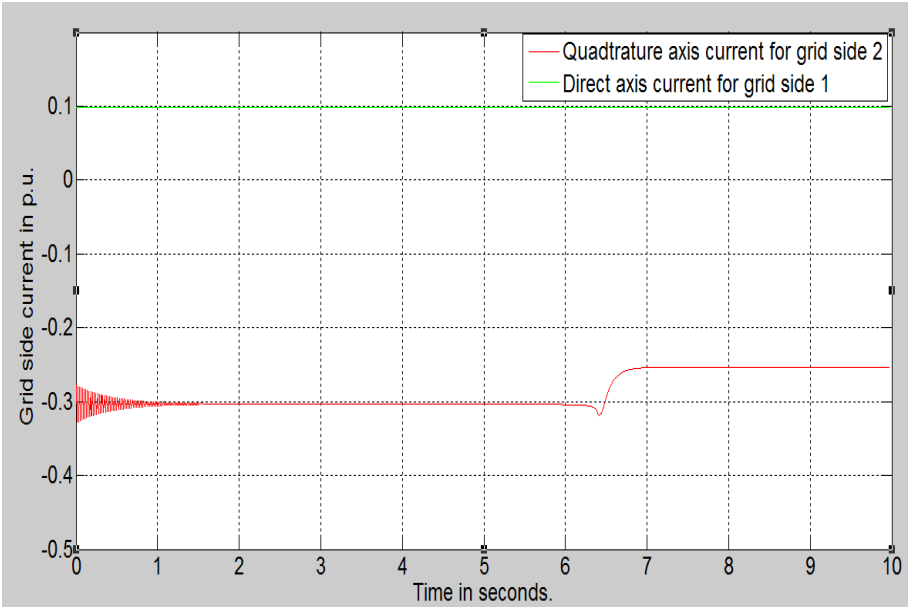

Figure 4.18: Inner current controller.

Figure 4.18 shows an inner current controller with some variations on the q-axis current components and less variation on d-axis current components in response to the active

power reversal. This is a true reflection of an independent control of the reactive and active power. It also demonstrates that reactive power is dependent on q-axis components while active power depends on d-axis current component. The stability of the inner current controller is attained.

4.3.2 Reactive power flow direction reversal

Reactive power control is a continuous process carried out in power transmission systems. In this research, the reactive power is delivered to the AC system by VSC through the control of phase and magnitude of the converter voltage. Therefore, the ability to control reactive power is important to any applications and the voltage is dependent on the reactive power in the system.

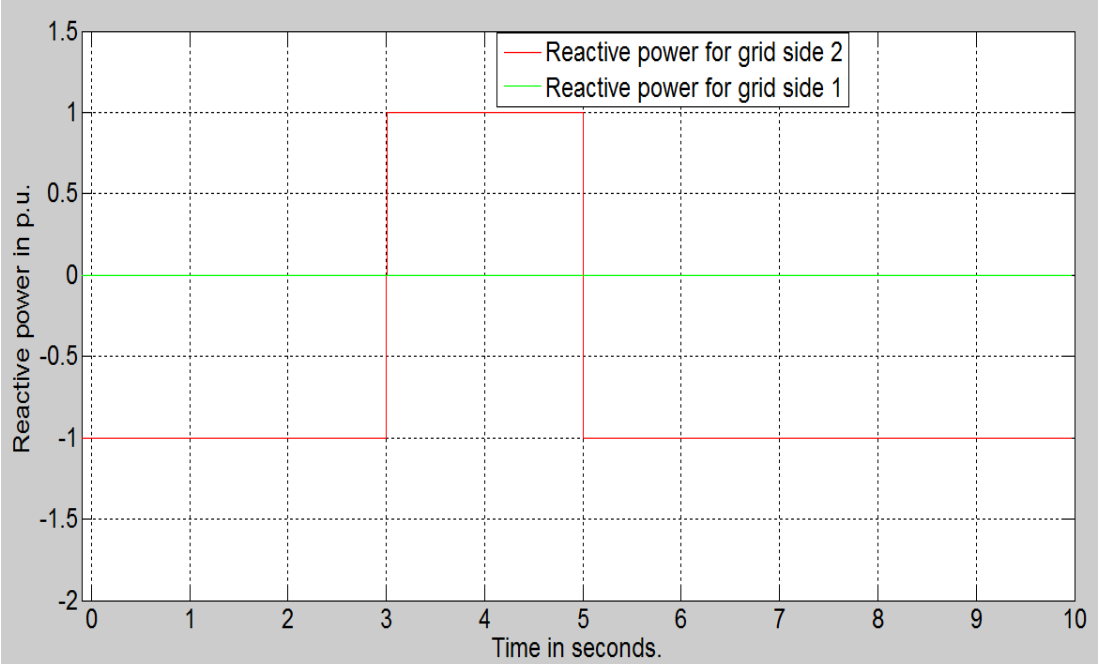

Figure 4.19: PQ controller.

The reactive power reversal at PQ controller took place at 3 s and 5 s respectively. Figure 4.19 shows that the reactive power is reversed from 1P.u to -1P.u for grid side 2 while that for grid side 1 is unaffected an indication of grid independence.

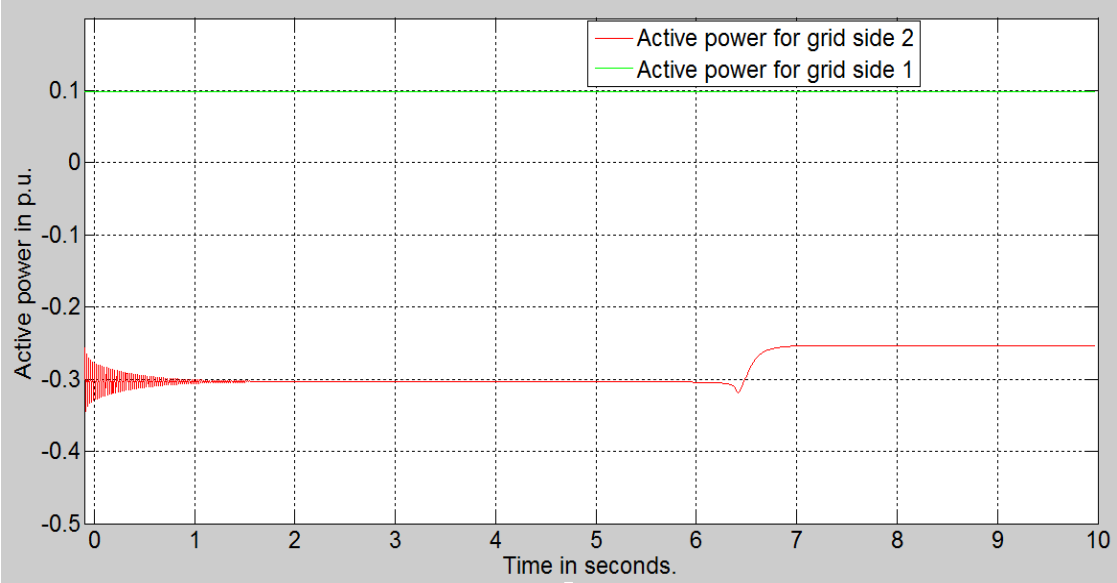

Figure 4.20: Active power controller.

Figure 4.20 shows very slight variations in active power. This shows a well-designed VSC-HVDC system with independent control of active and reactive power.

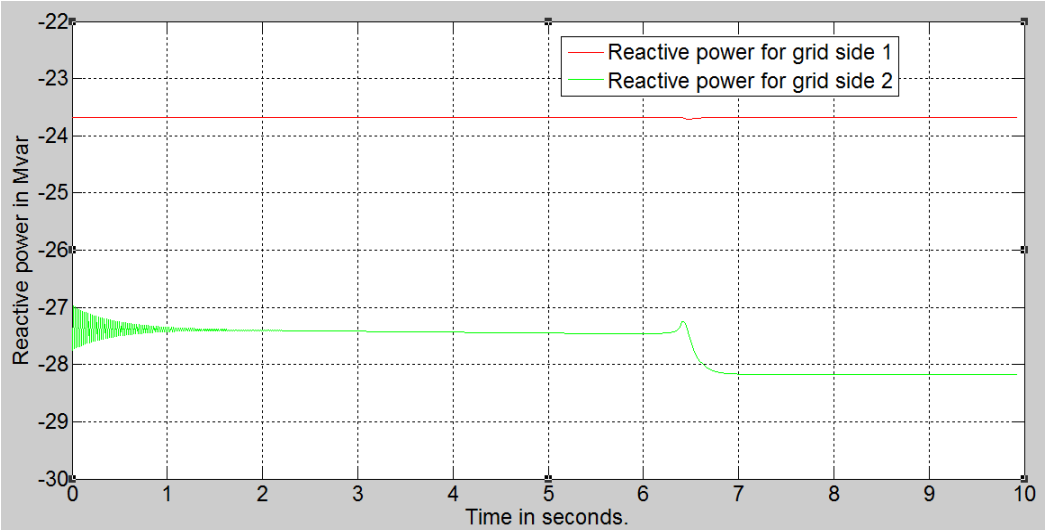

Figure 4.21: Reactive power controller.

Figure 4.21: shows reactive power changes at grid side 2 while at grid side 1, there is no variation in reactive power. This shows that the reactive power at the two grids is independent of each other.

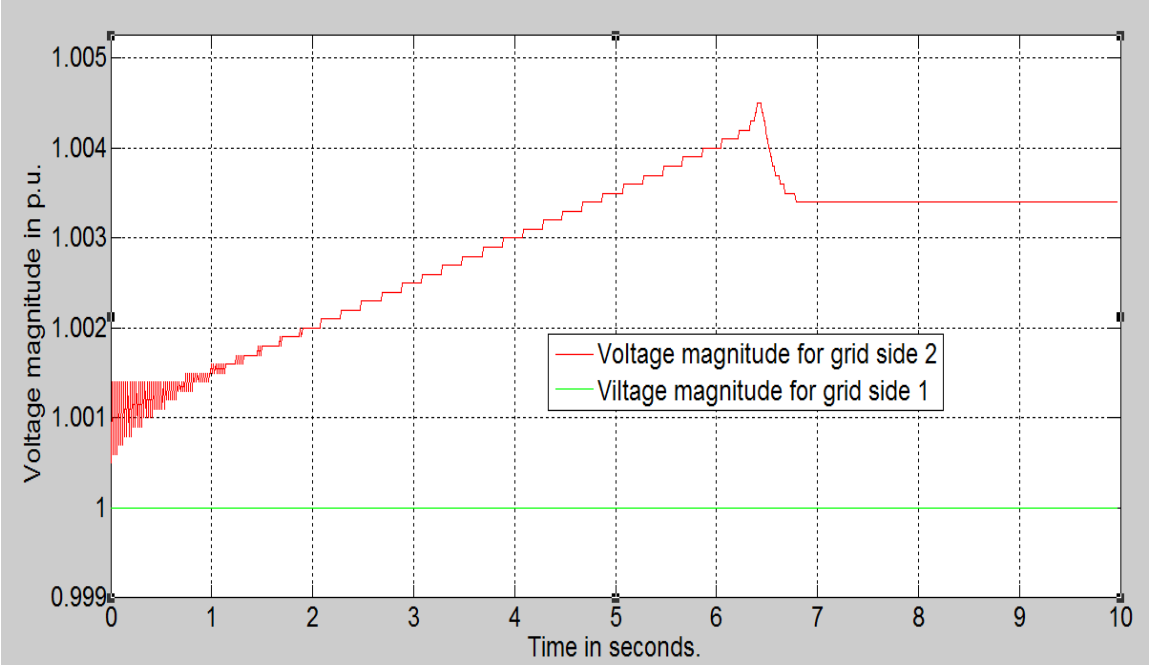

Figure 4.22: VSC voltage magnitude.

Figure 4.22 shows the converter bus voltage at VSC 2 (grid side 2) achieved transient stability from its pre-disturbance value without affecting the converter bus voltage at VSC1. When the reactive power returns to its pre-disturbance value, VSC 2 bus voltage returns to a value close to 1pu (nominal value). This is an indication of dependency of bus voltage on the reactive power injected or absorbed to/from it. Consequently, the bus voltage at VSC1 (grid side 1) shows no change due to the fact that the reactive power at this side is unaffected. Hence, during contingencies, the transmission system operator monitors the system voltage by adjusting the reference reactive power set value until the desired system voltage and stability is achieved.

4.3.3 DC voltage step responses

In this case, at t=3 s the dc reference value Vdc_{ref} increased from 1 p.u. value to 1.5 p.u. and then at 5 s the value is again reduced to the value 1pu. It is a normal practice for power Transmission Company to transfer power across the DC link at a certain DC

voltage; this can be done through changing the DC voltage reference value as shown in Figure 4.23.

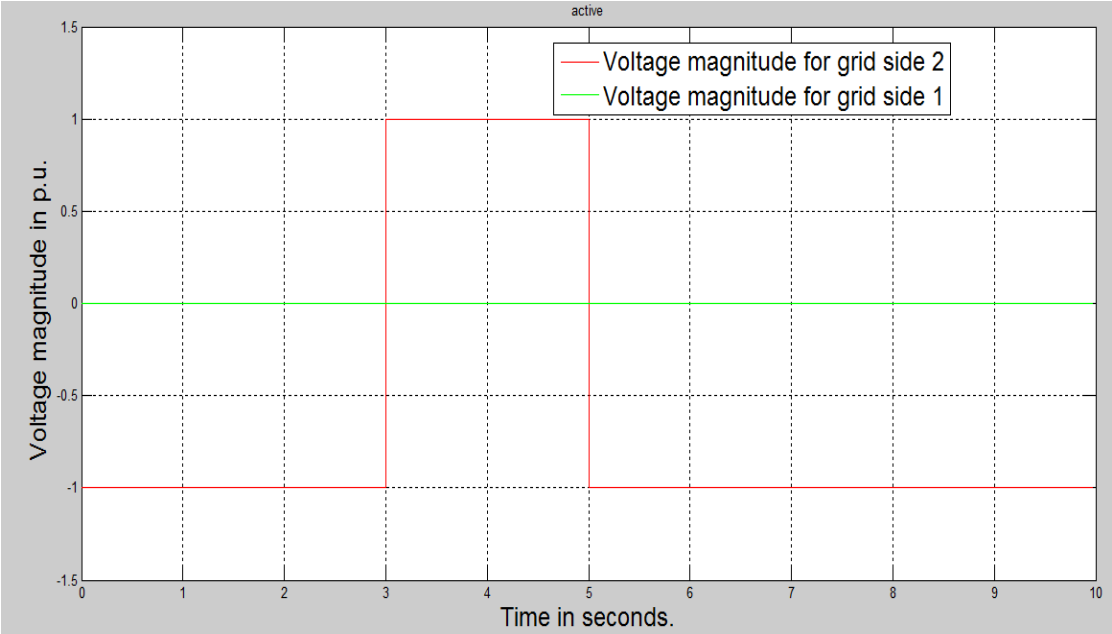

Figure 4.23: Voltage controller.

Figure 4.23 represent the characteristics of voltage controller when step voltage is increased. This shows that a fault on grid side 2 has no impact on grid side 1, an indication of correct designed voltage controller.

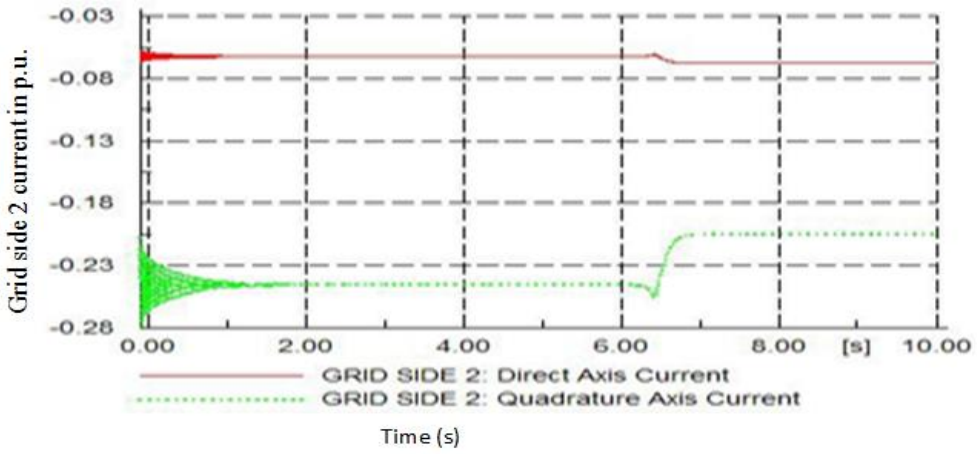

Figure 4.24: Inner current controller.

Figure 4.24 shows small variations for grid side 2 which quickly track the pre-disturbance value.

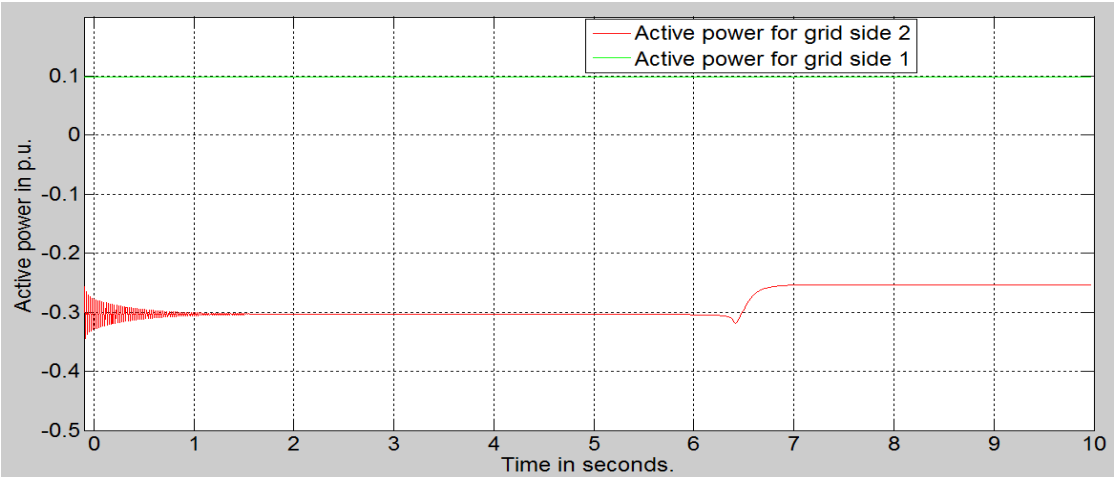

Figure 4.25: Active power controller.

Figures 4.25 and 4.26 shows very slight variations for active power on grid side 2 and are thus insignificant. This shows good design of the active and reactive power controllers.

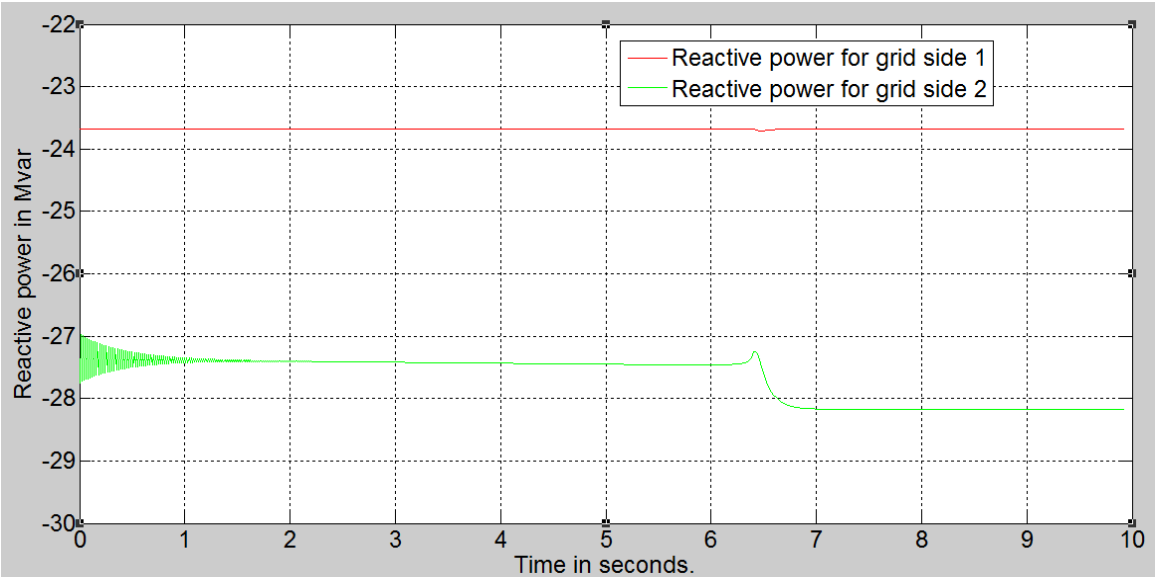

Figure 4.26: Reactive power controller.

Figures 4.13-4.26 shows the performance of the developed VSC-HVDC controllers. From the simulations, it is clear that the VSC-HVDC controllers carry out their functions of controlling the DC voltage, active and reactive power effectively. For example, the PQ controller designed is able to control the active and reactive power independently by ensuring that what happens on one grid has no impact on the other grids. This ensures that the power flow balance is maintained thus reducing the power losses that would have been generated by the unbalanced powers. The voltage controller maintained the DC voltage constant by controlling the reactive power flow in the power network.

4.4 Analysis of VSC-HVDC system for transient stability improvement of a power system with wind power integration.

Figures 4.28-4.31 shows the critical clearing time of a conventional grid connected without wind farm, conventional grid with wind farm and a conventional grid connected with wind farm through a VSC-HVDC transmission system. A three-phase to ground fault was initiated along the transmission line and cleared after the Preset time. Figure 3.14 in chapter 3 was modeled in DigSilent software and Load flow simulation results shown in figures 4.27- 4.31 respectively.

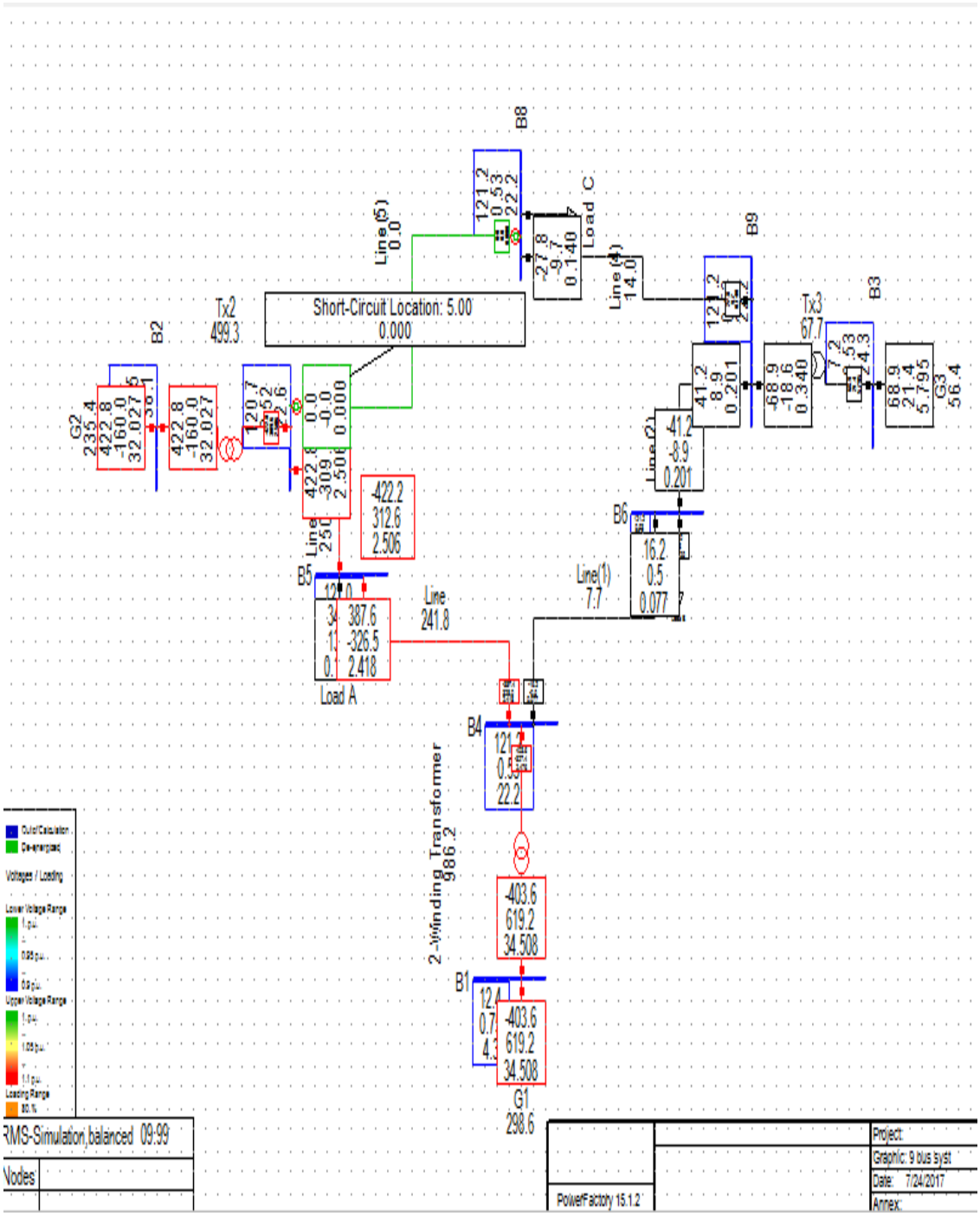

Figure 4.27: An IEEE 9-bus system indicating point of fault with load flow solution.

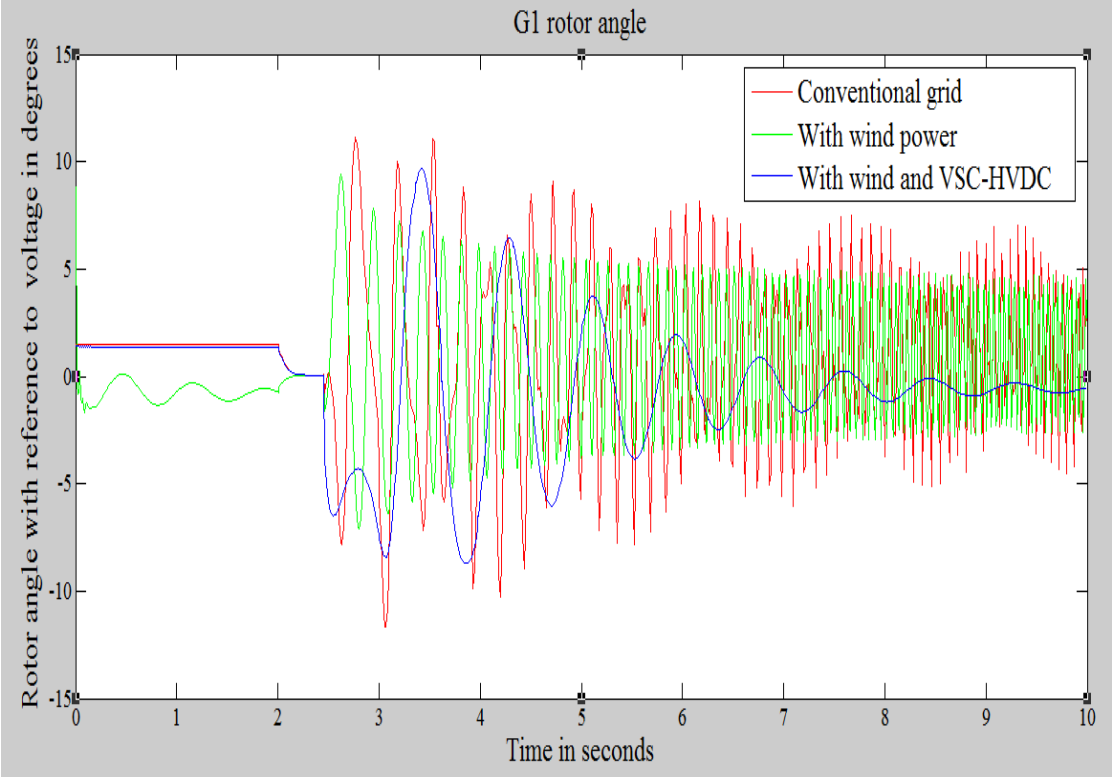

Figure 4.28: G1 rotor angle for a fault created at 2 s and cleared at 2.45 s.

Figure 4.28 shows a conventional grid connected with a wind farm through a VSC-HVDC system were stable with a critical clearing time of 0.45 s while the other two combinations were unstable at 2.45 s. This indicates that transmission system based on VSC-HVDC enhanced controllability with large wind power integration and improves power system transient stability.

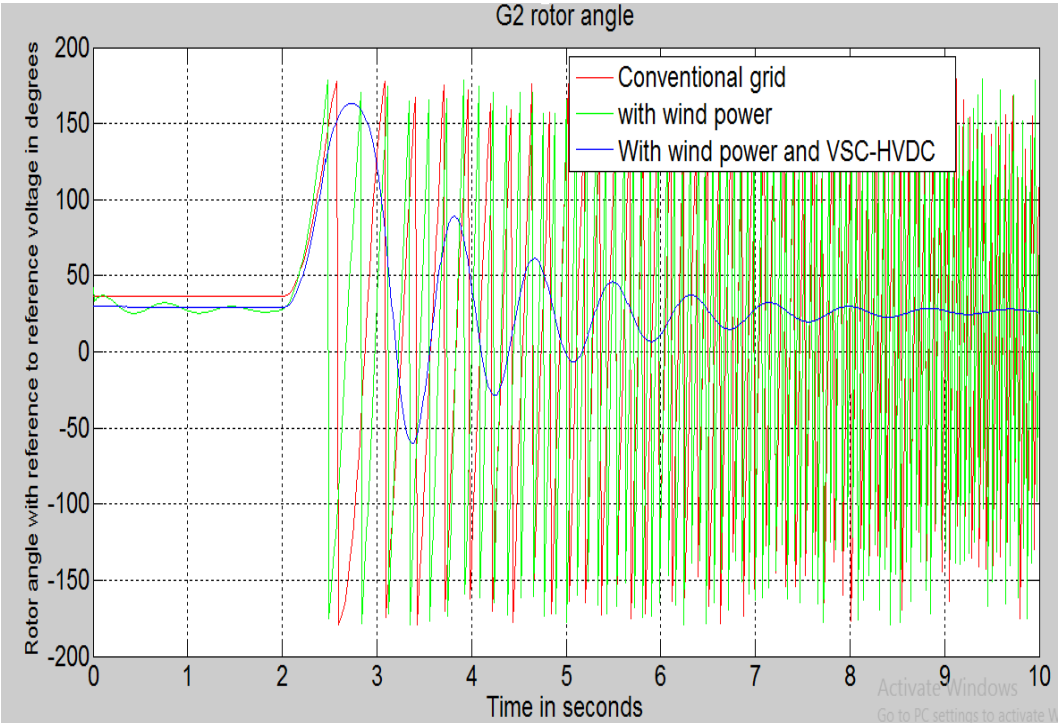

Figure 4.29: G2 rotor angle for a fault at 2 s cleared at 2.45 s.

Figure 4.29 shows G2 with a fault near bus 7. The rotor angle attained stability at 2.45 s for the IEEE 9-bus connected with wind farm through a VSC-HVDC transmission system whereas the other two configurations are unstable at 2.45 s.

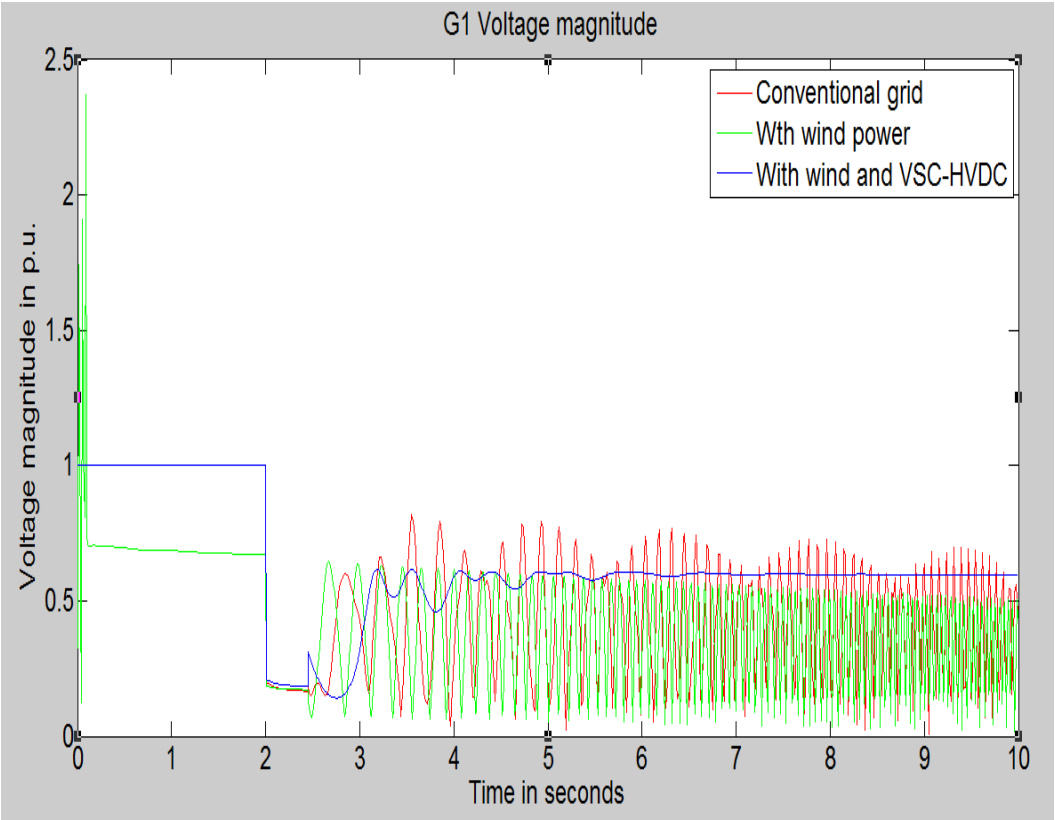

Figure 4.30: G1 Voltage magnitude for a fault 2 s cleared at 2.45 s.

Figure 4.30 shows the 9-bus with wind power connected through a VSC-HVDC system attained transient stability at 2.45 s for G1 while the other two configurations are unstable.

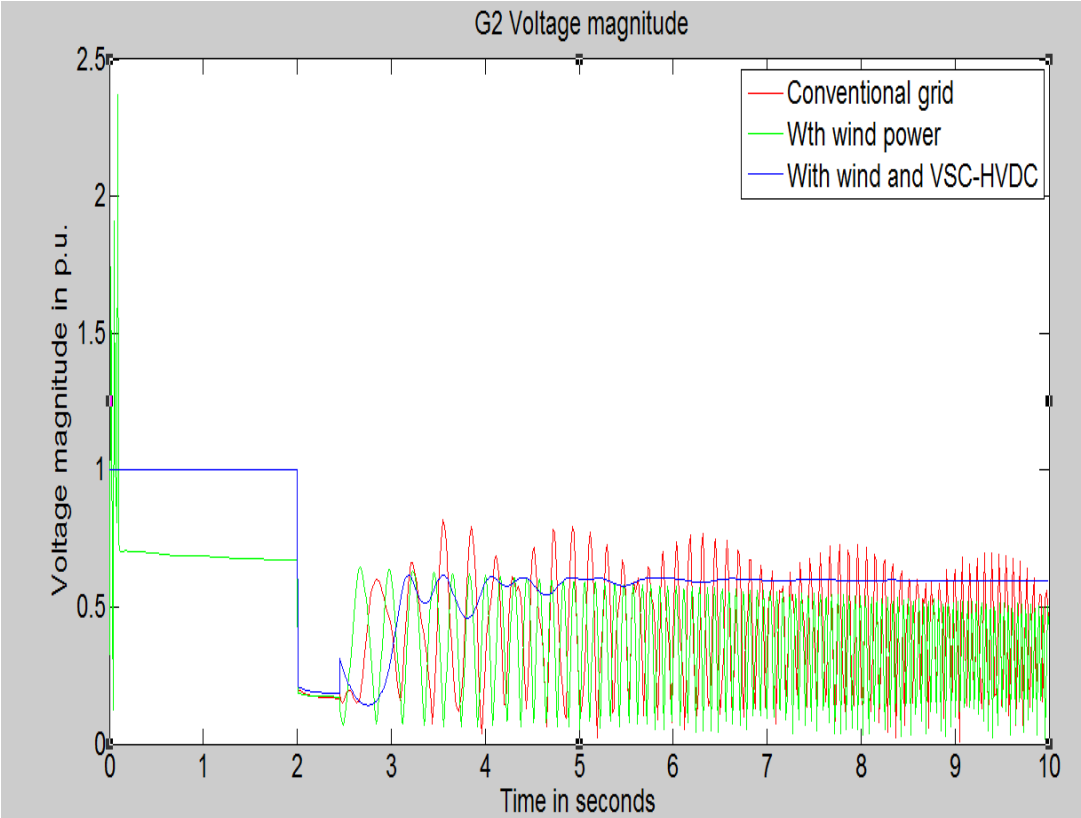

Figure 4.31: G2 voltage magnitude for a fault at 2 s cleared at 2.45 s.

Figure 4.31 shows the wind farm connected through a VSC-HVDC transmission system attained transient stability at 2.45 s whereas the other two configurations are unstable.

Figures 4.28-4.31 shows that rotor angle and voltage magnitude for both generator 1 and 2 took less time to attain stability at 2.45 s for an IEEE 9-bus system connected to a wind farm through a VSC-HVDC system. The simulation results for the other two scenarios indicate that after the fault is cleared at 2.45 s, the system oscillatory characteristics continued an indication of system instability.

4.5 Wider tuning of the proposed VSC-HVDC controllers

The analytical expressions for the inner current controller and the DC voltage controller are presented in the form of second order closed loop systems using the two tuning

techniques namely, Modulus Optimum Criteria (MOC) and Symmetrical Optimum Criterion (SOC) with diverse values of symmetrical distance selected. Simulation results generated based on MOC and SOC are shown in the subsections that follow.

4.5.1 Tuning of inner current controller by modulus optimum criterion (MOC).

Table 4.1 shows the calculated inner current controller parameters based on equations (3.40) and (3.51) for different values of symmetrical distance while figures 4.32-4.42 shows the bode plots and step responses of the inner current controller generated for various values of symmetrical distances.

Table 4.1: Calculated parameters for the Inner current controller.

A	**T_i**	**K_p**	**T_a**
2	0.063694	64.51	0.0001
3	0.063694	96.3	0.000067
4	0.063694	129	0.00006
5	0.063694	161.1	0.00004
6	0.063694	195.5	0.000033
8	0.063694	258	0.000025

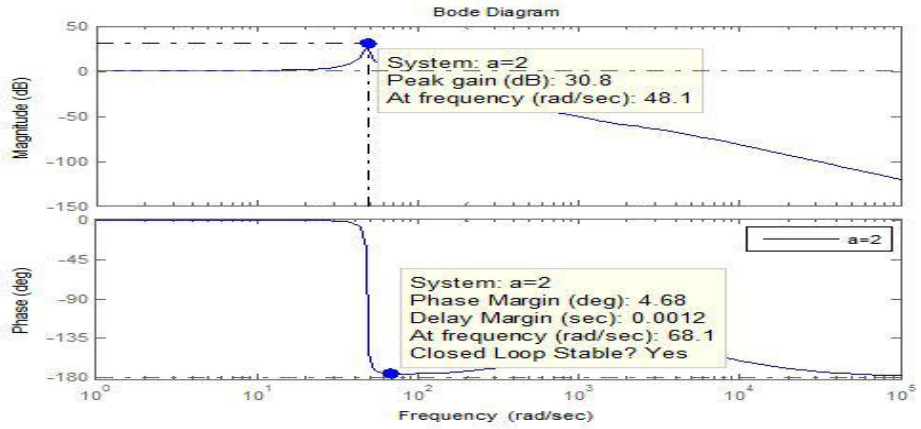

Figure 4.32: Bode plot of inner current controller with a=2.

Figure 4.32 shows the bode plot of inner current controller tuned based on modulus optimum criterion with symmetrical distance equal to 2. Figure 4.32 further indicates phase margin of 4.68° and time delay of 0.0012 s. At a=2, shown in table 4.1, the proportional gain and time constant are 64.51 and 0.063694 respectively. The system is stable since it has shorter response time and improves the damping factor conditions necessary for system to be stable.

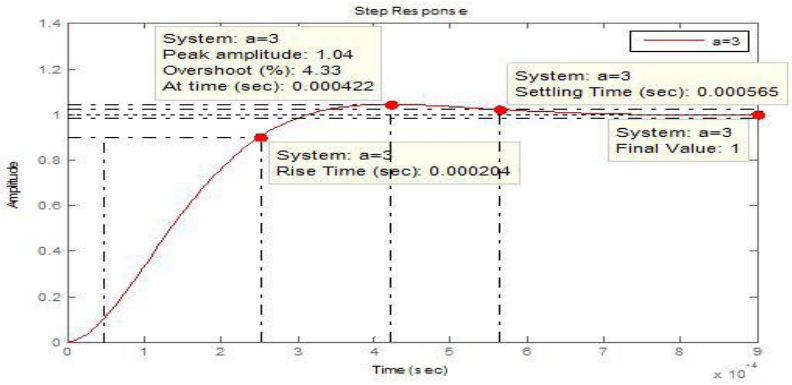

Figure 4.33: Step response of inner current controller with a=3.

Figure 4.33 shows the step time response of inner current controller with a==3 which gives the maximum Overshoot of 4.33, peak amplitude of 1.04, Time for maximum overshoot, *tm* = 0.00042s, Settling time, using 2% criteria, *ts* = 0.000565 s. Figure 4.37 further shows good system response time of 0.000204 s.

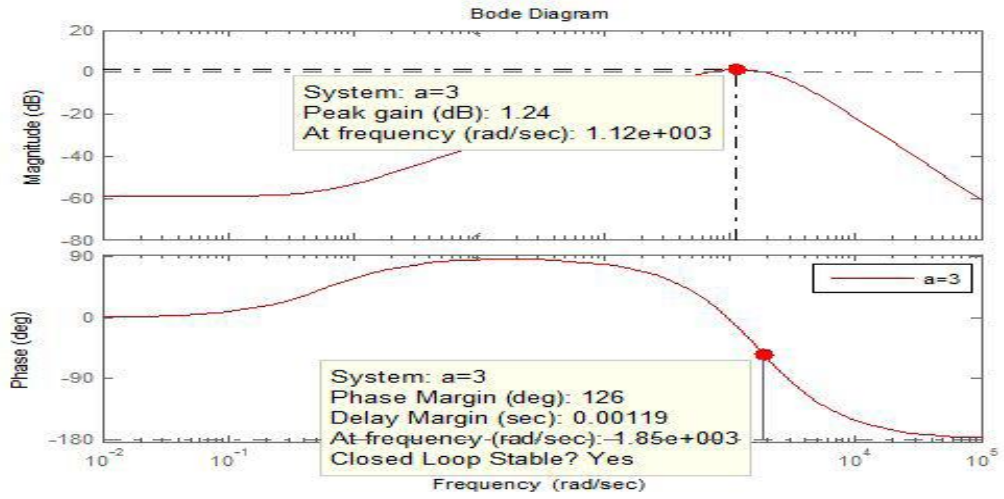

Figure 4.34: Bode plot of inner current controller with a=3.

Figure 4.34, shows the bode plot of inner current controller with a=3. The open loop bode plot gives the open loop crossover frequency of $1.12 \times 10^3 rad/sec$ =(180Hz), which is about 27 times smaller than the switching frequency of 5kHz, indicating acceptable ratio (Mohan, 2003). Figure 4.38 shows that increased value of symmetrical distance increases the phase margin and improves the damping ratio though the system response has become slower than that at a=2.

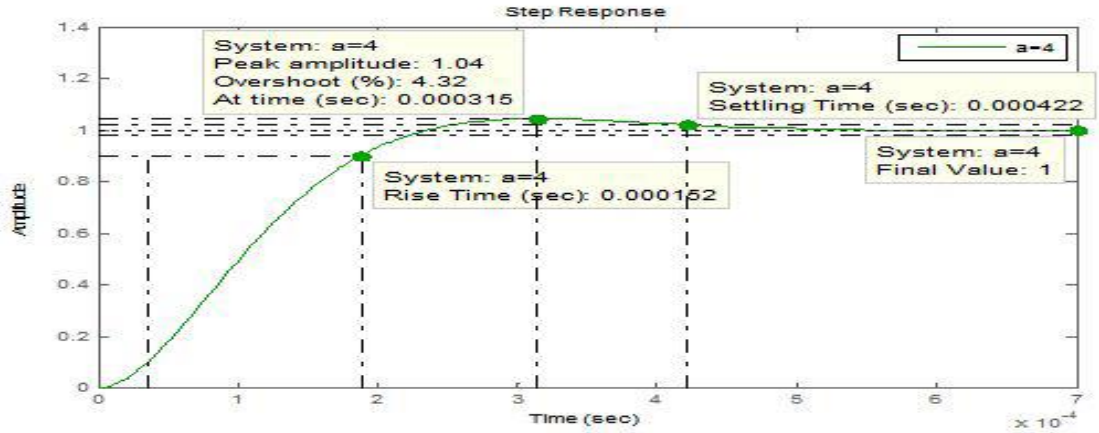

Figure 4.35: Step response of inner current controller with a=4.

Figure 4.35 shows the step time response of inner current controller with a==4 which gives the maximum Overshoot of 4.32%, peak amplitude of 1.04, time for maximum overshoot, *tm* = 0.000315s, Settling time, using 2% criteria, *ts* = 0.000422 s. Figure 4.35 further shows good system response time of 0.000152 s.

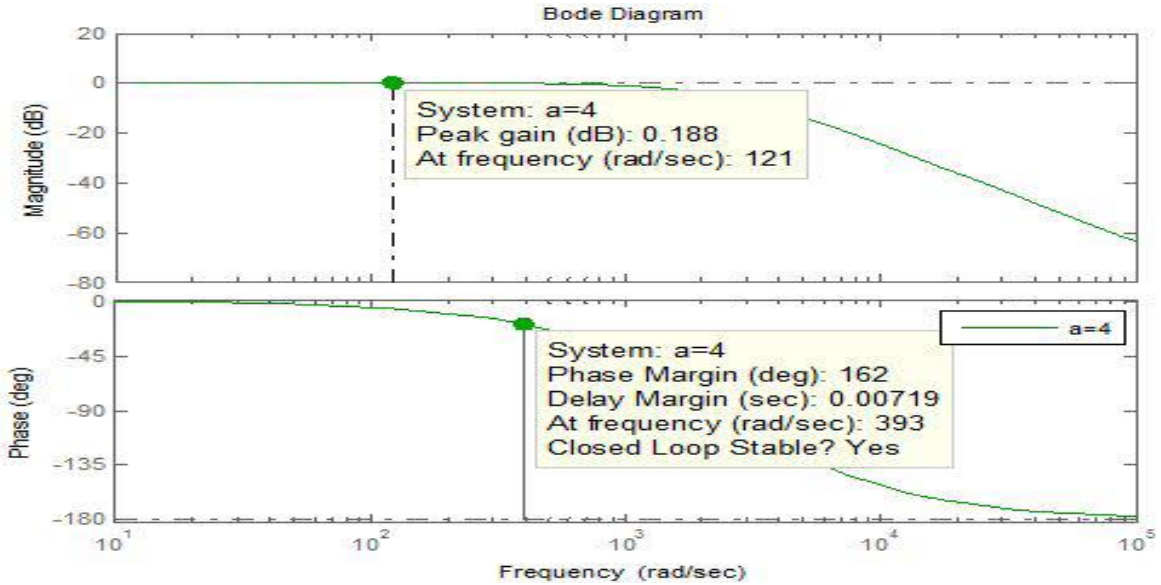

Figure 4.36: Bode plot of inner current controller with a=4.

Figure 4.36, shows the bode plot of inner current controller with symmetrical distance ‘a’=4.

The system has a controller gain of 129 with integral time constant of 0.063694. in addition, the open loop transfer function has a phase margin of 162° and gain margin infinity indicating that the closed loop system is stable at a=4.

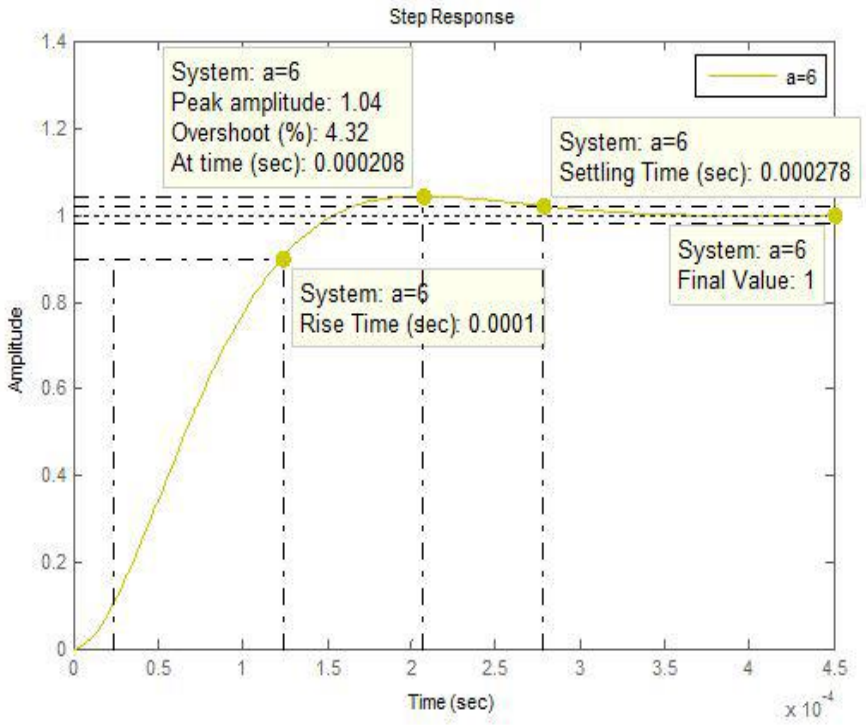

Figure 4.37: Step response of inner current controller with a=6.

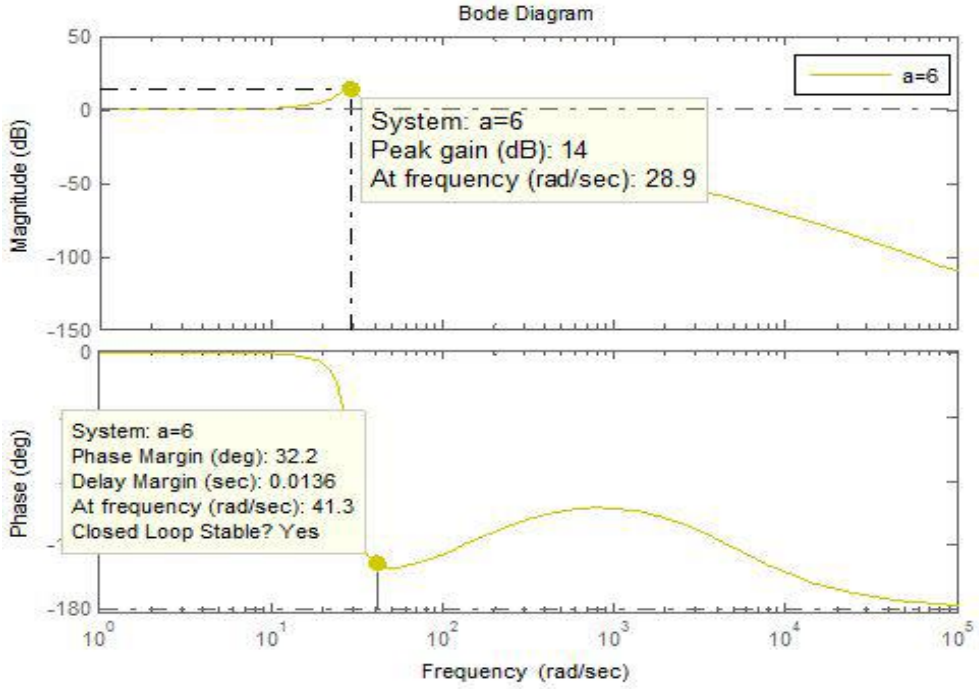

Figure 4.38: Bode plot of inner current controller with a=6.

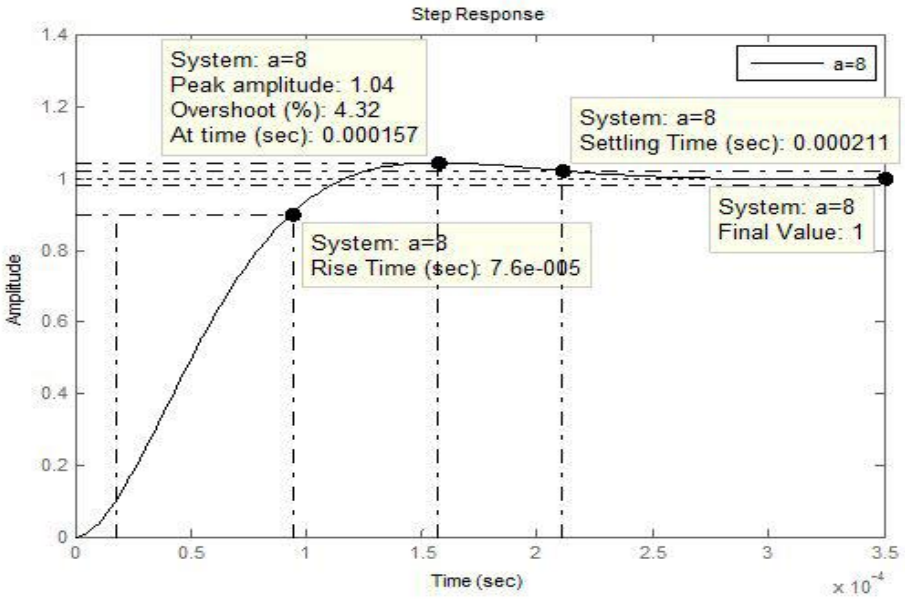

Figure 4.39: Step response of inner current controller with a=8.

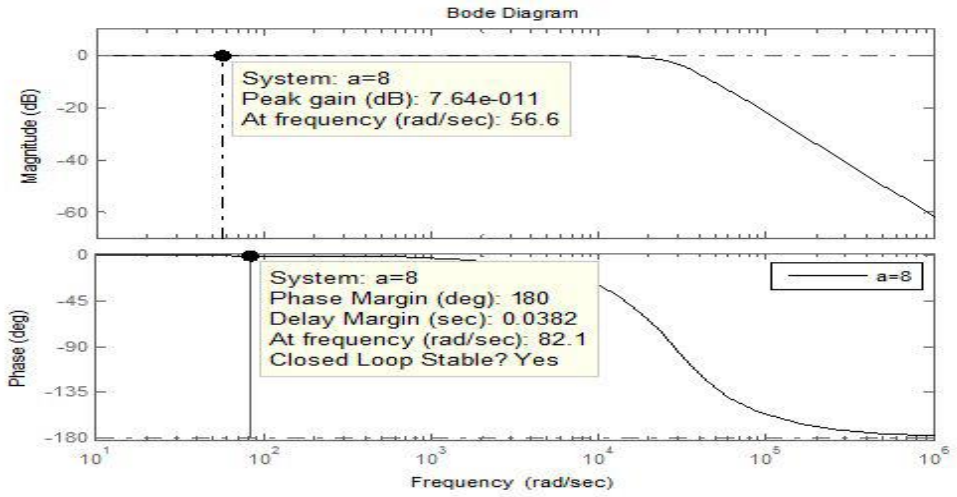

Figure 4.40: Bode plot of inner current controller with a=8.

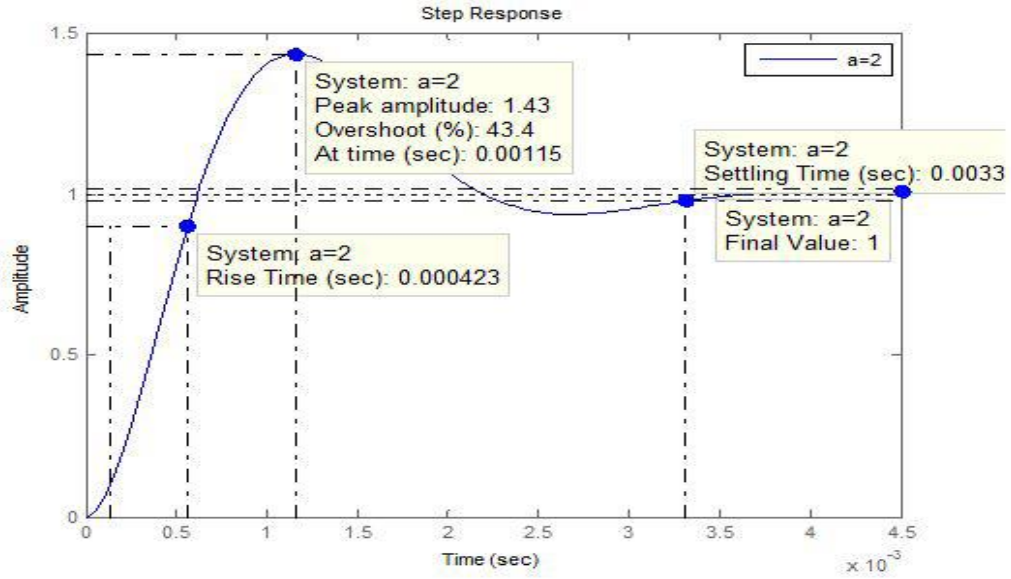

Figure 4.42: Step response of DC voltage controller with a=2.

Figures 4.32-4.42 shows the bode plots generated through tuning of the inner current controller by Modulus Optimum Criterion for diverse values of symmetrical distance ranging from 2 to 8. Comparing the characteristics of the inner current controller based on overshoot, rise time, settling time, phase margin, cross-over frequency and the peak

gain for various values of symmetrical distance it is crystal clear that at a=8, the system is still stable and damps out the oscillations within reasonable response time of 0.0382s. Comparing various values of symmetrical distances in figure 4.41, it shows that the rise time at a=3 (0.000204 s) in figure 4.33 is higher than that at a=8 (0.000076 s) in figure 4.39. This further shows that the controlled system attains stability faster at a=8. In addition, further comparison of the step response time and bode plots of figures 4.33, 4.35, 4.37, 4.39 and 4.42 evidently shows that based on settling time, rise time, phase margin and the damping values, the system with higher value of symmetrical distance increases the phase margin and improves the damping but still the system response time is better than that at a=4, thus ensuring stable system.

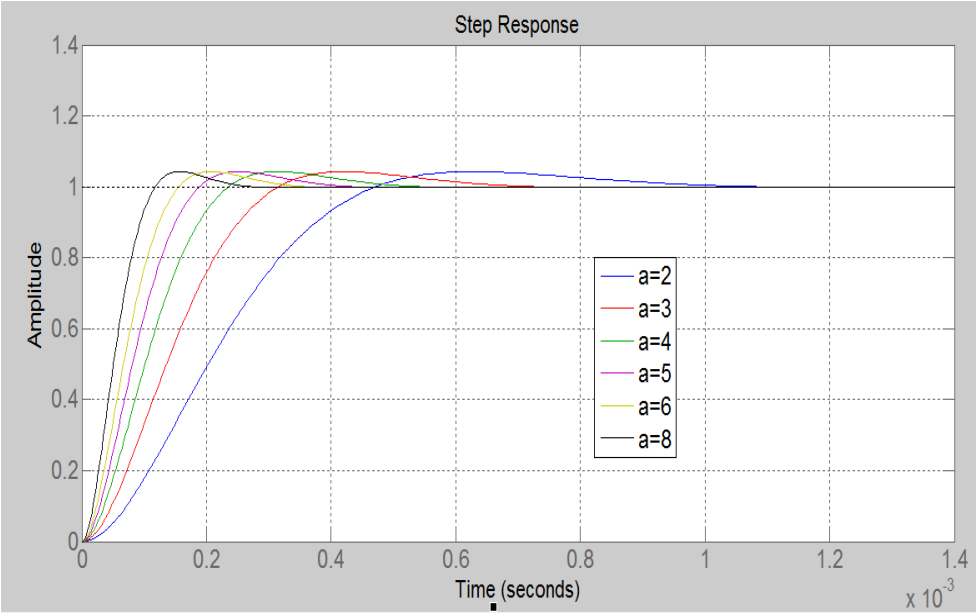

Figure 4.43: Step response plot showing settling time points for various values of symmetrical distance based on MOC.

Figure 4.43 shows the step responses of various values of symmetrical distance when inner current controller is tuned based on MOC.

4.5.2 Tuning the DC voltage controller using the symmetrical optimum criterion

Calculated parameters of various values of symmetrical distance for the DC voltage controller are shown in table 4.2 while the bode plots are shown in figures 4.44-4.50 respectively.

Table 4.2: Calculated parameters for the DC voltage controller.

A	**T_i**	**K_p**	**K**	**KT_i**
2	0.0008	0.1632	0.1347	0.00011
3	0.0027	0.07253	0.05993	0.0001618
4	0.0064	0.0408	0.03371	0.0002157
5	0.0125	0.02611	0.02157	0.00027
6	0.0216	0.01813	0.01498	0.000324
8	0.0612	0.0102	0.00843	0.000432

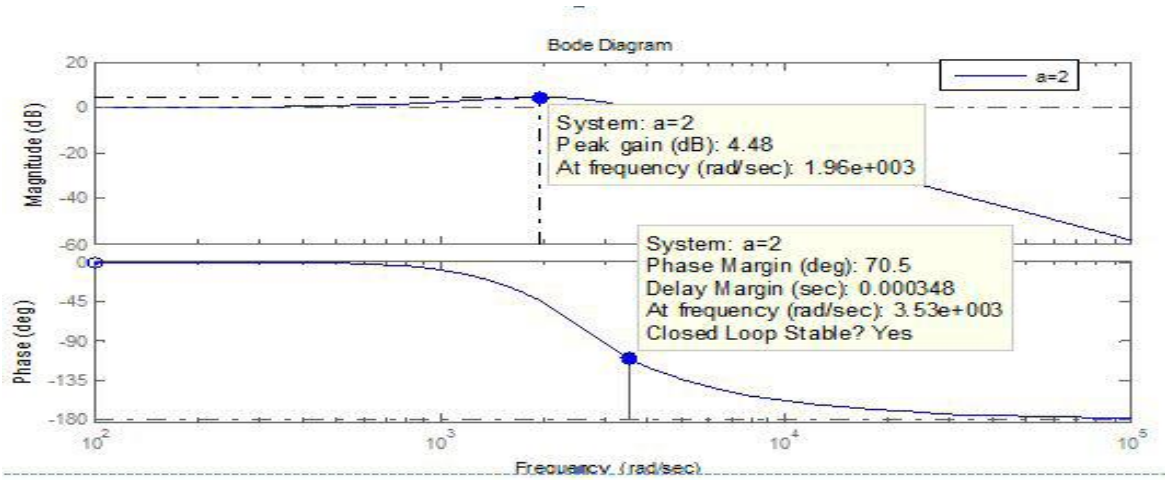

Figure 4.44: Bode plot of DC voltage controller with a=2.

Figure 4.44 shows the bode plot of DC voltage controller tuned based on SOC at a=2. It shows stable operating limits with a maximum phase margin of 70.5°, occurring at the crossover frequency of $3.53 \times 10^3 rad/sec$ (564.8Hz).

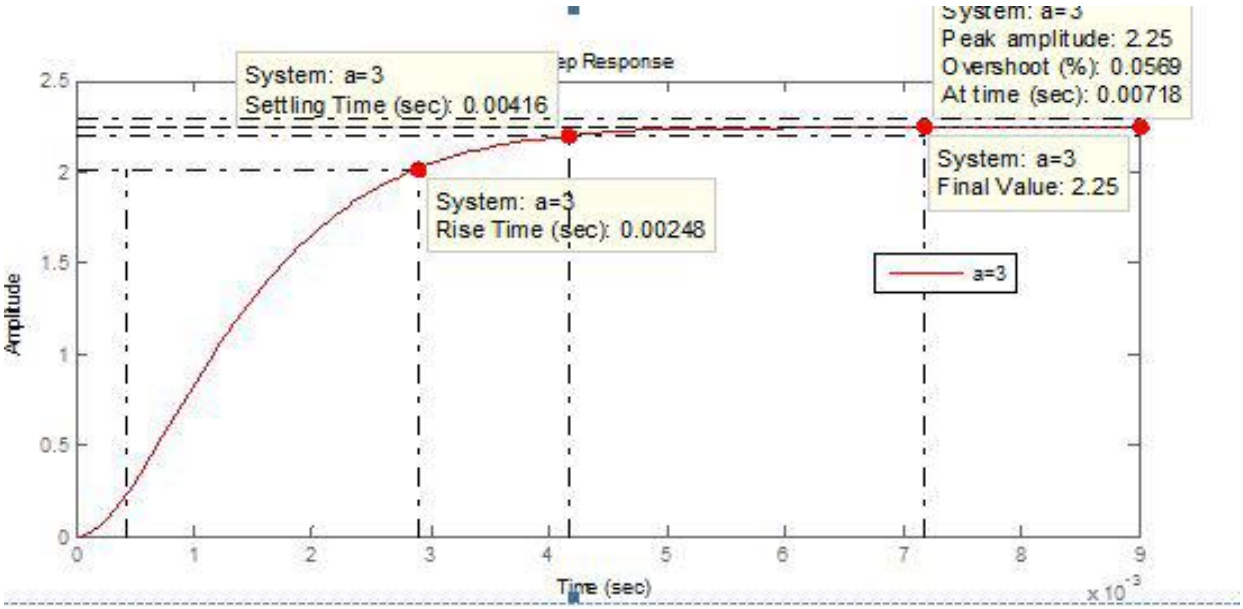

Figure 4.45: Step response of DC voltage controller with a=3.

Figure 4.45 shows the step response of DC voltage controller based on SOC at a=3.The step response of the system has following characteristics: Maximum Overshoot, *M* = 2.25, Time for maximum overshoot, *tm* = 0.00718 s, Settling time, using 2%criteria, *ts* = 0.004164 s and rise time of 0.00246 s. The system is stable at a=3.

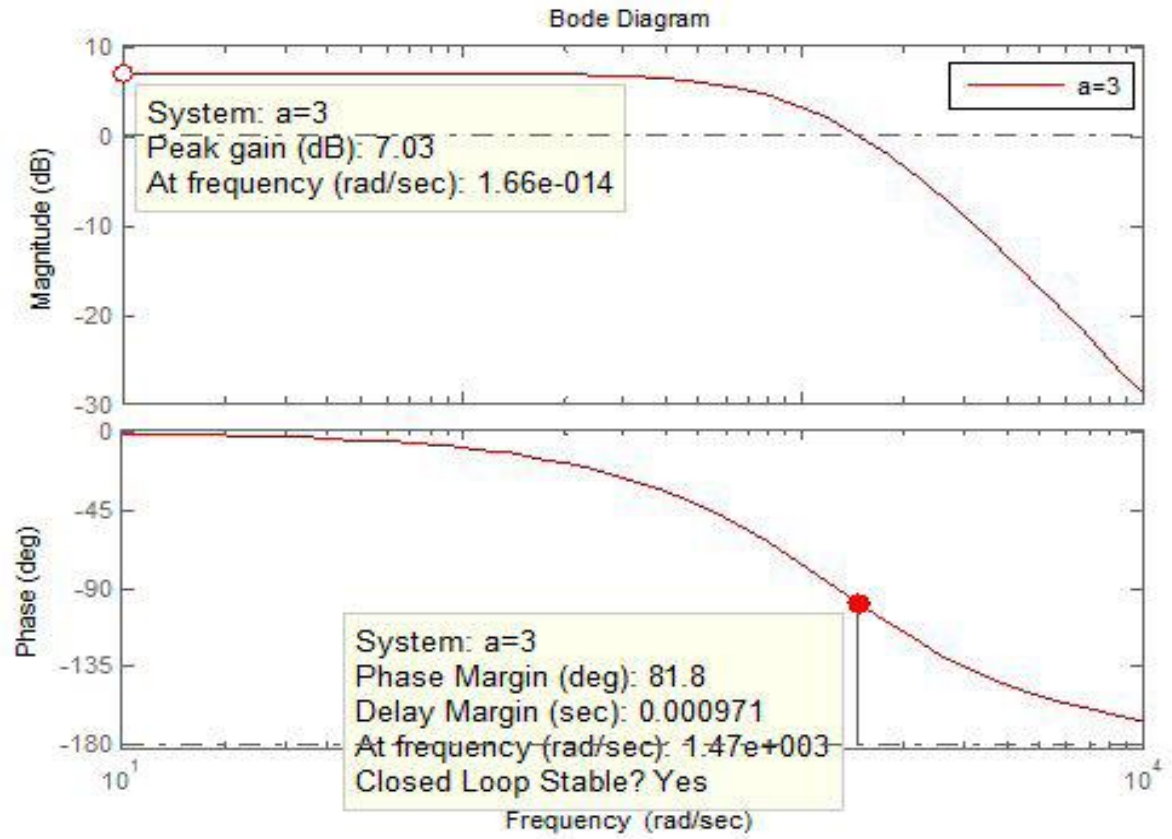

Figure 4.46: Bode plot of DC voltage controller with a=3.

Figure 4.46 shows bode plot of DC voltage controller for a=3. The system is stable with phase margin of 81.8° at crossover frequency of $1.470 \times 10^3\ rad/sec$ (235.2Hz) and delay margin of 0.000971s.

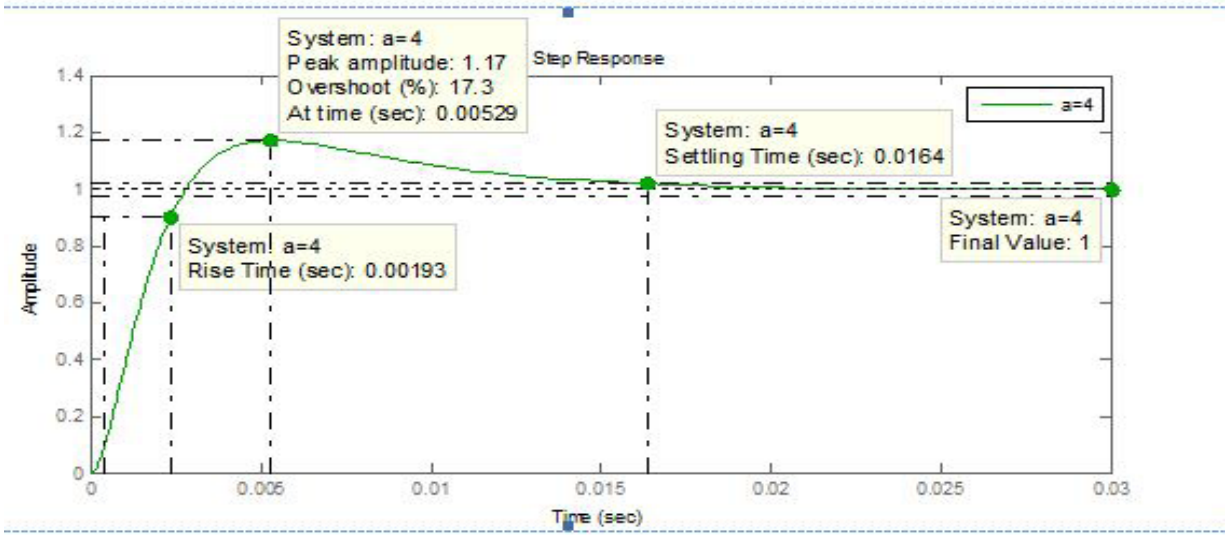

Figure 4.47: Step response of DC voltage controller with a=4.

The time domain response of the system to step input for figure 4.47 show the following characteristics: Maximum Overshoot, M = 1.17, time for maximum overshoot, tm = 0.00529 s, settling time, using 2% criteria, ts = 0.0164 s and rise time of 0.00193 s. It shows stable system.

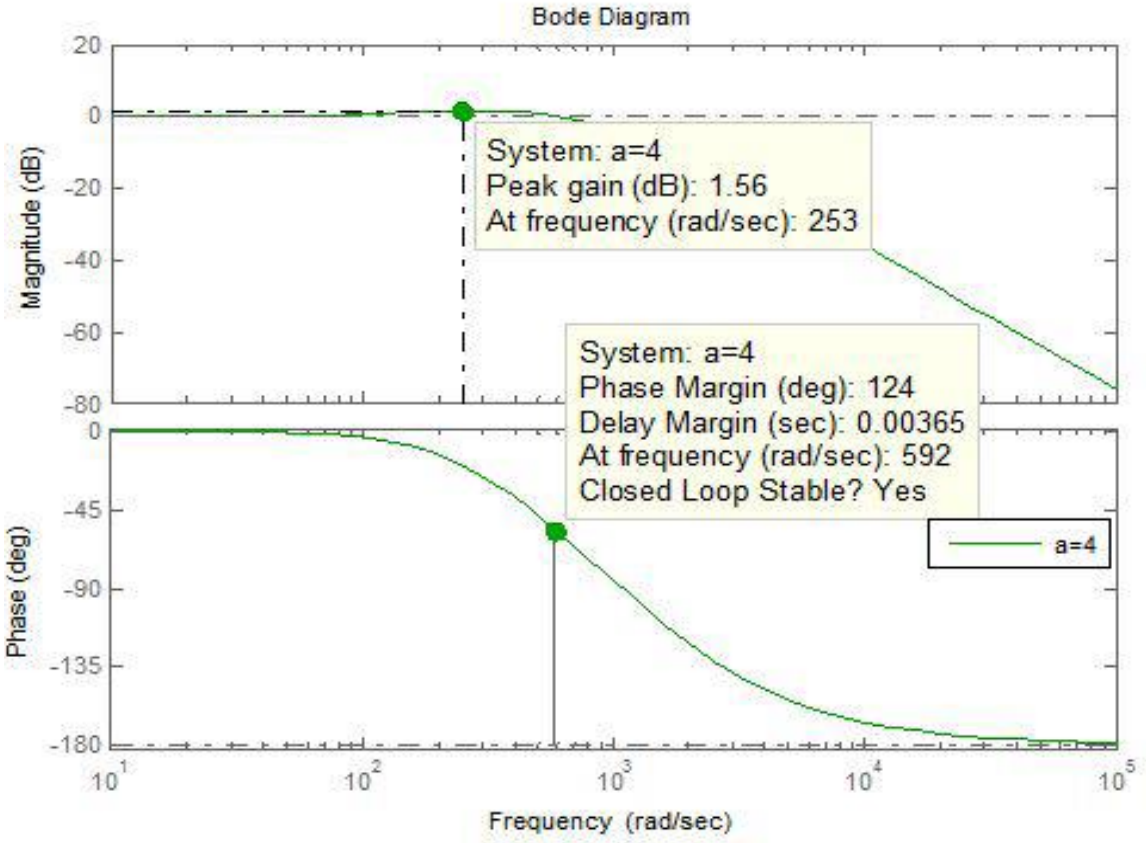

Figure 4.48: Bode plot of DC voltage controller with a=4.

Figure 4.48 shows bode plot of DC voltage controller for a=4. The system is stable with phase margin of 124° at crossover frequency of $592\ rad/sec$ (94.7Hz) and delay margin of 0.00365 s.

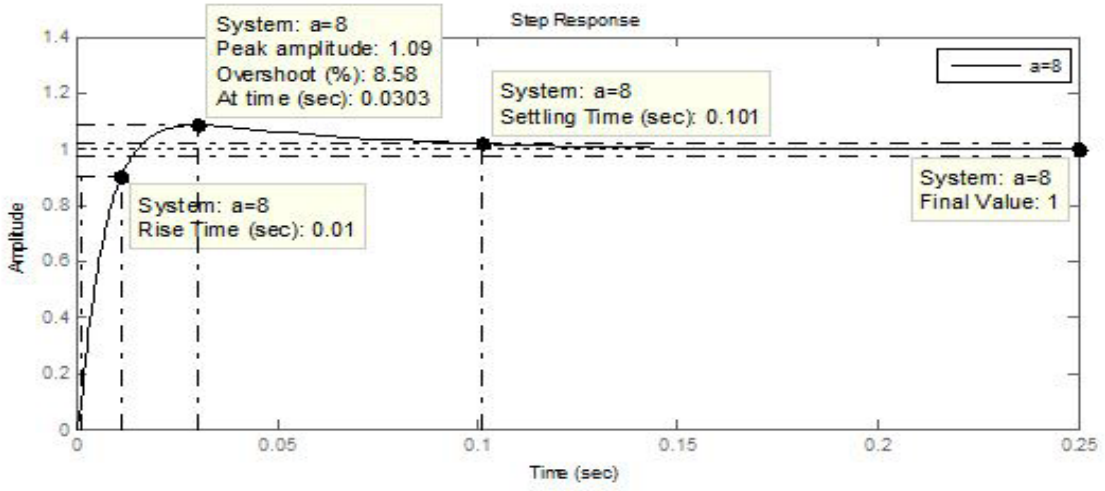

Figure 4.49: Step response of DC voltage controller with a=8.

The time domain response of the system to step input for figure 4.49 shows the following characteristics: Maximum Overshoot, M = 1.09, time for maximum overshoot, tm = 0.0303 s, settling time, using 2% criteria, ts = 0.101 s and rise time of 0.01 s. It shows stable system.

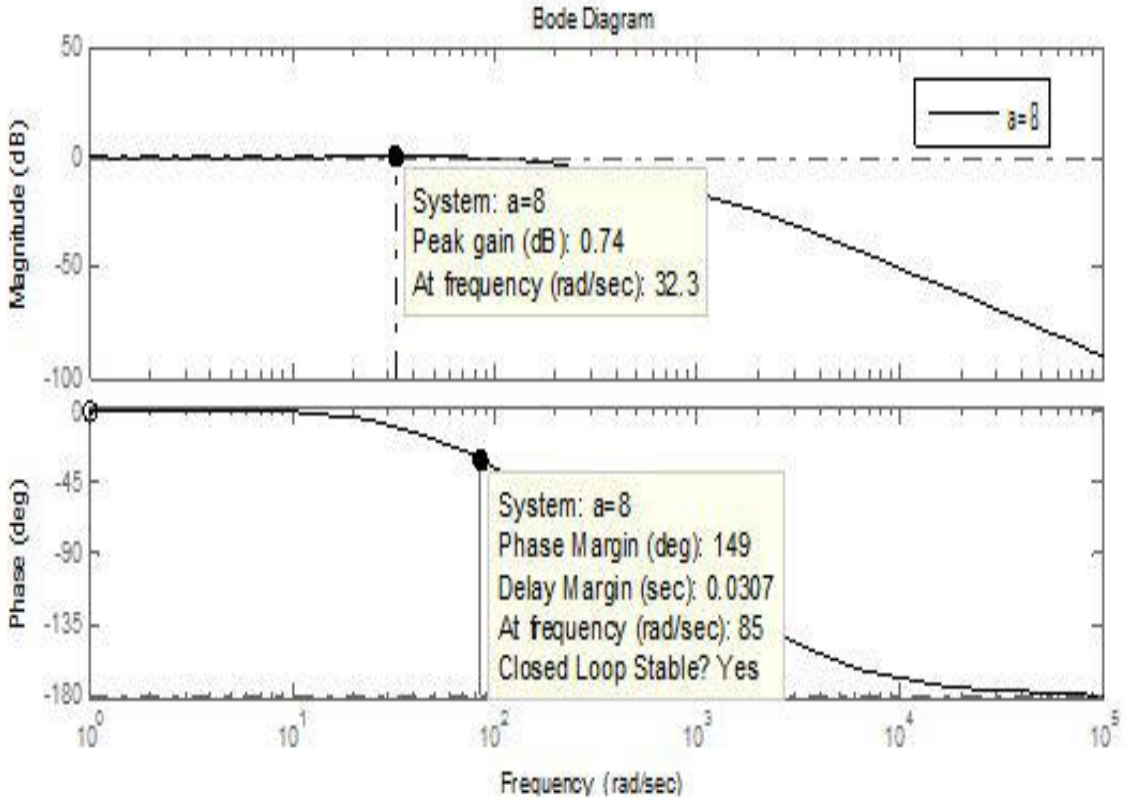

Figure 4.50: Bode plot of DC voltage controller with a=8.

Figure 4.50 shows bode plot of DC voltage controller for a=8. The system is stable with phase margin of 149° at crossover frequency of $85 rad/sec$ and delay margin of 0.0307 s. Figures 4.44-4.50 shows the behavior of the DC voltage controller when tuned using symmetrical optimum criteria at different values of symmetrical distance. Further comparison of DC voltage controller with diverse values of symmetrical distance shows that at a=2, the system is stable and damps out the oscillations very fast. Further, figure 4.50 shows that at a=8, there is increased phase margin, increased delay time and settling time and the system is stable. Therefore, tuning the controller based on SOC slower the system response however, the system stability is acceptable.

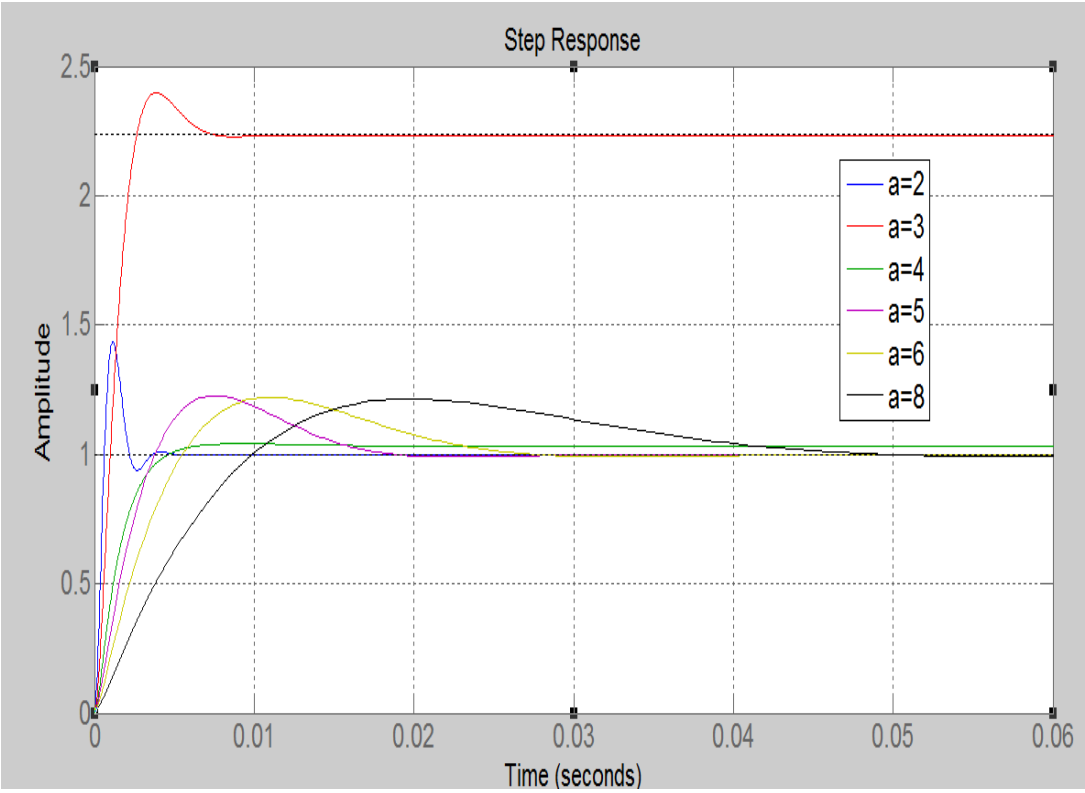

Figure 4.51: Step response plot showing settling time points for different values of symmetrical distance based on SOC.

Figure 4.51 shows the step response of various symmetrical distances for the tuned DC voltage controller based on SOC.

4.6 Simulation results of a novel fast DC Circuit breaker for transient stability improvement of the developed VSC-HVDC system.

A novel fast DC breaker modeled has a maximum break current of 5.25KA. A three-phase short-circuit fault was initiated at 0.3 s along the power transmission line. The developed DC breaker was set to clear the fault at 0.6 s. Table 4.3 compares the characteristics of the novel DC breaker developed in this research against the existing DC breakers.

Table 4.3: Comparison of existing DC breakers against the Novel DC breaker.

DC breaker type	Interruption time	% of the VSC station power losses.	Voltage rating	Current rating
Electromechanical	60ms	0.001%	550kv	**5KA**
Solid state	40ms	30%	800kv	**5KA**
Hybrid	2-30ms	0.1%	320kv	**9KA**
New solid state	5ms	30%	800kv	**5KA**
Novel DC breaker	1ms	30%	220kv	**5.25KA**

$$Current\ rating\ of\ the\ novel\ DC\ breaker = \left(\frac{2000}{\sqrt{3} \times 220 \times 1000}\right) \times 10^3)KA$$

$$= 5.25KA$$

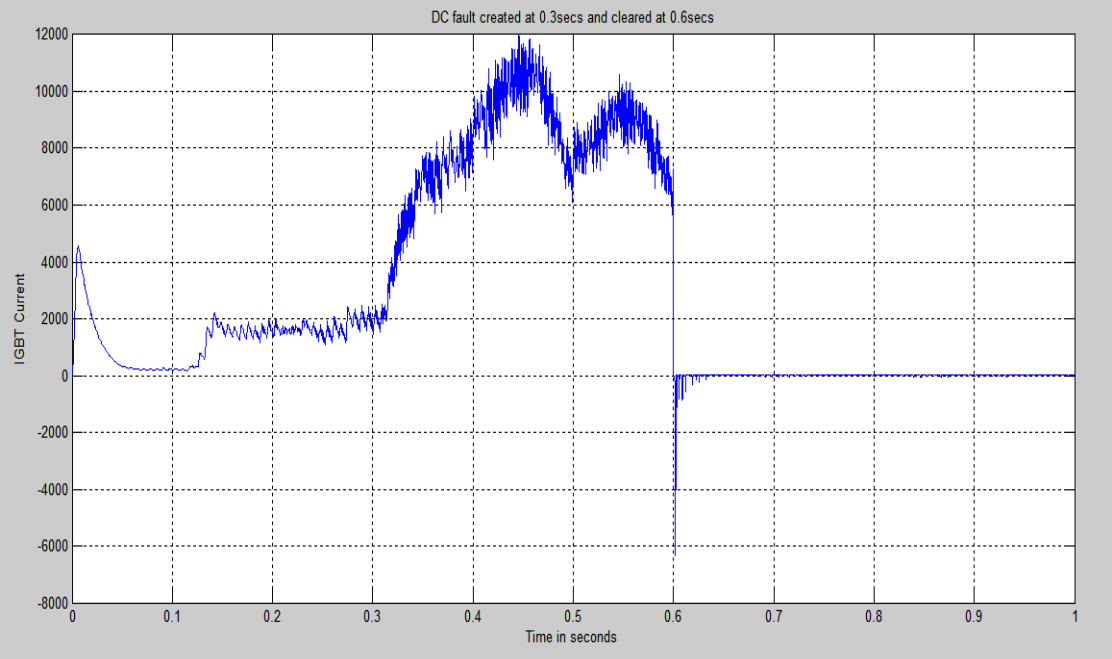

Figure 4.52: Voltage magnitude vs. Time in seconds.

Figure 4.52 shows the voltage response of the modified HVDC MATLAB model upon occurrence of the short-circuit fault. The fault was created at 0.3s and cleared at 0.6s respectively. The figure indicates that after the fault is cleared at 0.6 s, simulations continued for few s before reaching the steady-state condition. This is an indication of time delay in clearing the fault thus delaying the system from attaining stability. Figure 4.52 also shows some instability before the 0.3 s due to the on-state losses exhibited by the IGBT during the quick switching operation.

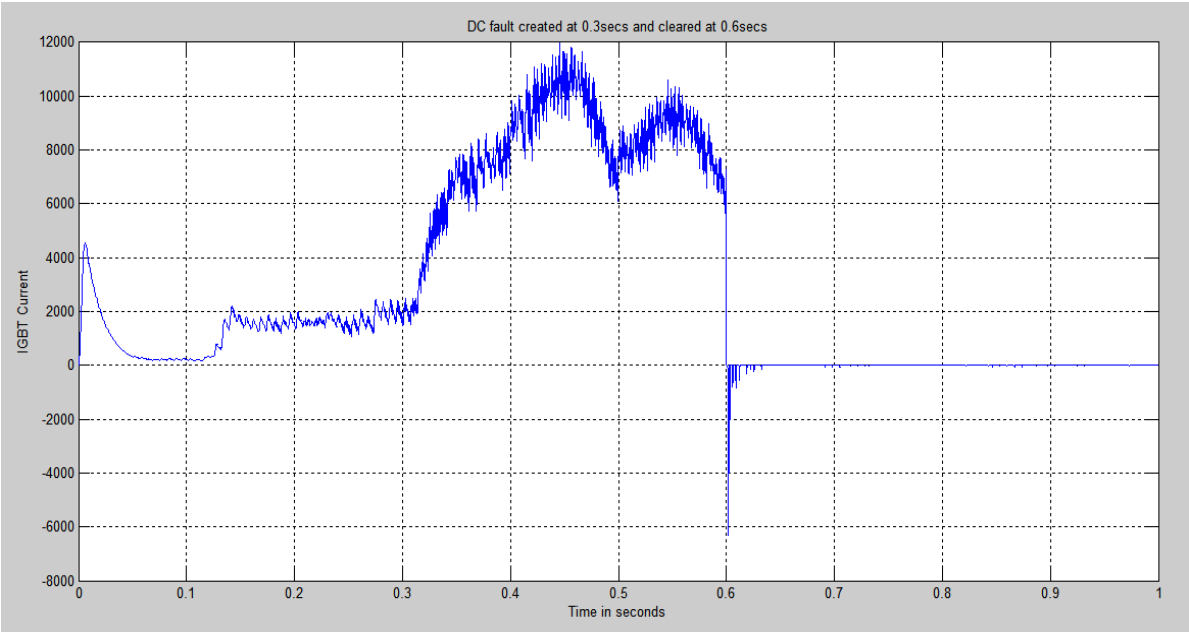

Figure 4.53: IGBT current Vs. Time in seconds.

Figure 4.53 shows a short-circuit fault created at 0.3 s with the developed model of novel fast DC breaker set to operate at 0.6s. Though the novel DC breaker interrupted the current at 0.6 s, oscillations continued up to 0.601 s where they died out. This indicates that the designed novel fast DC breaker has a fault clearing time of 1ms. This is a great improvement from the past designed and commercialized DC breakers whose fault clearing time is 5ms (Negari, 2015) and (Eriksson, Backman & Halen, 2014),.

CHAPTER FIVE

CONCLUSIONS AND RECOMMENDATIONS

5.1 Conclusions

VSC-HVDC system employing IGBTs is the leading semiconductor technology for long distance bulk power transmission and distribution by both overhead lines and underground cables. Currently, the generating power plants consists of various energy mix with diverse dynamic and unique characteristics that makes VSC-HVDC systems the most competitive power transmission media for the future. Further, they have the ability to independently control active and reactive power, fewer requirements for high pass filters because of the fast switching speed of the IGBT and ability for active power reversal by simply changing the direction of the current flow. It was noted that VSC-HVDC system requires smaller substation space as compared to LCC-HVDC and HVAC systems. These features make VSC-HVDC systems the most adopted transmission technology and continue to attract a lot of interest from researchers and other energy stakeholders.

The critical clearing time was used to find the longest time a fault can sustain without losing the power system transient stability on a conventional generation and when wind power is connected. The analysis shows that the system without wind power achieved a critical clearing time of 0.123s while that with 22% wind power integration attained a critical clearing time of 0.129s. When more wind power was integrated to the conventional generation at 34%, a critical clearing time of 0.127 s was realized. This shows that system with wind power have improved transient system stability because of the longer critical clearing times. This also shows that despite the clearing time being 0.129s for 22% wind power penetration, the system was still stable at 34% wind power penetration with critical clearing time of 0.127s. Therefore, in this research wind power

penetration level of 34% was achieved which is better than 20% of what other researchers have done.

Further, in this thesis, the VSC-HVDC system was modified with an objective of analyzing the impact of large wind power integration. A three-phase short-circuit fault was created on one of the transmission line to analyze power system transient stability. Three scenarios were analyzed: an IEEE 9-bus conventional grid, an IEEE 9-bus conventional grid with wind power and an IEEE 9-bus conventional grid with wind power integrated through the developed VSC-HVDC system. For each of the configuration, load flow was run in DigSilent software and data for various parameters transferred to workspace in Matlab software for ease of analysis. The analysis shows that the configuration with wind power through the developed VSC-HVDC system attained transient stability at 2.45s for all the three configurations. This shows that the configurations without wind power and that with wind power were unstable at 2.45s. This further demonstrated that VSC-HVDC systems contribute significantly to the independent control of DC voltage, active and reactive power subsequently facilitating the improvement of the power system transient stability.

The designed novel fast DC circuit breaker has a fault clearing time of 1ms. It has the ability to discriminate and quickly isolate the faulty section of the network while the healthy network continues with its normal operation. This is a major contribution towards a fast switching device, protection of VSC-HVDC converters and transmission systems against short-circuit faults.

Tuning the controllers is important task carried out in power systems. The objective of tuning the controller is to ensure that the system has fast response by increasing the cut-off frequency and stability where the system has small overshoot and good damping oscillations that dies out fast. However, in a real power system, a compromise has to be arrived at since a fast system response result into worst stability and a better controllability causes a slower system response. In this thesis, SOC and MOC tuning

techniques were used. Tuning the DC voltage controller was achieved by use of SOC technique where the controlled system has one dominant time constant and other minor time constant. Therefore, the design of the DC voltage controller and the tuning of the PI parameter in a modified VSC-HVDC system carried out in this thesis is an important step towards realization of a properly tuned controller. Researchers such as (Machaba, 2008) and [59] concluded that for a properly tuned DC voltage controller, the values of the symmetrical distance should be between 2 and 4. Based on wider tuning of the DC voltage controller, the analysis carried out in this thesis shows that the system was found to have good response time and stability at a=8.

The inner current controller built in PowerFactory was tuned based on MOC because of its simplicity and fast response time. In reality, the inner current controller is tuned with the aim of making it faster than the outer controller loop for the purpose of quickly driving the system to stability. Therefore, through the wider tuning of the controller, the simulation results shows that at a=8, the system still had better response time and stability thus enabling the modified VSC-HVDC system in thesis to operate efficiently and swiftly. In this thesis, the designed novel fast DC breaker (NFDCB) has a fault clearing time of 1ms.

The main objective of this thesis was to analyze the control strategy of a VSC-HVDC transmission system with high wind power penetrations and develops a novel DC circuit breaker for transient stability improvement of a power system. The wind farm and VSC-HVDC system models were developed and analyzed for various scenarios using time domain simulations. Mitigation measures for VSC's that often fail under short-circuit fault were realized through optimal tuning of the designed controllers and novel fast DC circuit breaker with a fault clearing time of 1ms. This is a great achievement in the development of a fast switching DC circuit breaker.

5.2 Recommendations

In this thesis, it has been found that with enhanced power system stability and optimal control of the VSC-HVDC controllers, it is possible to integrate large amount of wind power in a conventional generation. It has also been shown that the VSC's that often fail under short-circuit faults are safe with a novel fast DC circuit breaker model developed with a fault clearing time of 1ms. This makes independent control of active and reactive power feasible thus enabling stable operation of the power network. Despite the above advantages, there are challenges that need further research as highlighted below:

i. VSC-HVDC systems employ Insulated Gate Bipolar Transistor (IGBT) for quick switching operation. Due to the fast switching speed, IGBTs are known to have high on-state losses. This is contrary to Thyristors that have very minimal power losses but with slow switching speed. Future designs for the DC circuit breakers should focus on the possibility of limiting the high current magnitude generated during short-circuit faults without necessarily reducing the speed of the DC breaker operation. This will ensure good system response and stability of the power system.

ii. Since the fault on the DC system causes damage to converters and transmission network in a VSC-HVDC system, a bypass switch may be of help by providing alternative route thus preventing frequent interruptions affecting the power system.

iii. In this thesis, a novel fast DC breaker model is developed and simulated on MATLAB software. The DC breaker has a fault clearing time of 1ms and to enable validation of the simulation results, it is important to have a practical experimental working setup implemented.

iv. VSC-HVDC system connected to weak AC system continues to encounter challenges in operation causing system failure. Therefore, control strategies need to be carefully selected to ensure optimal active and reactive power flow.

v. In this thesis, wider tuning was carried out on DC voltage controller using SOC and inner current controller using MOC to analyze its impacts on power system transient stability. The results indicated good system response and stability at a=8. It is therefore important to carryout wider tuning of other types of controllers such as AC voltage controllers, active and reactive power controllers to assess their impacts on power system transient stability under short-circuit faults.

REFERENCES

Abido, M. A. (2009). Power system stability enhancement using FACTS controllers: A review. *The arabian journal for science and engineering, 34*(1B), 153-172.

Ackermann, T. (Ed.). (2005). *Wind power in power systems*. John Wiley & Sons.

Adapa, R. (2012). High-wire act: Hvdc technology: The state of the art. *IEEE power and energy magazine, 10*(6), 18-29.Tang, G. F. (2010). Voltage source converter based high voltage direct current transmission technology. *China Electric Power Press, Beijing, China (in Chinese)*.

Al-Ismail, F. S. & Abido, M. A. (2011, November). The impact of statcom based stabilizers on power system stability, using intelligent computational optimization approach. In *Innovative Smart Grid Technologies Asia (ISGT), 2011 IEEE PES* (pp. 1-13). IEEE.

Amutha, N., Aarthi, S. & Kumar, B. K. (2012, May). Improving critical clearing time of grid connected squirrel cage induction generator based wind generation system using DVR. In *Environment and Electrical Engineering (EEEIC), 2012 11th International Conference on* (pp. 519-524). IEEE.

Arrillaga, J. (1998). *High Voltage Direct Current Transmission*. London: IEEE

Asplund, G., Eriksson, K. & Svensson, K. (1997, September). DC transmission based on voltage source converters. In *CIGRE SC14 Colloquium, South Africa* (pp. 1-7)

Bahrman, M. P. & Johnson, B. K. (2007). The ABCs of HVDC transmission technologies. *IEEE power and energy magazine, 5*(2), 32-44.

Bahrman, M. P. & Johnson, B. K. (2007). The ABCs of HVDC transmission technologies. *IEEE power and energy magazine, 5*(2), 32-44.

Bajracharya, C. (2008). *Control of VSC-HVDC for wind power* (Master's thesis, Institutt for elkraftteknikk).

Bajracharya, C. (2008). *Control of VSC-HVDC for wind power* (Master's thesis, Institutt for elkraftteknikk, Norwegian University of Science and Technology, Trondheim)

Bollen, M. H. J., (2000). *Understanding power quality problems: Voltage sags and interruptions*, 'New York: IEEE Press,

Callavik, M., Blomberg, A., Häfner, J. & Jacobson, B. (2012). The hybrid HVDC breaker. *ABB Grid Systems Technical Paper*, *361*, 143-152..

Chaudhary, S. K., Teodorescu, R. & Rodriguez, P. (2008, November). Wind farm grid integration using vsc based hvdc transmission-an overview. In *Energy 2030 Conference, 2008. ENERGY 2008. IEEE* (pp. 1-7). IEEE..

Chen, Y. & Liu Z., (2010). Effect of large scale wind farm on transient stability, *International Conference on Electrical and Control Engineering, p. 3680*,

Cigre. (2004). *Analysis of HVDC Thyristor Converter Transformer Performance*. Cigre.

Cole, C & Belmans, R. (2011). A proposal for standard VSC HVDC dynamic models in power system stability studies", Electric Power System Research 81(2011*)*, pp. 967-973.

Cole, S., Beerten, J. & Belmans, R. (2010). Generalized dynamic VSC MTDC model for power system stability studies. *IEEE Transactions on Power Systems*, *25*(3), 1655-1662.

Council, G. W. E. (2008). Global wind 2013 report. *Brussels, Belgium: GWEC*. Retrieved fromhttp://www.gwec.net/fileadmin/documents/Publications/Report 2008/Global wind 2008 Report.

Damsky, B. L., Imam, I. & Premerlani, W. (1979, April). A New HVDC Circuit Breaker System Design for-+ 400 kV. In *Transmission and Distribution Conference and Exposition, 1979. 7 IEEE/PES* (pp. 230-236). IEEE

DeCesaro, J., Porter, K. & Milligan, M. (2009). Wind energy and power system operations: A review of wind integration studies to date. *The Electricity Journal*, *22*(10), 34-43.

Durrant, M., Werner, H. & Abbott, K. (2003, June). Model of a VSC HVDC terminal attached to a weak AC system. In *Control Applications, 2003. CCA 2003. Proceedings of 2003 IEEE Conference on* (Vol. 1, pp. 178-182). IEEE

Elansari, A. S., Finney, S. J., Burr, J. & Edrah, M. F. (2015, February). Frequency control capability of VSC-HVDC transmission system. In *AC and DC Power Transmission, 11th IET International Conference on* (pp. 1-6). IET.

El-Sayed, M. & Moussa, E. (2008). Effect of Large Scale Wind Farms On the Egyptian Power System Dynamics. *ICREPQ*, *8*, 12-14.

Eping, C., Stenzel, J., Pöller, M. & Müller, H. (2007). Impact of large scale wind power on power system stability. In *Proceedings of the 5th International Workshop on Large-Scale Integration of Wind Power and Transmission Networks for Offshore Wind Farms* (pp. 1-9).

Eriksson, K. (2001, November). Operational experience of HVDC Light/sup TM. In *AC-DC Power Transmission, 2001. Seventh International Conference on (Conf. Publ. No. 485)* (pp. 205-210). IET..

Eriksson, K. (2001, November). Operational experience of HVDC Light/sup TM. In *AC-DC Power Transmission, 2001. Seventh International Conference on (Conf. Publ. No. 485)* (pp. 205-210). IET.

Eriksson, T., Backman, M. & Halén, S. (2014). A low loss mechanical HVDC breaker for HVDC Grid applications. *Proc. Cigré Session, Paris, France*..

European Wind Energy Association. (2009). *The economics of wind energy*. EWEA.

European Wind Energy Association. (2011). *Pure power-wind energy targets for 2020 and 2030*. Ewea.

Franck, C. M. (2011). HVDC circuit breakers: A review identifying future research needs. *IEEE Transactions on Power Delivery*, *26*(2), 998-1007.

Gomis-Bellmunt, O., Liang, J., Ekanayake, J., King, R. & Jenkins, N. (2011). Topologies of multiterminal HVDC-VSC transmission for large offshore wind farms. *Electric Power Systems Research, 81*(2), 271-281.

Graham, J., Menzies, D., Biledt, G., Carvalho, A. R., Ping, W. W. & Wey, A. (2000, August). Electrical system considerations for the Argentina-Brazil 1000 MW Interconnection. In *CIGRE 2000 Conference, Paris* (Vol. 9).

Hafner, J. (2011). Proactive Hybrid HVDC Breakers-A key innovation for reliable HVDC grids. In *Proc. CIGRE Bologna Symposium* (pp. 1-8).

Hasan, M. R., Vanfretti, L., Li, W. & Khan, N. A. (2014, June). Generic high level VSC-HVDC grid controls and test systems for offline and real time simulation. In *Electric Power Quality and Supply Reliability Conference (PQ), 2014* (pp. 57-64). IEEE.

Hausler, M. (1999). Multiterminal HVDC for high power transmission in Europe. *CWPEX99, Pozan, Poland*.

Hingorani, N. G. (1991, September). FACTS-flexible AC transmission system. In *AC and DC Power Transmission, 1991., International Conference on* (pp. 1-7). IET.

Holaus, W.; Frohlich, K., "Ultra-fast switches- a new element for medium voltage fault current limiting switchgear," Power Engineering Society Winter Meeting, 2002. IEEE, vol.1, no., pp.299, 304 Vol.1, 2002

Jauch, C., Sørensen, P., Norheim, I. & Rasmussen, C. (2007). Simulation of the impact of wind power on the transient fault behavior of the Nordic power system. *Electric power systems Research*, *77*(2), 135-144.

Jiang-Hafner, Y., Hyttinen, M. & Paajarvi, B. (2002, October). On the short circuit current contribution of HVDC Light. In *Transmission and Distribution Conference and Exhibition 2002: Asia Pacific. IEEE/PES* (Vol. 3, pp. 1926-1932). IEEE

Koldby, E. & Hyttinen, M. (2009, September). Challenges on the Road to an Offshore HVDC Grid. In *Nordic Wind Power Conference* (Vol. 19).

Kostoulas, N., Sitokonstantinou, V., Idris, M., Sterling, P., Sayed, S. & Karaiskos, P. (2012). *DC circuit breakers and their use in HVDC grids*. Technical report, 2012. URL http://www2. ee. ic. ac. uk/patrick. sterling10/yr2proj/HVDCCircuitBreakersReport. pdf.

Kundur, P., Balu, N. J. & Lauby, M. G. (1994). *Power system stability and control* (Vol. 7). New York: McGraw-hill.

Kundur, P., Paserba, J., Ajjarapu, V., Andersson, G., Bose, A., Canizares, C., ... & Van Cutsem, T. (2004). IEEE/CIGRE joint task force on stability terms and definitions. *IEEE transactions on power systems*, *19*(3), 1387-1401

Lindberg, A. (1995). PWM and control of two and three level high power voltage source converters,‖ Licentiate thesis. *Royal Inst. of Technology, Stock-holm, Sweden*.

Lindberg, A. (1995). PWM and control of two and three level high power voltage source converters,‖ Licentiate thesis. *Royal Inst. of Technology, Stock-holm, Sweden*.

Lipu, M. S. H. & Karim, T. F. (2013). Effectiveness of FACTS controllers and HVDC transmissions for improving power system stability and increasing power transmission capability. *International Journal of Energy and Power Engineering*, *2*(4), 154-163.

Liserre, M. (2001). *Innovative control techniques of power converters for industrial automation* (Doctoral dissertation, Politecnico di Bari).

Liu, H., Xu, Z. & Huang, Y. (2003, September). Study of protection strategy for VSC based HVDC system. In *Transmission and Distribution Conference and Exposition, 2003 IEEE PES* (Vol. 1, pp. 49-54). IEEE.

Machaba, M. & Braae, M. (2003). Explicit damping factor specification in symmetrical optimum tuning of PI controllers. In *Proc. of First African Control Conference* (pp. 3-5).

Magnusson, J., Saers, R., Liljestrand, L. & Engdahl, G. (2014). Separation of the energy absorption and overvoltage protection in solid-state breakers by the use of parallel varistors. *IEEE transactions on power electronics*, *29*(6), 2715-2722.

Malesani, L., Rossetto, L., Tenti, P. & Tomasin, P. (1993, March). AC/DC/AC PWM converter with minimum energy storage in the DC link. In *Applied Power Electronics Conference and Exposition, 1993. APEC'93. Conference Proceedings 1993., Eighth Annual* (pp. 306-311). IEEE.

Mohan, N. (2003). *Electric drives: an integrative approach*. Mnpere.

Mokhberdoran, A., Carvalho, A., Leite, H. & Silva, N. (2014, September). A review on HVDC circuit breakers. In *Renewable Power Generation Conference (RPG 2014), 3rd* (pp. 1-6). IET.

Molinas, M., Naess, B., Gullvik, W. & Undeland, T. (2006). Robust wind turbine system against voltage sag with induction generators interfaced to the grid by power electronic converters. *IEEJ Transactions on Industry Applications*, *126*(7), 865-871.

National Grid Electricity Transmission plc (2013). The grid code national grid," Tech. rep. London: NGET

Negari, S. & Xu, D. (2014, June). A new solid-state HVDC circuit breaker topology for offshore wind farms. In *Power Electronics for Distributed Generation Systems (PEDG), 2014 IEEE 5th International Symposium on* (pp. 1-5). IEEE.

Netz, E. O. N. (2008). Requirements for offshore grid connections in the e. on netz network. *GmbH, Batreuth, Germany*.

Noroozian, M., Edris, A. A., Kidd, D. & Keri, A. J. (2003). The potential use of voltage-sourced converter-based back-to-back tie in load restorations. *IEEE transactions on Power Delivery*, *18*(4), 1416-1421.

Ottosson, J. &. Rudberg, M. (2003). *Simplified models for two and three-level voltage Source converters (*Master's thesis, Chalmers University of Technology, Goteborg, Sweden).

Paulinder, J. (2003). *Operation and Control of HVDC links embedded in AC systems* (Doctoral dissertation, Chalmers tekniska högsk.).

Paulinder, J. (2003). *Operation and Control of HVDC links embedded in AC systems* (Doctoral dissertation, Chalmers tekniska högsk.).

Pavella, M., Ernst, D. & Ruiz-Vega, D. (2012). *Transient stability of power systems: a unified approach to assessment and control*. New york: Springer Science & Business Media.

Polinder, H., VanderPilj, F., G. DeVilder, G. &. Tavner, T.J. (2006). Comparison of direct drive and geared generator concepts for wind turbines. *IEEE. Transactions on Energy Conversion*, *21*(3), 725–733,

Povh, D. (1998, May). FACTS Controller in Deregulated Systems. In *Power Systems Symposium, Rio de Janeiro, Brazil*.

Preitl, S. & Precup, R. E. (1999). An extension of tuning relations after symmetrical optimum method for PI and PID controllers. *Automatica*, *35*(10), 1731-1736..

Railing, B. D., Miller, J. J., Steckley, P., Moreau, G., Bard, P., Ronström, L. & Lindberg, J. (2004, July). Cross sound cable project second generation VSC technology for HVDC. In *Cigré conference, Paris, France, Aug*.

Rezek, Á. J., Coelho, C. A., Vicente, J. M. E., Cortez, J. A. & Laurentino, P. R. (2001, June). The modulus optimum (MO) method applied to voltage regulation systems: modeling, tuning and implementation. In *Proc. International Conference on Power System Transients, IPST* (Vol. 1, pp. 24-28).

Sano, K. & Takasaki, M. (2012, September). A surge-less solid-state dc circuit breaker for voltage source converter based HVDC transmission systems. In *Energy Conversion Congress and Exposition (ECCE), 2012 IEEE* (pp. 4426-4431). IEEE.

Schauder, C. & Mehta, H. (1993, July). Vector analysis and control of advanced static VAR compensators. In *IEE Proceedings C-Generation, Transmission and Distribution* (Vol. 140, No. 4, pp. 299-306). IET.

Schettler, F., Huang, H. & Christl, N. (2000). HVDC transmission systems using voltage sourced converters design and applications. In *Power Engineering Society Summer Meeting, 2000. IEEE* (Vol. 2, pp. 715-720). IEEE. [28]

Shewarega, F. & Erlich, I. (2014). Simplified modeling of vsc-hvdc in power system stability studies. *IFAC Proceedings Volumes*, *47*(3), 9099-9104.

Shire, T.W. (2009). *VSC-HVDC based network reinforcement,* (M.Sc. Thesis Electrical Power Engineering Department, Delft University of Technology).

Shukla, A. & Demetriades, G. D. (2015). A survey on hybrid circuit-breaker topologies. *IEEE Transactions on Power Delivery*, *30*(2), 627-641..

Singh, G. (2015, August). Controller design and stability analysis of VSC based HVDC transmission system. In *Power and Advanced Control Engineering (ICPACE), 2015 International Conference on* (pp. 344-349). IEEE.

Steurer, M.; Frohlich, K.; Holaus, W.; Kaltenegger, K., "A novel hybrid current-limiting circuit breaker for medium voltage: principle and test results," Power Delivery, IEEE Transactions on, vol.18, no.2, pp.460, 467, April 2003

Suzuki, K. I., Nakajima, T., Konishi, H. & Nakamura, T. (1992). A study of control system for self-commutated converter compensator. *IEEJ Transactions on Power and Energy*, *112*(1), 67-73.

Svensson, J. (1998). *Grid-Connected Voltage Source Converter* (Doctoral dissertation, Chalmers University of Technology Göteborg, Sweden).

Van Kuik, G.A.M., (2007).The lanchester-betz-joukowsky limit, *Wind Energy, 10*, . 289–291,

Wang, L. & Ertugrul, N. (2010, December). Selection of PI compensator parameters for VSC-HVDC system using decoupled control strategy. In *Power Engineering Conference (AUPEC), 2010 20th Australasian Universities* (pp. 1-7). IEEE.

Wang, W., Beddard, A., Barnes, M. & Marjanovic, O. (2014). Analysis of active power control for VSC–HVDC. *IEEE Transactions on Power Delivery*, *29*(4), 1978-1988.

Wasserrab A, Balzer G. Calculation of short circuit currents in HVDC systems. ‘‘Proceedings of the 46th international universities’’ power engineering conference (UPEC’11), Soest, Germany, 5–8 Sep 2011,

Wasserrab, A. & Balzer, G. (2011, September). Calculation of short circuit currents in HVDC systems. In *Universities' Power Engineering Conference (UPEC), Proceedings of 2011 46th International* (pp. 1-6). VDE

Woodford, D. A. (1998). HVDC transmission. *Manitoba HVDC Research Centre*, 400-1619..

Wu, R., Blaabjerg, F., Wang, H., Liserre, M. & Iannuzzo, F. (2013, November). Catastrophic failure and fault-tolerant design of IGBT power electronic

converters-an overview. In *Industrial Electronics Society, IECON 2013-39th Annual Conference of the IEEE* (pp. 507-513). IEEE.

Xu, L. & Fan, L. (2012, September). System identification based VSC-HVDC DC voltage controller design. In *North American Power Symposium (NAPS), 2012* (pp. 1-6). IEEE.

Zhang, G., Xu, Z. & Cai, Y. (2001). An equivalent model for simulating VSC based HVDC. In *Transmission and Distribution Conference and Exposition, 2001 IEEE/PES* (Vol. 1, pp. 20-24). IEEE.

APPENDICES

APPENDIX A: VSC-HVDC CONTROLLERS TUNING

Tuning the controllers is an important activity carried out in VSC-HVDC system to enable selection of controller parameters to meet specific performance specifications. The controllers are classified as inner current controller and the outer controllers; the outer controller is further classified as active and reactive power controllers, AC voltage controller, DC voltage controller and the frequency controllers. Two tuning techniques namely; symmetrical optimum criterion and the modulus optimum criterion were applied in this thesis and the Matlab codes for DC voltage controller and inner current controller generated:

Appendix A.1: DC voltage controller tuning based on symmetrical optimum criteria

%TUNNING THE DC VOLTAGE CONTOLLER USING THE SYMMETRICAL OPTIMUM CRITERION (SOC)

T_i=0.0008; Kp=0.163; K=0.134; %for a=2

T_{i1}=0.0018; Kp1=0.109; K1=0.05993; %for a=3

T_{i2}=0.032; Kp2=0.082; K2=0.03371; %for a=4

T_{i3}=0.005; Kp3=0.065; K3=0.02157; %for a=5

T_{i4}=0.0072; Kp4=0.054; K4=0.01498; %for a=6

T_{i5}=0.0128; Kp5=0.0408; K5=0.00843;%for a=8

C=0.000053933;

T_{eq}=0.0002;

num=[K*$_{Ti}$ K];

num1=[K1*T_{i1} K];

num2=[K2*T_{i2} K2];

num3=[K3*$_{Ti3}$ K3];

num4=[K4*T_{i4} K4];

num5=[K5*T_{i5} K5];

den=[Ti*T_{eq}*C T_i*C K*T_i K];

den1=[Ti1*T_{eq}*C T_{i1}*C K1*T_{i1} K1];

den2=[Ti2*T_{eq}*C T_{i2}*C K2*T_{i2} K2];

den3=[Ti3*T_{eq}*C T_{i3}*C K3*T_{i3} K3];

den4=[Ti4*T_{eq}*C T_{i4}*C K4*T_{i4} K4];

den5=[Ti5*T_{eq}*C T_{i5}*C K5*T_{i5} K5];

G=tf(num,den);

G1=tf(num1,den1);

G2=tf(num2,den2);

G3=tf(num3,den3);

G4=tf(num4,den4);

G5=tf(num5,den5);

ylabel('dq-currents amplitude');

xlabel('time');

title('Step response of DC Voltage Controller');

step(G,'b',G1,'r',G2,'g',G3,'m',G4,'y',G5,'k');

legend('a=2','a=3','a=4','a=5','a=6','a=8')

Appendix A.2: Inner current controller tuning based on modulus optimum criteria.

%TUNNING THE INNER CURRENT CONTOLLER USING THE MODULUS OPTIMUM CRITEIA

T_i=0.063694; Kp=64.51; T_a=0.0001; %for a=2

T_{i1}=0.063694;Kp1=96.3; T_{a1}=0.000067; %for a=3

T_{i2}=0.063694; Kp2=129; T_{a2}=0.00005; %for a=4

T_{i3}=0.063694; Kp3=161.1; T_{a3}=0.00004; %for a=5

T_{i4}=0.063694; Kp4=195.5; T_{a4}=0.000033; %for a=6

T_{i5}=0.063694; Kp5=258; T_{a5}=0.000025;%for a=8

R=0.20253;

num=[Kp/(T_i*T_a*R)];

num1=[Kp1/(T_{i1}*T_{a1}*R)];

num2=[Kp2/(T_{i2}*T_{a2}*R)];

num3=[Kp3/(T_{i3}*T_{a3}*R)];

num4=[Kp4/(T_{i4}*T_{a4}*R)];

num5=[Kp5/(T_{i5}*T_{a5}*R)];

den=[1 1/T_a Kp/(T_i*T_a*R)];

den1=[1 1/T_{a1} Kp1/(T_{i1}*T_{a1}*R)];

den2=[1 1/T_{a2} Kp2/(T_{i2}*T_{a2}*R)];

den3=[1 1/T_{a3} Kp3/(T_{i3}*T_{a3}*R)];

den4=[1 1/T_{a4} Kp4/(T_{i4}*T_{a4}*R)];

den5=[1 1/T_{a5} Kp5/(T_{i5}*T_{a5}*R)];

G=tf(num,den);

G1=tf(num1,den1);

G2=tf(num2,den2);

G3=tf(num3,den3);

G4=tf(num4,den4);

G5=tf(num5,den5);

ylabel('dq-currents amplitude');

xlabel('time');

title('Tunning the inner current controller by modulus optimum criteria ');

step(G,'b',G1,'r',G2,'g',G3,'m',G4,'y',G5,'k');

legend('a=2','a=3','a=4','a=5','a=6','a=8')

APPENDIX B: USER DEFINED MODELS

Various user defined models for various controllers were modeled. Based on the desired applications, various combinations of controllers were selected per VSC converter aimed at efficient control of DC voltage, active and reactive power.

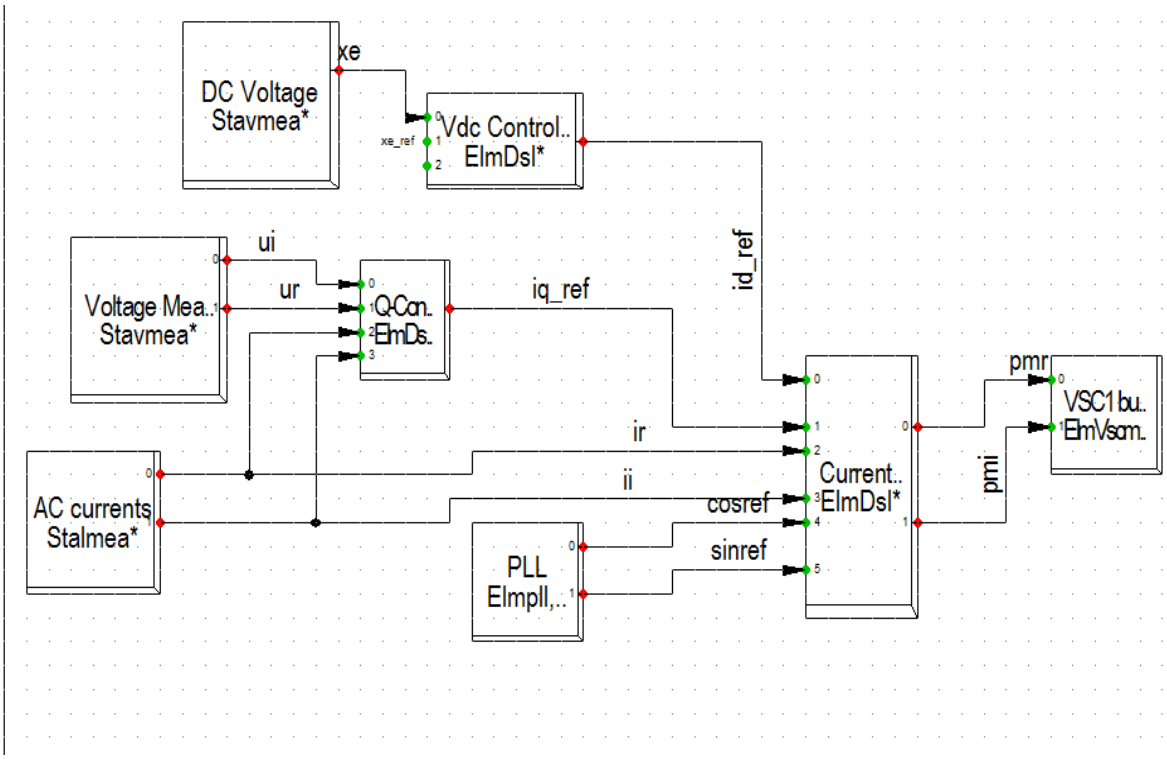

Figure B.1: VSC 1 controller.

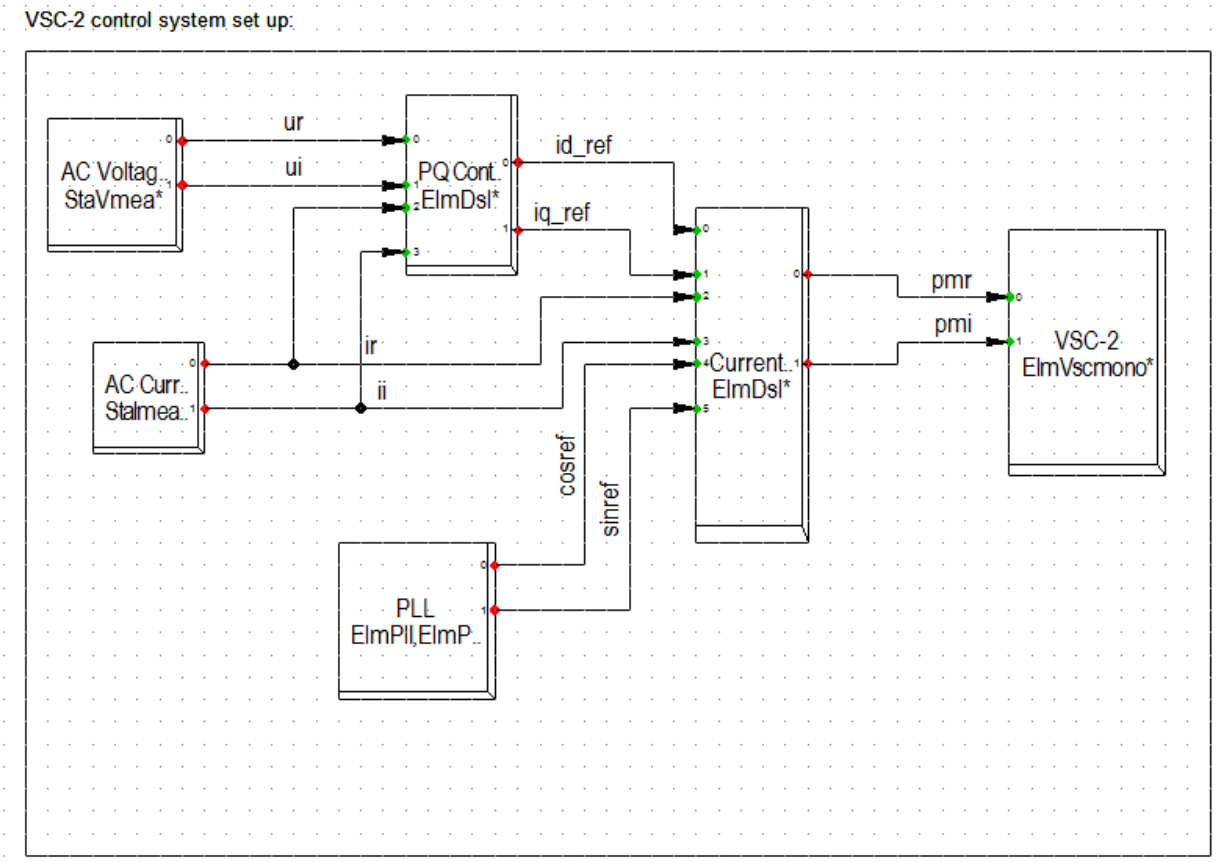

Figure B.2: VSC 2 controller.

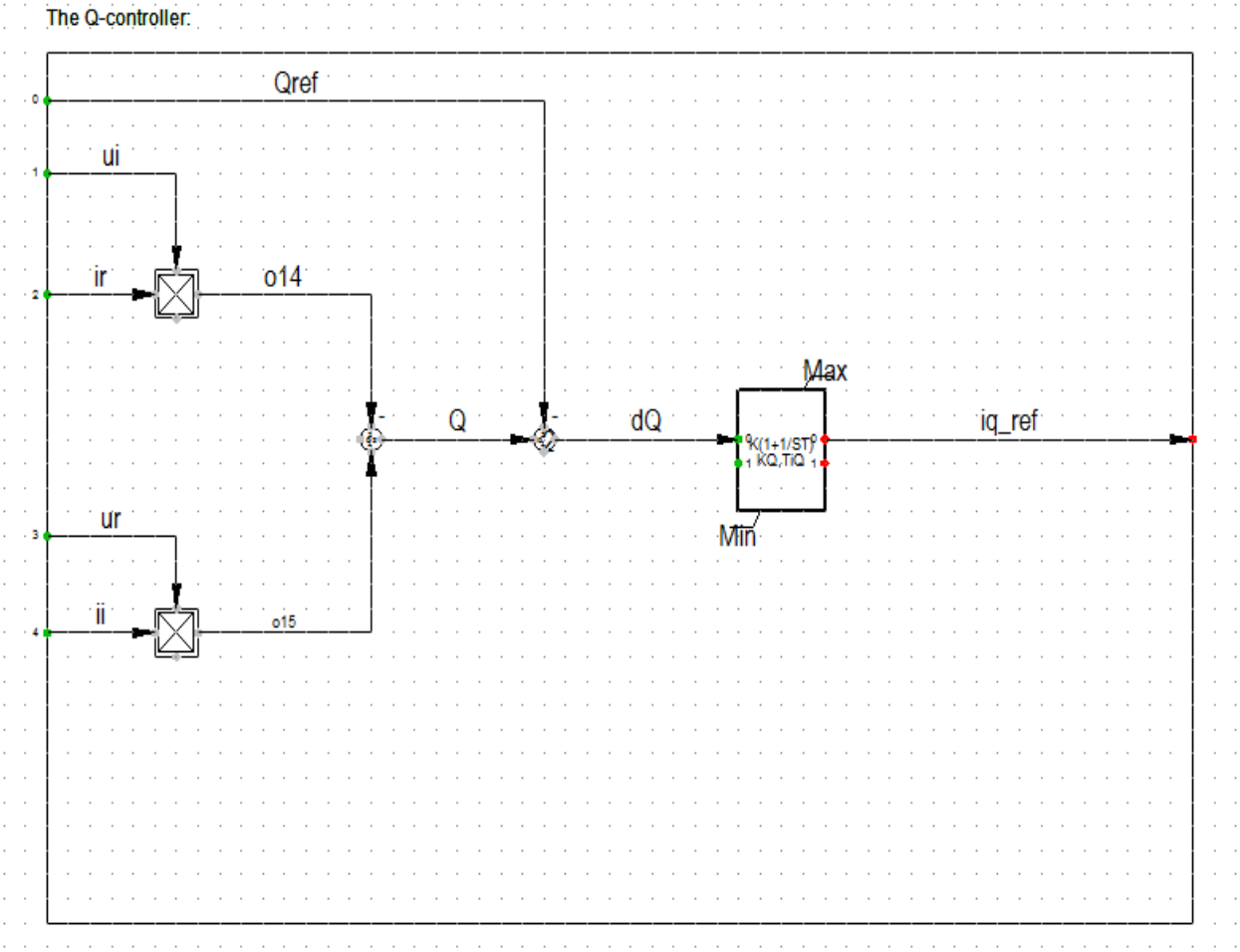

Figure B.3: Q controller.

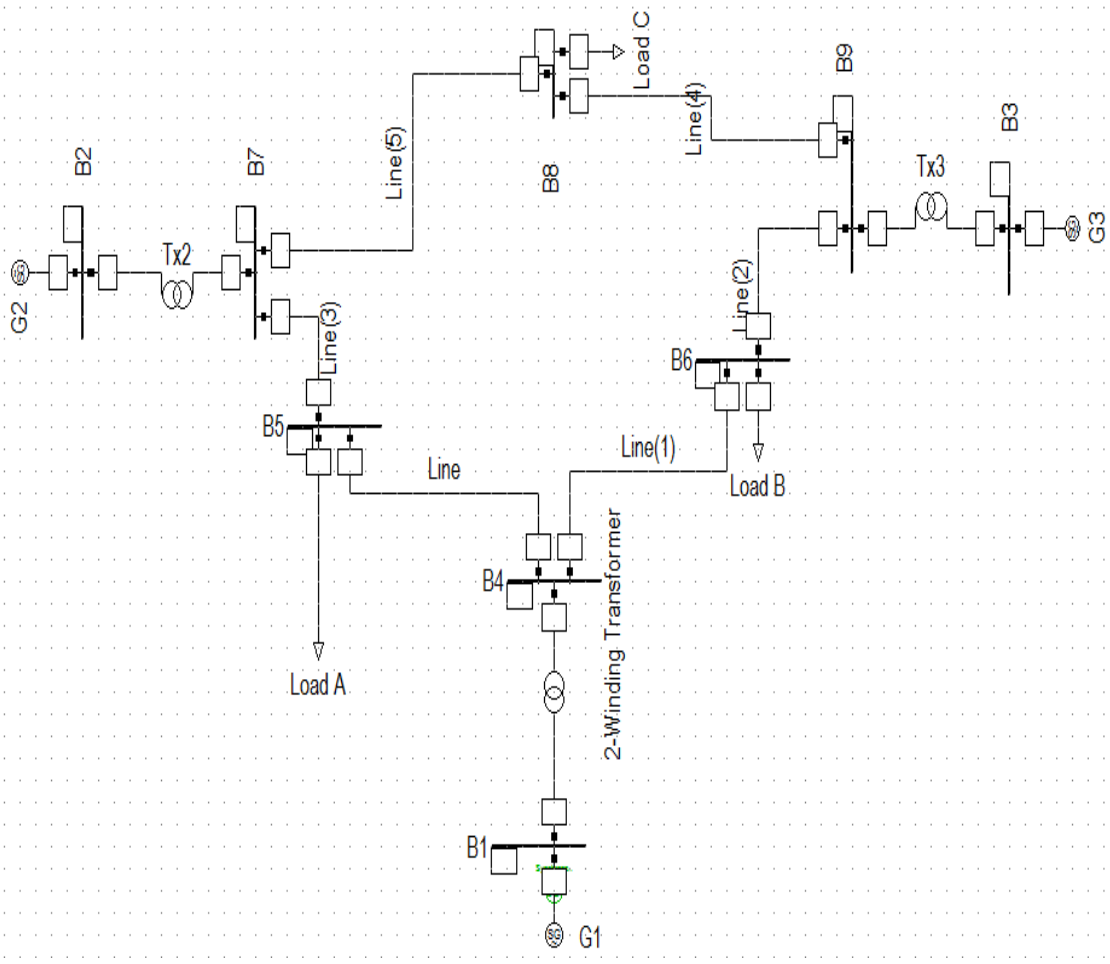

Figure B.4: IEEE 9-bus Data

Appendix C:

Table C.1: IEEE 9-bus data in p.u.

Bus number	**Bus type**	**P.U voltage**	**Active power (MW)**	**Reactive power (MVAR)**	**Generation (MW)**	**Generation (MVAR)**	**Rated voltage in KV**
1	3	1.04	0	0	0	0	16.5
2	2	1.025	0	0	163	0	18
3	2	1.025	0	0	85	0	13.8
4	0	1	0	0	0	0	230
5	0	1	125	50	0	0	230
6	0	1	90	30	0	0	230
7	0	1	0	0	0	0	230
8	0	1	100	35	0	0	230
9	0	1	0	0	0	0	230

Table C.2: Generator data.

Generator identification	**G1**	**G2**	**G3**
Rated Mva	247.5	192	128
Kv	16.5	18	13.8
Power factor	1	0.85	0.85
Speed	180rpm	3600rpm	3600rpm
x_d	0 146	0.8958	1.3125
x'_d	0.0608	0.1198	0.182
x_q	0.09 9	0.8645	1.2578
x'_q	.0969	0.1969	0.2
x_l	0.0336	0.0521	0.0742

T'_{do}	8.96	6	5.89
T'_{qo}	0	0.535	0.6
T''_{do}	0.15	0.075	0.005
T''_{qo}	0.024	0.07	075
x''_{d}	0.04	0.112	0.12
x''_{q}	0.024	0.112	0.2
Inertia time constant(H)	9.5438	6.214	2.3516

Table C.3: Line data in p.u.

From bus	**o bus**	**Branch resistance 'R'**	**Branch reactance 'X'**	**Line charging 'B'**
1			0.0576	0

2	7	0	0.0625	0
			0.0586	0
4	5	0.01	0.085	0.176
4	6	0.017	0.092	0.158
5	7	0.032	0.161	0.306
6	9	0.039	0.17	0.358
7	8	0.0085	0.072	0.149
8	9	0.0119	0.1008	0.209

APPENDIX D: TRANSFORMATIONS FOR THREE-PHASE SYSTEMS

Transformations used in this research are selected from three-phase quantities into vectors in stationary $\alpha\beta$ and rotating *dq-reference* frames.

Appendix D.1: Transformation of three-phase quantities to vectors

Three-phase reference quantities $v_a(t)$, $v_b(t)$ and $v_c(t)$ are translated from the three-phase reference frame into a vector $\vec{v}^{(\alpha\beta)}(t)$ in stationary orthogonal reference frame quantities $\alpha\beta$ frame, by applying the following transformation equation.

$$v^{(\alpha\beta)}(t) = v^{\alpha}(t) + jv^{\beta}(t) = K_{tans}(v_a(t) + v_b(t)e^{j\frac{2\pi}{3}} + v_c(t)e^{j\frac{4\pi}{3}} \qquad (D.1)$$

The transformation constant *K*trans can be chosen to be $\sqrt{\frac{2}{3}}$ to ensure power invariant or amplitude invariant transformation respectively between the two systems. This thesis considers a power invariant transformation. Equation (D.1) can be expressed in matrix form as:

$$v^{\alpha}(t) = T_{32}\begin{vmatrix} v_a(t) \\ v_b(t) \\ v_c(t) \end{vmatrix} \qquad (D.2)$$

Where the matrix T_{32} is given by

$$T_{32} = K_{trans}\begin{bmatrix} 1 & -\frac{1}{2} & -\frac{1}{2} \\ 0 & \frac{\sqrt{3}}{2} & -\frac{\sqrt{3}}{2} \end{bmatrix} \qquad (D.3)$$

The inverse transformation, assuming no zero-sequence, i.e. $v_a(t) + v_b(t) + v_c(t) = 0$, is given

by the relation;

$$\begin{bmatrix} v_a(t) \\ v_{b(t)} \\ v_c(t) \end{bmatrix} = T_{23}\begin{bmatrix} v^{\alpha}(t) \\ v^{\beta}(t) \end{bmatrix} \qquad (D.4)$$

Where the matrix $\mathbf{T}_{23}$ is given by

$$T_{23} = \frac{1}{K_{trans}}\begin{bmatrix} \frac{2}{3} & 0 \\ -\frac{1}{3} & \frac{1}{\sqrt{3}} \\ -\frac{1}{3} & -\frac{1}{\sqrt{3}} \end{bmatrix} \qquad (D.5)$$

Appendix D.2: Transformation between fixed $\alpha\beta$ and rotating dq coordinate systems

For the vector $\vec{v}^{(\alpha\beta)}(t)$ rotating in the $\alpha\beta$ frame with the angular frequency $\omega(t)$ in the positive (counter-clockwise direction), a *dq*-frame that rotates in the same direction with the same angular frequency $\omega(t)$ can be defined. The vector $\vec{v}^{(\alpha\beta)}(t)$will appear as fixed vectors in this rotating reference frame as shown in figure D.1. A projection of the vector $\vec{v}^{(\alpha\beta)}(t)$ on the *d*-axis and *q*-axis of the *dq*-frame gives the components of the vector on the *dq*-frame as illustrated in figure D.1

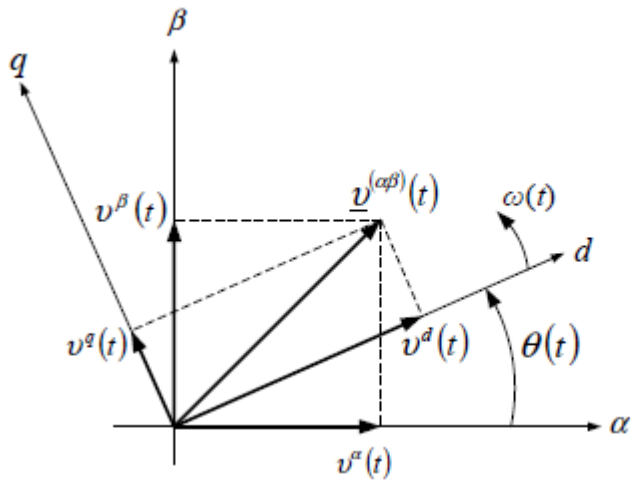

Figure D.1: Relation between stationery αβ-frame and dq rotating frame.

In vector form, the transformation below is used;

$$\vec{v}^{(dq)}(t) = v^{d}(t) + jv^{q}(t) = \vec{v}^{(\alpha\beta)}(t)e^{-j\theta(t)} \qquad (D.6)$$

The angle $\theta(t)$ in figure D.1 is given by;

$$\theta(t) = \theta_0 + \int_0^t \omega(\tau)d\tau \qquad (D.7)$$

The inverse transformation from the rotating *dq*-frame to the stationery $\alpha\beta$ frame is normally given by;

$$\vec{v}^{(\alpha\beta)}(t) = \vec{v}^{(dq)}(t)e^{j\theta} \qquad (D.8)$$

The transformation between the fixed $\alpha\beta$ frame and the rotating *dq*-frame can be written as;

$$\begin{bmatrix} v^d(t) \\ v^q(t) \end{bmatrix} = R\lfloor -\theta(t) \rfloor \begin{bmatrix} v^\alpha(t) \\ v^\beta(t) \end{bmatrix} \qquad (D.9)$$

$$\begin{bmatrix} v^\alpha(t) \\ v^\beta(t) \end{bmatrix} = R\lfloor \theta(t) \rfloor \begin{bmatrix} v^d(t) \\ v^q(t) \end{bmatrix} \qquad (D.10)$$

The projection matrix is given by;

$$R\lfloor \theta(t) \rfloor = \begin{bmatrix} \cos(\theta(t)) & -\sin(\theta(t)) \\ \sin(\theta(t)) & \cos(\theta(t)) \end{bmatrix} \qquad (D.11)$$

Appendix E: Coding for the VSC-HVDC controllers

Appendix E.1: PQ Controller codes

id_ref,iq_ref='The PQ-

controller'(Pref,ur,ir,ui,ii,Qref;x,x1;KP,TiP,KQ,TiQ,yP_min,yQ_min,yP_max,yQ_max;P,Q,dP,dQ,o1,o1l,o12,o13)

id_ref='\kpl16588.IntUser\working converter(14).IntPrj\Library.IntPrjfolder\User Defined Models.IntPrjfolder\K(1+1/sT)ant_.BlkDef'(dP;x;KP,TiP,yP_min,yP_max;)

x.=dP/TiP

limits(TiP)=(yP_min,yP_max]

limits(KP)=[yP_min,yP_max]

id_ref=lim(yP_min>=-1000,dP,yP_max<=1000)

iq_ref='\k**james**.IntUser\working **converter** **(**14).IntPrj\Library.IntPrjfolder\User Defined Models.IntPrjfolder\K(1+1/sT).BlkDef'(dQ;x1;KQ,TiQ,yQ_min,yQ_max;)

x1.=dQ/TiQ

limits(TiQ)=[yQ_min,yQ_max]

limits(KQ)=[yQ_min,yQ_max]

iq_ref=lim(yQ_min>=-1000,dQ,yQ_max<=1000)

o1=ir*ur

o11=ii*ui

o12=ir*ui

o13=ii*ur

dP=-P+Pref

P=o11+o1

dQ=Q-Qref

Q=-o13+o12

inc(o1)=ir*ur

inc(o11)=ii*ui

inc(o12)=ir*ui

inc(o13)=ii*ur

inc(P)=o11+o1

inc(Q)=-o13+o12

inc(dP)=-P+Pref

inc(dQ)=Q-Qref

inc(x)=id_ref*TiP/KP

inc(x1)=iq_ref*TiQ/KQ

```
inc(Pref)=P

inc(Qref)=Q

inc0(ur)=1

inc0(ir)=-1

inc0(ui)=0

inc0(ii)=0

inc(id_ref)=1000

inc0(iq_ref)=-1

vardef(Pref)='pu';'[-1]'

vardef(Qref)='pu';'[-1]'

vardef(Q)='pu';'[1]'

vardef(P)='pu';'[1]'

vardef(id_ref)='pu';'[1]'

vardef(iq_ref)='Pu';'[1]'

vardef(yP_max)='pu';'[1]'

vardef(yQ_max)='Pu';'[1]'

vardef(yP_min)='pu';'[-1]'
```

vardef(yQ_min)='pu';'[-1]'

vardef(iq_ref)='Pu';'[1]'

Appendix E.2: Q controller codes

iq_ref='The Q-controller'(Qref,ui,ir,ur,ii;xiQ;KQ,TiQ,Min,Max;Q,dQ,o14,o15)

! iq_ref='\kjames.IntUser\working converter (14).IntPrj\Library.IntPrjfolder\User Defined Models.IntPrjfolder\K(1+1/ST).BlkDef'(dQ;xiQ;KQ,TiQ,Min,Max;)

xiQ.=dQ/TiQ

iq_ref=lim(Max<=10,dQ,Min>=-10)

o14=ir*ui

o15=ii*ur

Q=o15-o14

dQ=Q-Qref

inc(o14)=ir*ui

inc(o15)=ii*ur

inc(dQ)=Q-Qref

inc(Q)=o15-o14

inc(b0)=1

inc(b1)=1

```
inc(Qref)=Q

inc(x)=1

inc0(ii)=1

inc0(ir)=1

inc0(ui)=1

inc0(ur)=1

vardef(KQ)='pu';'gain'

vardef(TiQ)='s';'time'

vardef(Max)='pu';

vardef(Min)='pu';

b0=KQ

b1=KQ/TiQ

inc(iq_ref)=b1*x+b0*dQ
```

Appendix E.3: Inner current controller codes.

Pmr,Pmi='The inner dq-current controller'(id_ref,ir,ii,cosref,sinref,iq_ref;x1,xid,x4,xiq;Kr,Tr,Ki,Ti,MinPmd,MinPmq,MaxPmd,MaxPmq;yunb1,dev1,dev3,b2,a2,b4,b5,a1,yunb,uq,bo,b3,dev,dev4,Pmd,Pmq,did,diq,id,iq)

! Pmr,Pmi='\kjames.IntUser\working converter (14).IntPrj\Library.IntPrjfolder\User Defined Models.IntPrjfolder\dq-Back(1).BlkDef'(Pmd,Pmq,cosref,sinref;;;)

Pmr=Pmd*cosref-Pmq*sinref

Pmi=Pmd*sinref+Pmq*cosref

! Pmd='\kjames.IntUser\working converter(14).IntPrj\Library.IntPrjfolder\User Defined Models.IntPrjfolder\K(1+1/sT)ant..BlkDef'(did;x1,xid;Kr,Tr,MinPmd,MaxPmd;yunb1,dev1,

dev3,b2,a2,b4,b5,a1)

xid.=dev3

x1.=dev1

a1=1/Tr

b4=Kr

b5=Kr/Tr

dev1=id

dev3=-a1*xid+did

yunb1=b5*x1*b4*id

a2=1/Tr

b2=1/Tr

Pmd=lim(did,MinPmd>=-1000,MaxPmd<=1000)

Pmq='\k**james**.IntUser\working converter(14).IntPrj\Library.IntPrjfolder\User Defined Models.IntPrjfolder\K(1+1/sT)ant-
.BlkDef'(diq;x4,xiq;Ki,Ti,MinPmq,MaxPmq;yunb,uq,bo,b3,dev,dev4)

xiq.=dev4

x4.=dev

bo=Ki

b3=Ki/Ti

dev=uq

dev4=-a2*xiq+diq

yunb=b3*x4-bo*uq

uq=b2*xiq

Pmq=lim(diq,MinPmq>=-1000,MaxPmq<=1000)

id,iq='\kjames.IntUser\working converter(14).IntPrj\Library.IntPrjfolder\User Defined Models.IntPrjfolder\dq_Trans.BlkDef'(ir,ii,cosref,sinref;;;)

id=ir*cosref+ii*sinref

iq=-ir*sinref+ii*cosref

did=id_ref-id

diq=iq_ref-iq

inc(id_ref)=id

inc(iq_ref)=iq

inc(did)=id_ref-id

inc(xid)=did

inc(xiq)=diq

inc(x1)=Pmd*Tr/Kr

inc(x4)=Pmq*Ti/Ki

inc(dev1)=0

inc(dev)=0

inc(dev3)=0

inc(dev4)=0

inc0(ir)=1

inc0(ii)=1

inc0(cosref)=1

inc0(sinref)=0

inc0(Pmr)=0

inc0(Pmi)=1

inc(Pmd)=Pmr*cosref+Pmi*sinref

inc(Pmq)=-Pmr*sinref+Pmi*cosref

Appendix E.4: DC voltage controller codes.

id_ref='Voltage controller'(Vdc_ref,Vdc;x;K,Ti,Minid_ref,Maxid_ref;yunb,b1,b0,dev,u)

id_ref='\kjames.IntUser\working converter(14).IntPrj\Library.IntPrjfolder\User Defined Models.IntPrjfolder\K(1+1/sT)ant.BlkDef'(u;x;K,Ti,Minid_ref,Maxid_ref;yunb,b1,b0,dev)

x.=dev

```
dev=u

b0=K

b1=K/Ti

yunb=b1*x+b0*u

limits(Ti)=(0,]

id_ref=lim(Maxid_ref<=10,u,Minid_ref>=-10)

u=Vdc-Vdc_ref

inc(Vdc_ref)=Vdc

inc(u)=Vdc-Vdc_ref

inc(x)=id_ref*Ti/K

inc(dev)=0

inc0(Vdc)=1

inc(id_ref)=100

vardef(id_ref)='pu';'[1]';'reference curent'

vardef(K)='pu';'[0.109]';'Gain'

vardef(Ti)='s';'[0.0018]';'time'

vardef(Maxid_ref)='pu';'[1]'
```

vardef(Minid_ref)='pu';'[-1]'

vardef(Vdc_ref)='pu';'[1]';'reference voltage'

vardef(Vdc)='pu';'[1]';'actual voltage'

vardef(u)='pu';'[1]'

vardef(dev)='pu';'[1]';'voltage error'